

eman ta zabal zazu



Universidad
del País Vasco

Euskal Herriko
Unibertsitatea

**Elucidation of the molecular and bioenergetic
mechanisms underlying the resistance to
oxidative stress and the pro-recovery effect of
H₂O₂-preconditioned adipose-derived stem cells**

Patricia Garrido Pascual

Leioa, 2020

Supervisors:

Prof. Ana Alonso Varona

Prof. Teodoro Palomares Casado

A mis padres

Agradecimientos

En primer lugar, quiero agradecer a mis directores, la Doctora Ana Alonso y el Doctor Teodoro Palomares, la oportunidad que me dieron de incorporarme a su grupo de investigación, la confianza depositada en mí para llevar a cabo este proyecto, su asesoramiento, paciencia y dedicación durante todos estos años.

En segundo lugar, María y Vero, gracias por haber sido tan buenas compañeras de laboratorio, por todos los buenos momentos (que son muchos) y por vuestro apoyo incondicional, sin el cual hubiera sido muy difícil llegar hasta aquí. Gracias también a las veteranas, María y Cris, por su ayuda en mis inicios como investigadora y a las nuevas incorporaciones Sheila y Ander por su apoyo en la recta final.

Gracias a mis compañeros de departamento Maddalen, Alba, Arantza, Mainer, Igor, Xandra, Noelia, Lutxu, Miguel, María, Aitor, Cris, Patri, Olatz, Miren, Vero, Andrea y Jose. Me siento muy afortunada de haber contado con todos vosotros durante todo este tiempo, gracias por compartir tan buenos momentos dentro y fuera del labo. Habéis hecho que venir a trabajar sea un verdadero placer. Mención especial para Irene, *my partner in crime*, gracias por apoyarme siempre en todo, por tus consejos, por tus ánimos y sobre todo por enseñarme que con humor todo se lleva mejor.

Gracias a los miembros de SGIker por su colaboración para sacar adelante esta investigación.

A la fundación Jesus de Gangoiti Barrera por financiar parte de mi investigación y apoyar año tras año a jóvenes investigadores.

Al mismo tiempo, quiero expresar mi agradecimiento a la empresa HistoCell por permitirme formar parte de este proyecto y por todo lo que me han enseñado en el proceso.

Agradecer a la Doctora Begoña Ochoa, por su ayuda y consejos en el mundo del metabolismo energético.

Muchas gracias también a la Doctora Yolanda Calle, por abrirme las puertas de su laboratorio en Londres y darme la oportunidad de disfrutar de aquella maravillosa experiencia.

Gracias a mis amigas por estar ahí desde hace tanto tiempo. A las que estáis lejos y las que estáis cerca, gracias por vuestros ánimos y vuestro cariño. Sois las mejores.

Por último, quiero dar las gracias a toda mi familia por vuestro apoyo e interés en saber sobre mi tesis. En especial gracias mamá y papá, esta tesis no habría sido posible sin vosotros.

Index

Resumen.....	1
Summary.....	13
I. Introduction.....	17
I.1. Tissue Injury and Regenerative Medicine	19
I.2. Stem Cells	22
I.2.1. Stem Cells Types.....	22
I.2.1.1. Totipotent Stem Cells	22
I.2.1.2. Pluripotent Stem Cells	23
Embryonic stem cells (ESCs)	23
Induced pluripotent stem cells (iPSCs).....	23
I.2.1.3. Multipotent Stem Cells.....	24
Adult stem cells	25
I.2.2. Stem Cell Research: Then and Now.....	26
I.3. MSCs in Regenerative Medicine	28
I.3.1. Benefits.....	30
I.3.1.1. Homing Ability	30
I.3.1.2. Immunomodulatory Properties.....	32
I.3.1.3. Antioxidant Properties	33
I.3.1.4. Metabolic Plasticity	35
I.3.1.5. Paracrine Activity.....	36
I.3.1.6. Differentiation Capacity	39
I.3.2. Limitations	39
I.3.2.1. Pre- transplantation Limitations.....	40

Index

I.3.2.2. Post-transplantation limitations	42
I.3.3. Strategies to Overcome Limitations.....	43
I.3.3.1. Optimization of MSCs culture	44
I.3.3.2. Gene Modification	46
I.3.3.3. Preconditioning.....	47
II. Hypothesis and Aims.....	51
III. Chapter 1.....	55
III.1. Materials and methods	58
III.1.1. Cell culture	58
III.1.2. hASCs H ₂ O ₂ -preconditioning	59
III.1.3. Senescence, cell cycle analysis and proliferation rate.....	59
III.1.3.1. Senescence Assay.....	59
III.1.3.2. Cell cycle analysis	60
III.1.3.3. Proliferation rate assay	60
III.1.4. Proteomic profile analysis.....	61
III.1.5. Oxidative stress induction.....	63
III.1.6. PC-hASCs tolerance to H ₂ O ₂ -induced oxidative stress.....	64
III.1.6.1. Measurement of ROS.....	64
III.1.6.2. Apoptosis assay.....	64
III.1.6.3. Cytotoxicity assay.....	65
III.1.7. Statistical analysis	66
III.2. Results.....	67

III.2.1. Preconditioning does not alter morphology, senescence, cell cycle or proliferation rate	67
III.2.2. hASCS preconditioning modify the proteomic profile	70
III.2.3. Preconditioning protects cells against oxidative stress	73
IV. Chapter 2	77
IV.2. Materials and methods	80
IV.1.1. Cell culture	80
IV.1.2. Western blot analysis	80
IV.1.3. Assessment of mitochondrial stress	82
IV.1.4. Cellular bioenergetic evaluation	83
IV.1.4.1. Mitochondrial respiration	84
IV.1.4.1. Glycolysis	85
IV.1.4.1. ATP production	87
IV.1.5. Statistical analysis	88
IV.2. Results	89
IV.2.1. Preconditioning promotes the antioxidant response and reduces the pro-inflammatory proteins expression	89
IV.2.1. Preconditioning alters cells metabolism	93
IV.2.1.1. Mitochondrial respiration	93
IV.2.1.2. Glycolysis	98
IV.2.1.3. ATP production	101
V. Chapter 3	105
V.2. Materials and methods	109
V.2.1. Cell culture	109

Index

V.2.1.1. Human adipose-derived stem cells.....	109
V.2.1.2. Human oligodendrogloma (HOG)	109
V.2.2. HOG differentiation	110
V.2.3. Immunofluorescence assay	112
V.2.4. Oxidative stress induction and co-culture	113
V.2.5. Proliferation assay	114
V.2.6. Measurement of ROS.....	115
V.2.7. Total antioxidant capacity assay	115
V.2.8. Western blot analysis	116
V.2.9. Migration assay.....	117
V.2.10. Statistical analysis	118
V.3. Results.....	119
V.3.1. HOG cells differentiation	119
V.3.2. $oxHOGd$ repair	121
V.3.3. Antioxidant capacity	124
V.3.4. Homing ability.....	128
VI. Discussion	131
VII. Conclusions	147
VIII. References	151

Figures index

Figure 1. Stem cells properties. Modified from the image prepared by Catherine Twomey for the National Academies, Understanding Stem Cells: Overview of the Science and Issues from the National Academies.....	22
Figure 2. Differentiation potentials of stem cells.....	25
Figure 3. Schematic timeline showing the main discoveries in stem cell research.	27
Figure 4. Map of the different MSC-based clinical trials ongoing worldwide...	28
Figure 5. Ongoing MSC-based clinical trials classified by disease.	29
Figure 6. Mesenchymal stem cells homing mechanisms.	31
Figure 7. The NRF2-Keap1 signaling pathway. Under normal conditions, NRF2 is constantly ubiquitinated through Keap1 and degraded in the proteasome. Under stress conditions, Keap1 is inactivated, NRF2 translocates into the nucleus and promotes transcriptional activation of antioxidants and detoxification enzymes.	34
Figure 8. Overview of metabolic features contributing to MSCs maintenance and differentiation.	35
Figure 9. Overview of the MSC secretome. The secretome comprises of soluble proteins and extracellular vesicles. The proteins include biologically active factors such as cytokines, chemokines and growth factors, and the extracellular vesicles include exosomes and microvesicles..	37
Figure 10. Overview of senescence in MSCs. MSC senescence is characterized by an irreversible cell cycle arrest, a change in morphology and an impairment in differentiation ability. In addition, senescent cells secrete SASPs, decrease the level of certain surface antigens (CD13, CD29 and CD44) and increase the levels of ROS.	42
Figure 11. <i>Hormesis</i> concept. In normal conditions cells exposed to an intense stress undergo cell death. However, cells preconditioned with mild stress can	

become resistant to subsequent intense stresses. This process is called hormesis: an adaptive behavior that is crucial for survival in a stress environment.	48
Figure 12. Phase contrast microscopy image of 80% confluent hASCs culture (scale bar: 100 μ m).	58
Figure 13. Representative images of 80% confluent hASCs and PC-hASCs morphology by contrast phase microscope. Scale: 100 μ m.	67
Figure 14. (A) Representative images of hASCs and PC-hASCs dyed with X-GAL staining (senescent cells are dyed in blue, scale bar: 100 μ m) and (B) their quantification. Data are expressed as mean \pm SD. * $p < 0.05$	68
Figure 15. (A) Flow cytometry analysis for cell-cycle distribution (B) Evaluation of the proliferation rate of hASCs and PC-hASCs under standard conditions. Experiments were, at least, performed in triplicate. Data are expressed as mean \pm SD. * $p < 0.05$	69
Figure 16. Volcano plot for hASCs vs PC-hASCs. Differentially expressed proteins are within the quadrants in green. hASCs overexpressed proteins (19, left quadrant) and PC-hASCs overexpressed proteins (21, right quadrant). A Student's t-test was used to determine statistically significant changes in protein expression. Proteins that showed $p < 0.05$ and a change in LFQ greater or less than 1.5 times were considered as differentially expressed proteins ($n=5$).	70
Figure 17. Graphical representation of the percentage of differentially expressed proteins according to their function.	72
Figure 18. Intracellular ROS levels of hASCs and PC-hASCs during the oxidative stress insult. ROS generation was induced by H_2O_2 (0.25 or 0.5 mM) and measured for 1 hour every 10 minutes. At least three different experiments were performed ($n \geq 5$). Data are expressed as mean \pm SD. * $p < 0.05$	73
Figure 19. Analysis of hASCs and PC-hASCs undergoing early and late apoptosis. (A). Annexin V/PI assay was performed by flow cytometry. Annexin V-/PI- represents live cells; Annexin V+/PI- or Annexin V-/PI+ represents early or late	

apoptosis phase respectively; Annexin V+/PI+ reflects necrosis. (B) Quantification of cells undergoing early and late apoptosis. Experiments were performed in triplicate. Data are expressed as mean \pm SD. *p < 0.05.....	74
Figure 20. Determination of H ₂ O ₂ cytotoxic effect on hASCs and PC-hASCs. LDH release was quantified at 24 and 48 hours post-stimulus (0.25 or 0.5 mM H ₂ O ₂). At least three different experiments were performed (n \geq 5). Data are expressed as mean \pm SD. *p < 0.05.	75
Figure 21. Agilent Seahorse XF Cell Mito Stress Test profile, showing the key parameters of mitochondrial function.....	85
Figure 22. Principle of the Agilent Seahorse XF Glycolytic rate assay.....	86
Figure 23. Agilent Seahorse XF Glycolytic rate assay profile. Proton efflux from live cells comprises both glycolytic and mitochondrial-derived acidification. Inhibition of mitochondrial function by Rot/AA enables calculation of mitochondrial-associated acidification to Total Proton Efflux Rate (PER) results in Glycolytic Proton Efflux Rate (glycoPER).	87
Figure 24. Agilent Seahorse XF Real-Time ATP rate assay. This assay removes contributions from non-ATP production related signals through sequential injection of energy pathway modulators (oligomycin and Rot/AA).....	88
Figure 25. Expression and quantification of nuclear NRF2 in hASCs and PC-hASCs exposed to oxidative stress. Cells were treated with 0.25 mM H ₂ O ₂ for 1 hour, and lysed just after the insult. Values were normalized to their corresponding loading control. At least three different experiments were performed. Data were relativized to control hASCs (dotted line) and expressed as mean \pm SD. *p < 0.05, compared with control hASCs, #p < 0.05.	89
Figure 26. Expression and quantification of HO-1, SOD-1, GPx1 and CAT in hASCs and PC-hASCs exposed to oxidative stress. Cells were treated with 0.25 mM H ₂ O ₂ for 1 hour, and lysed just after the insult. Values were normalized to their corresponding loading control. At least three different experiments were	

performed. Data were relativized to control hASCs (dotted line) and expressed as mean ± SD. *p < 0.05, compared with control hASCs, #p < 0.05.90

Figure 27. Expression and quantification of NF-κB, COX-2 and IL-1β in hASCs and PC-hASCs exposed to oxidative stress. Cells were treated with 0.25 mM H₂O₂ for 1 hour, and lysed 24 hours after the insult. Values were normalized to their corresponding loading control. At least three different experiments were performed. Data were relativized to control hASCs (dotted line) and expressed as mean ± SD. *p < 0.05, compared with control hASCs, #p < 0.05.91

Figure 28. Expression and quantification of p-ERK and p-AKT. hASCs and PC-hASCs were exposed to 0.25 mM H₂O₂ for 1 hour, and lysed 24 hours after the insult. At least three different experiments were performed. Data were relativized to control hASCs (dotted line), and expressed as mean ± SD. *p < 0.05, compared with control hASCs, #p < 0.05.92

Figure 29. Mitochondrial morphology. Confocal microscopy images of PC-hASCs and hASCs under standard and oxidative stress situation; cells labeled live with MitoTracker Red CMXRos. Scale bar: 30 μm.93

Figure 30. Δψ_m quantification. hASCs and PC-hASCs under standard and oxidative stress situation were labeled live with MitoTracker Red CMXRos and fluorescence was quantified. At least three different experiments were performed and results were expressed as mean ± SD. *p < 0.05.94

Figure 31. Coupling efficiency. Mitochondrial respiration parameters were assessed in hASCs and PC-hASCs following sequential injections of oligomycin, FCCP, and a ROT/AA under control conditions or after 0.25 mM H₂O₂ exposure. At least three different experiments were performed and results were expressed as mean ± SD. *p < 0.05.95

Figure 32. Mitochondrial respiration parameters. Mitochondrial respiration was assessed in hASCs and PC-hASCs following sequential injections of oligomycin, FCCP, and a ROT/AA under control conditions or after 0.25 mM H₂O₂ exposure. (A) Basal respiration, (B) Maximal respiration. At least three different

experiments were performed and results were expressed as mean \pm SD. *p < 0.05.....	96
Figure 33. ATP-linked respiration. Mitochondrial respiration parameters were assessed in hASCs and PC-hASCs following sequential injections of oligomycin, FCCP, and a ROT/AA under control conditions or after 0.25 mM H ₂ O ₂ exposure. At least three different experiments were performed and results were expressed as mean \pm SD. *p < 0.05.	97
Figure 34. Percentage of PER from glycolysis. Both, hASCs and PC-hASCs present a glycolytic phenotype suggested by % PER (proton efflux rate, the number of protons exported by cells into the assay medium over time) from glycolysis. At least three different experiments were performed. Data were expressed as mean \pm SD. *p < 0.05.....	98
Figure 35. Glycolysis parameters. Glycolysis was assessed in hASCs and PC-hASCs following sequential injections of ROT/AA and 2-DG under control conditions or after 0.25 mM H ₂ O ₂ exposure. (A) Basal glycolysis and (B) Compensatory glycolysis. At least three different experiments were performed. Data were expressed as mean \pm SD. *p < 0.05.....	99
Figure 36. Expression and quantification of HIF-1 α . hASCs and PC-hASCs were exposed to 0.25 mM H ₂ O ₂ for 1 hour, and lysed 24 hours after the insult. At least three different experiments were performed. Data were relativized to control hASCs (dotted line), and expressed as mean \pm SD. *p < 0.05, compared with control hASCs, #p < 0.05.	100
Figure 37. Total ATP production rate. Seahorse XF Real-Time ATP Rate Assay was performed in hASCs and PC-hASCs under control conditions or after 0.25 mM H ₂ O ₂ exposure to quantify the ATP production. At least three different experiments were performed and data were expressed as mean \pm SD. *p < 0.05.	101
Figure 38. Glycolytic ATP production rate. Seahorse XF Real-Time ATP Rate Assay was performed in hASCs and PC-hASCs under control conditions or after 0.25	

mM H₂O₂ exposure to quantify the ATP production. At least three different experiments were performed and data were expressed as mean ± SD. *p < 0.05.102

Figure 39. Mitochondrial respiration ATP production rate. Seahorse XF Real-Time ATP Rate Assay was performed in hASCs and PC-hASCs under control conditions or after 0.25 mM H₂O₂ exposure to quantify the ATP production. At least three different experiments were performed and data were expressed as mean ± SD. *p < 0.05.103

Figure 40. Phase contrast microscopy image of 80% confluent HOG cell line culture (scale bar: 100 μm).109

Figure 41. Chronogram of HOG cell line differentiation.111

Figure 42. Visual representation of hASCs or PC-hASCs CM obtaining for oxHOGd treatment.113

Figure 43. Visual representation of hASCs or PC-hASCs co-cultured with oxHOGd, with or without oxidative stress induction.114

Figure 44. HOG cell line differentiation. Phase contrast images of HOG and HOGd cells. Differentiated cells showed short ramified processes. Scale bar: 100 μm.119

Figure 45. HOG cell line differentiation. Representative images of the expression of MBP, CNPase and MOG evaluated by immunofluorescence (scale bar: 50 μm) and western blot. At least three different experiments were performed.120

Figure 46. Effect of oxidative induction on oxHOGd. (A) Cell viability, and (B) intracellular ROS levels after 24 and 48 hours of the H₂O₂ insult. Data are expressed as mean ± SD and relativized to control (HOGd, dotted line). *p < 0.05, compared with oxHOGd.121

Figure 47. Reparative effect of hASCs and their derivatives on the oxHOGd. The viability of oxHOGd was measured at different time points (24 and 48 hours), alone or cultured with: i, hASCs CM or PC-hASCs CM; ii, hASCs or PC-hASCs; and iii, hASCs or PC-hASCs subjected to oxidative stress. Four different experiments

were performed (n=3). Results were relativized to control (HOGd, dotted line) and expressed as mean \pm SD. *p < 0.05, compared with $_{ox}$ HOGd, #p < 0.05. 122	
Figure 48. Reparative effect of hASCs and their derivates on the $_{ox}$ HOGd. Intracellular ROS levels of $_{ox}$ HOGd were measured at different time points (24 and 48 h), alone or cultured with: i, hASCs CM or PC-hASCs CM; ii, hASCs or PC-hASCs; and iii, hASCs or PC-hASCs subjected to oxidative stress Four different experiments were performed (n=3). Results were relativized to control (HOGd, dotted line) and expressed as mean \pm SD. *p < 0.05, compared with $_{ox}$ HOGd, #p < 0.05.	123
Figure 49. Total antioxidant capacity (TAC) of the culture media. $_{ox}$ HOGd secretion of small molecule antioxidants and proteins in the culture media was measured with the Total Antioxidant Capacity Assay Kit at 24 hours, alone or cultured with: i, hASCs CM or PC-hASCs CM; ii, hASCs or PC-hASCs; and iii, hASCs or PC-hASCs subjected to oxidative stress. Four different experiments were performed (n=3). Results were relativized to control (HOGd, dotted line) and expressed as mean \pm SD. *p < 0.05, compared with $_{ox}$ HOGd + hASCs, #p < 0.05.	124
Figure 50. Expression and quantification of NRF2, HO-1 and SOD-1 in $_{ox}$ HOGd. HOGd were exposed to 0.25 mM H ₂ O ₂ for 1 hour, cultured with: i, hASCs or PC-hASCs; and ii, hASCs or PC-hASCs subjected to oxidative stress, and lysed 24 hours after the insult. At least three different experiments were performed. Data were relativized to control ($_{ox}$ HOGd + hASCs, dotted line), and expressed as mean \pm SD. *p < 0.05, compared with $_{ox}$ HOGd + hASCs, #p < 0.05.	125
Figure 51. Expression and quantification of NRF2, CAT, HO-1 and SOD-1 in hASCs. hASCs, PC-hASCs and hASCs and PC-hASCs subjected to oxidative stress co-cultured with $_{ox}$ HOGd were lysed 24 hours after the insult. At least three different experiments were performed. Data were relativized to control ($_{ox}$ HOGd + hASCs, dotted line), and expressed as mean \pm SD. *p < 0.05, compared with $_{ox}$ HOGd + hASCs, #p < 0.05.	126

Figure 52. Migration ability of hASCs, PC-hASCs, and hASCs and PC-hASCs subjected to oxidative stress towards $_{ox}HOGd$ at 24 hours after the co-culture. Representative images of phase contrast microscopy (x10 objective). At least three different experiments were performed.....128

Figure 53. Migration ability of hASCs, PC-hASCs, and hASCs and PC-hASCs subjected to oxidative stress migration towards $_{ox}HOGd$ at 48 hours after the co-culture. Representative images of phase contrast microscopy (x10 objective). At least three different experiments were performed.....129

Figure 54. Quantification of hASCs, PC-hASCs and hASCs and PC-hASCs subjected to oxidative stress migration towards $_{ox}HOGd$ at 24 and 48 hours after the co-culture. At least three different experiments were performed. Data are expressed as mean \pm SD. * $p < 0.05$130

Figure 55. Schematic overview of PC-hASCs mechanisms to adapt to an oxidative stress environment.145

Tables index

Table 1. Regenerative medicine strategies.....21

Table 2.Types of multipotent stem cells depending on their origin.....24

Table 3. Function of bioactive factors present in MSC-derived secretome.38

Table 4. List of overexpressed proteins in hASCs or PC-hASCs and their functions.71

Table 5. List of western blot antibodies used in the PC-hASCs analysis.....81

Table 6. List of different metabolic stressors used in the energetic metabolism analysis of PC-hASCs.83

Table 7. List of antibodies used in the immunofluorescence assay.112

Table 8. List of antibodies used in the western blot analysis.117

Glossary

·OH: hydroxyl radical

2-DG: 2-deoxy-D-glucose

AAV: adeno-associated virus

Ad-hHO-1: adenovirus vector harboring the HO-1 gene

AGC: automatic gain control

AKT: protein kinase B

Ang-1: angiotensin-1

ARE: antioxidant response element

ATP: adenosine triphosphate

BDNF: brain-derived neurotrophic factor

bFGF: basic fibroblast growth factor

BM-MSCs: bone marrow-derived stem cells

BSA: bovine serum albumin

CAT: catalase

CDM: chemically-defined media

CM: conditioned media

CNPase: 2', 3'-cyclic nucleotide 3'-phosphodiesterase

CNS: central nervous system

COMMD1: COMM domain-containing protein 1

COX-2: cyclooxygenase 2

COX7A2L: cytochrome c oxidase subunit 7A-related protein

DFC: 2',7'-dichlorofluorescein

DM: differentiation media

DMEM: Dulbecco's modified eagle medium

DTH: delayed-type hypersensitivity

DTT: dithiothreitol

ECAR: extracellular acidification rate

ECM: extracellular matrix

ERK: extracellular signal-regulated kinase

ESCs: embryonic stem cells

ETC: electron transport chain

ETFDH: electron transfer flavoprotein-ubiquinone oxidoreductase

EVs: extracellular vesicles

FASP: filter-aided sample preparation

FBS: fetal bovine serum

FCCP: carbonyl cyanide 4-(trifluoromethoxy) phenylhydrazone

FGF: fibroblast growth factor

GAPDH: glyceraldehyde 3-phosphate dehydrogenase

GFAP: glial fibrillary acidic protein

GlycoPER: glycolytic proton efflux rate

GPX-1: glutathione peroxidase

GvHD: graft-versus-host disease

H2-DFC-DA: 2'-7'-dichlorofluorescein diacetate

H₂O₂: hydrogen peroxide

hASCs: human adipose-derived stem cells

HB-EGF: heparin-binding epidermal growth factor-like growth factor

HCD: higher energy C-trap dissociation

HCs: hepatocytes

HGF: hepatocyte growth factor

HIF: hypoxia inducible factor

hMSCs: human mesenchymal stem cells

HO-1: heme-oxygenase 1

HOG: human oligodendroglioma

HOGd: oligodendrocyte-like cells

HPD: human platelet-derivatives

hUC-MSCs: human umbilical cord mesenchymal stem cells

IDO: indoleamine 2,3-dioxygenase

IGF: insulin-like growth factor

IL: interleukin

iNOS: inducible nitric oxide synthase

iPSCs: induced pluripotent stem cells

IRS1: insulin receptor substrate 1

ISCT: international society of cellular therapy

Keap1: Kelch-like ECH associating protein 1

LC-MS/MS: liquid chromatography tandem-mass spectrometry

LDH: lactate dehydrogenase

LFQ intensity: Label-free quantification intensity

LPS: lipopolysaccharide

MBP: myelin basic protein

MDC: macrophage-derived chemokine

MEFs: mouse embryo fibroblasts

MFN2: mitofusin 2

MI: myocardial infarction

MMPs: metalloproteinases

MOG: myelin oligodendrocyte glycoprotein

MSCs: mesenchymal stem cells

NF- κ B: nuclear factor

NO: nitric oxide

NRF2: nuclear factor E2-related factor 2

o/n: overnight

OCR: oxygen consumption rate

α HOGd: damaged oligodendrocyte-like cells

OXPPOS: oxidative phosphorylation

PBS: phosphate-buffered saline

PC-hASCs: preconditioned human adipose-derived stem cells

PDGF: platelet-derived growth factor

PER: proton efflux rate

PFA: paraformaldehyde

PGE-2: prostaglandin E2

PI: propidium iodide

PXN: paxillin

RECK: reversion-inducing cysteine-rich protein with Kazal motifs

RNS: reactive nitrogen species

ROS: reactive oxygen species

RT: room temperature

SASP: senescence-associated secretory phenotype

SA- α -Fuc: senescence-associated lysosomal α -L-fucosidase

SA- β -gal: senescence-associated β -galactosidase

SDF: stromal cell-derived factor

SDS: sodium Dodecyl

SOD-1: superoxide dismutase

T3: triiodothyronine

TAC: total antioxidant capacity

TCA cycle: tricarboxylic acid cycle

TCA: trichloroacetic acid

TGF- β : transforming growth factor- β

TIMPs: tissue inhibitors of metalloproteinases

TSG-6: tumor necrosis factor-stimulated gene

VCAM: vascular cell adhesion protein

VEGF: vascular endothelial growth factor

$\Delta\psi_m$: mitochondrial membrane potential

Resumen

La medicina regenerativa es una rama de la medicina que se ha desarrollado considerablemente en los últimos años. Su objetivo es reparar o reemplazar un tejido o la función de un órgano mediante la estimulación e inducción de su propia regeneración. En la actualidad, las células madre mesenquimales (MSCs) juegan un papel crucial en las estrategias de reparación o regeneración tisular ya que tienen la capacidad de diferenciarse hacia otros tipos celulares, presentan actividad paracrina y propiedades inmunorreguladoras. Además, la disponibilidad y versatilidad de estas células, junto al hecho de que no existen problemas éticos asociados a su uso ¹⁻³, han permitido su aplicación clínica para el tratamiento de enfermedades asociadas con la inflamación, isquemia o reacciones autoinmunes. Entre los distintos tipos de MSCs, destacan las células madre mesenquimales derivadas de tejido adiposo humanas (hASCs), puesto que son de fácil obtención por procedimientos mínimamente invasivos, mantienen sus propiedades *stem* en cultivo durante más tiempo que otras MSCs y liberan gran variedad de factores que pueden modular la neuroinflamación o el estrés oxidativo ^{4,5}. De hecho, actualmente están recogidos en la base de datos oficial de los Institutos Nacionales de Salud de EE. UU. (www.clinicaltrials.gov) más de 500 ensayos clínicos que utilizan MSCs en diferentes tipos de patologías, entre los cuales cerca de un 20 % emplean las hASCs.

Sin embargo, su actividad terapéutica presenta limitaciones. Entre ellas, destaca el hecho de que, una vez trasplantadas en el tejido dañado, todos los tipos de MSCs, incluidas las hASCs, tienen una baja tasa de supervivencia, debido principalmente a que en el lugar de implantación encuentran unas condiciones ambientales adversas, tales como la deprivación de nutrientes, la inflamación y/o un elevado estrés oxidativo local ^{6,7}.

Cuando se produce estrés oxidativo, ya sea por agotamiento de antioxidantes o por acumulación de especies reactivas de oxígeno (ROS) ⁸, se ocasiona un daño

y disfunción celular que disminuye la viabilidad y la actividad inmunomoduladora de las MSCs injertadas^{9,10}. Para sobrevivir en estas circunstancias, las células han desarrollado diversas estrategias que implican la activación de factores de transcripción, los cuales promueven la síntesis de moléculas responsables de la respuesta antioxidante celular.

Un importante mecanismo celular para reducir el estrés oxidativo es la vía de señalización del elemento de respuesta antioxidante (ARE) del factor 2 relacionado con el factor nuclear E2 (NRF2). El NRF2 es un factor de transcripción que regula la expresión de genes que codifican proteínas antioxidantes, antiinflamatorias y desintoxicantes^{11,12}. En ausencia de estrés, el NRF2 se localiza en el citoplasma, donde interactúa con la proteína de unión a actina, la proteína 1 asociada a ECH tipo Kelch (Keap1), lo que conduce a su ubiquitinación y degradación proteasómica¹³. Sin embargo, en condiciones de estrés oxidativo, el NRF2 se disocia de la Keap1 y se transloca al núcleo, induciendo la transcripción de diversas proteínas, como la hemo-oxigenasa-1 (HO-1), superóxido dismutasa-1 (SOD-1), glutatión peroxidasa-1 (GPx1) y catalasa (CAT), las cuales juegan un papel importante en la protección de las células contra el daño inducido por el estrés oxidativo¹⁴⁻¹⁶. Además de su participación en las respuestas antioxidantes y desintoxicantes, NRF2 también juega un papel importante en la respuesta inflamatoria.

En estudios recientes, se ha observado que, en condiciones de estrés, se produce una comunicación cruzada entre el NRF2 y las vías de señalización del factor nuclear κ B (NF- κ B)¹⁷. El NF- κ B es un factor de transcripción cuya translocación al núcleo inicia la transcripción de moléculas proinflamatorias, incluidas las citocinas como IL-1, IL-6 y TNF- α , la enzima ciclooxigenasa-2 (COX-2) y otras¹⁸. El NRF2 puede activarse por estrés oxidativo o inhibirse por la presencia de agentes antioxidantes. Por lo tanto, la activación del NRF2 evita la sobreproducción de mediadores proinflamatorios, mientras que su supresión se

asocia con un aumento de la expresión del NF- κ B^{19–21}. En definitiva, la interacción entre estas dos vías está estrechamente relacionada con el estado oxidativo / inflamatorio de la célula y, en consecuencia, con su supervivencia.

La supervivencia de los diferentes tipos de MSCs en un entorno oxidativo / inflamatorio conlleva un incremento del gasto de energía, razón por la cual la demanda bioenergética de estas células requiere una adaptación metabólica^{22,23}. La bioenergética desempeña un papel fundamental en la resistencia al estrés ambiental, donde el mantenimiento del equilibrio entre el aporte y el gasto de la energía es un requisito clave para la supervivencia²⁴. Las células obtienen energía libre en forma química a través del catabolismo de las moléculas de nutrientes y utilizan esta energía para producir ATP a partir de ADP + Pi. La hidrólisis de ATP libera energía libre que las células utilizan para mantener importantes funciones, como la síntesis de proteínas y ácidos nucleicos, el transporte de moléculas o iones en contra de un gradiente a través de las membranas, la motilidad celular, la división celular, etc. En las células de mamíferos, las vías de la glicólisis y la fosforilación oxidativa (OXPHOS) proporcionan la mayor parte del ATP celular. Todas las MSCs son células predominantemente glicolíticas pero con capacidad para transitar fácilmente entre la vía de la glicólisis y la vía OXPHOS, adaptándose así a los cambios del microambiente²⁵.

Con el fin de mejorar la resistencia de las MSCs en un entorno oxidativo / inflamatorio, aumentando así la tasa de supervivencia tras la implantación, se han propuesto diferentes estrategias de preconditionamiento celular^{3,26–28}. El proceso de preconditionamiento consiste en una exposición sub-lethal a estresores celulares que promueven la expresión y la secreción de algunas moléculas necesarias para reducir el daño y aumentar la supervivencia, proporcionando a las células la capacidad de responder eficientemente a un nivel más alto del mismo agente inductor de estrés^{29–31}. En un estudio previo,

demostramos que el preacondicionamiento con bajas dosis de H₂O₂ promovió una recuperación más rápida de hASCs tras su criopreservación, lo que mejoró su capacidad de adhesión, migración y supervivencia en entornos de estrés oxidativo³².

En el contexto de estas investigaciones, el presente estudio *in vitro* tiene como objetivos, en primer lugar, evaluar el efecto sobre el comportamiento biológico de las hASCs sometidas a un preacondicionamiento con dosis bajas de H₂O₂ (ver detalles en la patente HC016; WO / 2013/004859, 2013); en segundo lugar, analizar la capacidad de respuesta de las hASCs preacondicionadas (PC-hASCs) ante un microambiente de estrés oxidativo; en tercer lugar, dilucidar los mecanismos moleculares y bioenergéticos que subyacen en el incremento de la resistencia de estas células cuando son sometidas a un microambiente oxidativo; y en cuarto lugar, evaluar la capacidad terapéutica de las células preacondicionadas para reparar el daño oxidativo de otras poblaciones celulares.

En relación al primer objetivo, demostramos que las PC-hASCs, en condiciones de cultivo estándar, no presentan modificaciones significativas en los diferentes parámetros biológicos celulares, tales como la morfología, la senescencia, el ciclo celular o la actividad proliferativa. Sin embargo, en el análisis del perfil proteómico identificamos un 1% de proteínas expresadas de forma diferencial. Aunque este porcentaje no supone una gran variación, la función de las proteínas expresadas diferencialmente aporta información relevante sobre el efecto del preacondicionamiento en dichas células. De este modo, se observa que las funciones de dichas proteínas están principalmente relacionadas con la capacidad antioxidante y el metabolismo energético celular.

En lo relativo al segundo objetivo, evaluamos la supervivencia de las PC-hASCs bajo condiciones de estrés oxidativo. En esta parte del estudio, para inducir el estrés oxidativo se administró H₂O₂ directamente en el medio de cultivo a dos

concentraciones diferentes (0.25 o 0.5 mM). El H₂O₂ permaneció en contacto con las células durante 1 hora, en la cual el H₂O₂ produjo un aumento tiempo- y dosis- dependiente de los niveles de ROS, así como un aumento de la apoptosis y una reducción de la viabilidad celular. Sin embargo, las PC-hASCs toleraron mejor las diferentes concentraciones de H₂O₂, ya que los niveles intracelulares de ROS, la apoptosis y el porcentaje de citotoxicidad se redujeron en comparación con las hASCs no precondicionadas. Esta resistencia al estrés oxidativo inducido fue más evidente cuando se aplicó la concentración de 0.25 mM. Teniendo en cuenta estos resultados y el hecho de que esta concentración es similar a la observada en procesos inflamatorios desencadenados en algunos tejidos ³³, en el resto del estudio experimental se utilizó exclusivamente la concentración de 0.25 mM.

Para llevar a cabo el tercer objetivo, analizamos las vías de señalización implicadas en la resistencia de estas células al estrés oxidativo; en particular, nuestro estudio se centró en la vía del NRF2-ARE. Observamos que, en comparación con los controles, tras recibir un estímulo oxidativo las PC-hASCs muestran una mayor expresión de NRF2 y de las enzimas antioxidantes relacionadas con este factor de transcripción (HO - 1, SOD-1, GPx-1 y CAT).

Debido a la estrecha relación que existe entre el NRF2 y el NF-κB, se estudió también la expresión del NF-κB y las moléculas proinflamatorias COX-2 e IL-1β. Los resultados demostraron que las PC-hASCs sometidas a la acción tóxica del H₂O₂, reducen la expresión del NF-κB, COX-2 e IL-1β, probablemente debido a la sobreexpresión del NRF2 ocasionada por el precondicionamiento. Asimismo, evaluamos la expresión de p-AKT y p-ERK para determinar si estas proteínas de señalización están relacionadas con el incremento de la supervivencia de las PC-hASCs, ya que está descrito que también reaccionan ante la existencia de un estrés oxidativo ³⁴⁻³⁶. Nuestros resultados mostraron que el estrés oxidativo aumenta la expresión de p-AKT, tanto en hASCs como en PC-hASCs, si bien no

se observaron diferencias significativas en la respuesta de ambas poblaciones celulares. Este aumento en la fosforilación de AKT podría estar relacionado con la regulación positiva de las proteínas antiapoptóticas³⁷. Con respecto a ERK, observamos que, tras la estimulación con H₂O₂, se produjo una disminución en su fosforilación, siendo dicha reducción más evidente en las células preacondicionadas, lo que puede atribuirse al aumento de su respuesta antioxidante. Se ha descrito que la inducción de la fosforilación de ERK ante el estrés oxidativo conduce a la activación de NF-κB³⁸; de este modo, estos datos sugieren que, en condiciones de estrés oxidativo, el aumento de la respuesta antioxidante de las PC-hASCs puede atenuar la expresión de p-ERK y, así, reducir la expresión del NF-κB.

Tal y como ocurre con cualquier actividad celular, es lógico pensar que el aumento en la respuesta antioxidante de las PC-hASCs requiere una adaptación previa de su metabolismo energético. Dicha adaptación permitiría proporcionar la energía necesaria para la activación de las vías de señalización, así como para la supervivencia y la proliferación, y finalmente, la adaptación al entorno inmediato. En este trabajo hemos analizado las dos vías metabólicas principales de obtención de energía, la respiración mitocondrial y la glicólisis, tanto en condiciones estándar como oxidativas. Las hASCs utilizan tanto la fosforilación oxidativa como la vía glicolítica, siendo esta última la fuente principal para la generación de ATP³⁹⁻⁴¹. Nuestro estudio confirma estas observaciones, ya que alrededor del 95% de la producción total de ATP de estas células se obtuvo a partir de la glicólisis. Al analizar ambas vías por separado, observamos que, tras el daño ocasionado por el H₂O₂, las PC-hASCs incrementaron 1.8 veces la respiración basal y 1.4 veces la respiración máxima comparadas con las hASCs. En condiciones de estrés oxidativo, las hASCs parecen limitar la actividad mitocondrial en un intento de reducir los niveles intracelulares de ROS. Los ROS son generados por varios orgánulos, entre los cuales las mitocondrias son la principal fuente de oxidantes celulares y, por lo tanto, el lugar principal para la

posible sobreproducción de ROS ⁴². En cambio, las PC-hASCs aumentan la actividad mitocondrial en condiciones de estrés, ya que cuentan con una mayor concentración de antioxidantes que pueden compensar dicho incremento de ROS. Sin embargo, la vía metabólica OXPHOS constituye exclusivamente el 5% del metabolismo de las hASCs, por lo que el estudio de la glicólisis fue necesario para comprender el efecto del precondicionamiento en el metabolismo energético.

Tras la estimulación con 0.25 mM de H₂O₂, observamos que la actividad glicolítica basal disminuyó significativamente. Esta reducción fue más notable en las hASCs, lo que nos llevó a investigar los mecanismos subyacentes que podrían activarse para contrarrestar el estrés oxidativo e incrementar la glicólisis en las PC-hASCs. Por este motivo, analizamos la expresión de HIF-1 α , un factor clave que codifica proteínas relacionadas con la obtención de energía por la vía glicolítica; y pudimos observar un aumento significativo en su expresión en las PC-hASCs con respecto a las hASCs. Este resultado sugiere que el precondicionamiento activa HIF-1 α , lo que aumenta la actividad glicolítica basal, probablemente como un mecanismo para reducir los niveles intracelulares de ROS e incrementar la producción de ATP.

En el cuarto y último objetivo, estudiamos el potencial efecto terapéutico de las PC-hASCs o sus derivados (CM) sobre una población celular de estirpe oligodendroglial sometida a estrés oxidativo.

En esta parte del estudio, utilizamos la línea celular HOG, sobre la que se aplicó un protocolo de diferenciación (cultivo con DMEM con alto contenido de glucosa, suplemento de N2, T3 30 nM y SBF al 0.05%, durante 8 días) con el objetivo de obtener una población de células similares a los oligodendrocitos (HOGd). Tras la diferenciación, las HOGd mostraron proyecciones citoplasmáticas ramificadas y extensiones cortas de membrana, una disminución en la actividad proliferativa y un aumento en la expresión de MBP,

CNPasa y MOG, lo cual se corresponde con los resultados obtenidos por otros autores ⁴³⁻⁴⁶. Una vez que se estableció el protocolo de diferenciación y se obtuvo un cultivo estable de las HOGd, se estudió el efecto del estrés oxidativo en estas células. Así, como modelo de inducción del estrés oxidativo, utilizamos la administración de 0.25 mM H₂O₂, durante 1 hora. Este modelo nos permitió analizar el efecto de la oxidación sobre la viabilidad y proliferación celular, así como sobre los niveles intracelulares de ROS. Como era previsible, el H₂O₂ ocasionó un aumento significativo de los niveles intracelulares de ROS y una disminución de la viabilidad celular.

Una vez analizado el efecto de la oxidación sobre las HOGd, evaluamos el papel terapéutico de las PC-hASCs, tanto a través de su CM como del cocultivo indirecto de ambos tipos celulares. En presencia del CM de hASCs o de PC-hASCs, la población de oligodendrocitos sometida a estrés oxidativo (oxHOGd) recuperó su viabilidad a niveles similares a los de las células control, además de verse reducidos significativamente los niveles intracelulares de ROS a las 48 horas. Sin embargo, este efecto fue más pronunciado cuando las oxHOGd se cocultivaron mediante insertos con las hASCs o PC-hASCs. De hecho, a las 48 horas, los niveles intracelulares de ROS de las oxHOGd se redujeron significativamente y la viabilidad celular superó la del control.

Aunque las dos estrategias, CM y cocultivo indirecto, mostraron efectos reparadores en las oxHOGd, el cocultivo celular indujo una recuperación mayor de las funciones de las oxHOGd que el producido por CM. Estos resultados indican que la presencia de las oxHOGd es necesaria para inducir a las células madre mesenquimales a producir los factores requeridos para la recuperación de las oxHOGd.

Entre los diferentes cocultivos realizados, el constituido por las oxHOGd y las PC-hASCs sometidas a estrés oxidativo obtuvo un incremento mayor de la viabilidad

(1,4 veces mayor que la del control) y una mayor reducción de los niveles de ROS (reducción de 1,3 veces de los valores obtenidos por el control).

Por lo tanto, todos estos datos demuestran que el estrés oxidativo inducido por 0.25 mM de H₂O₂ estimula la respuesta antioxidante de las PC-hASCs, la cual tuvo un efecto beneficioso en la recuperación de las oxHOGd. A continuación, analizamos los mecanismos implicados en dicho efecto; para ello, evaluamos la capacidad antioxidante total y la expresión de proteínas relacionadas con la respuesta antioxidante, tanto en las oxHOGd como en las células mesenquimales. Los resultados sugieren que la sobreexpresión del NRF2, HO-1, SOD-1 y CAT en las PC-hASCs mejoró la recuperación de las oxHOGd al reducir los niveles de ROS y aumentar la viabilidad de estas células. Estos datos muestran que la adaptación al estrés oxidativo es una ventaja fundamental de las PC-hASCs, ya que pone en marcha mecanismos que mejoran su supervivencia y mantienen su funcionalidad tras ser sometidas a un estrés oxidativo adicional, incrementando su capacidad terapéutica.

Finalmente, evaluamos la capacidad migratoria de las células mesenquimales en respuesta a un estímulo quimiotáctico de las oxHOGd, mediante cocultivo indirecto. Nuestros resultados demostraron que las PC-hASCs presentan una capacidad de migración hacia las oxHOGd significativamente mayor que las hASCs control, lo que sugiere que las PC-hASCs pueden responder de manera más eficiente a las señales quimiotácticas presentes en el secretoma de las oxHOGd. Estas diferencias se observaron tanto en condiciones estándar como después de la exposición al H₂O₂, probablemente porque la adaptación al estrés oxidativo hace que las PC-hASCs permanezcan en un estado de alerta que acelera su respuesta a las señales emitidas por las oxHOGd.

En conclusión, este trabajo demuestra que el precondicionamiento de las hASCs con dosis bajas de H₂O₂ mejora su supervivencia y su capacidad de

adaptación a las condiciones de estrés oxidativo a través de dos mecanismos, el incremento de la actividad antioxidante y la plasticidad metabólica.

En condiciones de estrés oxidativo, las PC-hASCs *i*, reducen los niveles intracelulares de ROS al sobreexpresar el factor de transcripción NRF2 y las enzimas antioxidantes HO-1, SOD-1, GPx-1 y CAT; *ii*, disminuyen la secreción de moléculas proinflamatorias COX-2 e IL-1 β al atenuar la expresión de NF- κ B, y *iii*, aumentan la tasa de producción total de ATP, adaptando su metabolismo para satisfacer la demanda bioenergética requerida para sobrevivir.

Por último, las PC-hASCs muestran una mayor capacidad reparadora, como se ha demostrado en un modelo de células oligodendrogiales sometidas a estrés oxidativo, promoviendo la respuesta antioxidante de estas células dañadas.

En conjunto, estos hallazgos indican que las PC-hASCs podrían considerarse un avance importante en la terapia celular, ya que poseen mecanismos que permiten hacer frente a la baja tasa de supervivencia de las células injertadas en un microambiente tisular adverso y de este modo mejorar su eficacia terapéutica.

Summary

In the field of regenerative medicine, it has been pointed out the relevance of human adipose derived stem cells (hASCs) for cell therapy. They can be easily obtained, have low immunogenicity, and secrete soluble factors that could regulate neuroinflammation and oxidative stress. However, their transplantation at the site of injury results in a low percentage of survival and engraftment, mainly due to the harsh microenvironment they encounter. To address this issue, it is imperative to pre-adapt cells, so that they resist harmful environmental factors such as oxidative stress.

In this study, we preconditioned hASCs (PC-hASCs) with low doses of H₂O₂ and evaluated their resistance to an oxidative stress insult. PC-hASCs displayed lower levels of ROS, apoptosis and cytotoxicity than hASCs, indicating their increased capacity to resist to oxidative stress.

In addition, we analyzed the molecular and bioenergetic mechanisms underlying the survival and adaptation of PC-hASCs under oxidative stress. On these conditions, PC-hASCs *i*, reduce intracellular ROS levels by overexpressing the transcription factor NRF2 and their related antioxidant enzymes HO-1, SOD-1, GPx-1, and CAT; *ii*, reduce the secretion of pro-inflammatory molecules COX-2 and IL-1 β by attenuating the expression of NF- κ B, and *iii*, increase the total ATP production rate by adapting their metabolism in order to meet the bioenergetic demand required to survive.

Finally, we evaluated the therapeutic role of PC-hASCs to overcome the deleterious effect of oxidative stress in an oligodendroglial cell population, and proved that PC-hASCs restored cell viability and diminished the intracellular ROS levels of these damaged oligodendrocytes by promoting their antioxidant response.

Summary

Altogether, these findings support that PC-hASCs, given their beneficial advantages, might be considered an important breakthrough in cell-based therapies.

I. Introduction

I.1. Tissue Injury and Regenerative Medicine

Tissue injury, caused by disease, age or trauma, initiates a chemical signaling cascade in the body that, depending on the character or acuteness of the injury, triggers various healing mechanisms. These mechanisms include stimulation of cell proliferation, differentiation and metabolic activity of the tissue, initiation of the inflammatory response, and the recruitment of stem cells into the damaged tissue, where they differentiate to generate specific cells required for healing ⁴⁷.

However, there are several factors that can limit the efficiency of endogenous tissue repair. These limiting factors include the type and extent of the injury, its location, chronic inflammation, oxidative stress or metabolic failure ⁴⁸. Under normal conditions, inflammation's purpose is to minimize the injury, remove the deleterious stimuli, and finally initiate repair and regeneration of damaged tissue in order to restore the homeostasis ⁴⁹. Although inflammation is one of the main defense mechanisms of the body against injury, when uncontrolled or unresolved, can lead to persistent chronic inflammation, excessive tissue damage, and dysregulation of tissue healing. In addition, it may give rise to an array of diseases, such as cardiovascular diseases, atherosclerosis, type 2 diabetes, rheumatoid arthritis, and cancers ⁵⁰. Furthermore, the dysregulated inflammatory process is associated with overproduction of reactive oxygen species (ROS) and reactive nitrogen species (RNS), leading to oxidative stress and activation of different cell signaling pathways ⁵¹. During the inflammatory response, there is an increase in the levels of free radicals, generated mainly as a product of the metabolism of the cells of the immune system. In response to this, the cell's antioxidant systems remove the excess of reactive species and activate genes related to the repair of molecules damaged by oxidative stress. However, if inflammation is chronic, overproduction of ROS/RNS activates

I. Introduction

signaling pathways and create vicious cycles that maintain a high secretion of pro-inflammatory cytokines and chemokines, which also induce the production of ROS/RNS and the impairment of antioxidant systems, leading to an oxidative stress situation ⁵².

Oxidative stress is the consequence of an imbalance between the excessive production of ROS/RNS and the cellular antioxidant capacity. Although low basal levels of ROS/RNS are required to maintain cellular processes such as cell survival, proliferation, and inflammatory signaling, an overproduction causes cellular damage by inducing irreversible functional alterations or even destruction of cellular macromolecules, such as lipids, proteins, carbohydrates, and nucleic acids, resulting in the functional impairment of the cells ⁸ and, therefore, limiting the efficiency of endogenous tissue repair.

Another factor that limits the body's own healing process is the metabolic failure of the cells. Survival in an oxidative/inflammatory environment is an energy-demanding process for any cell, that requires an effective metabolic adaptation to fulfill the bioenergetic demand ^{22,23}. Bioenergetics plays a central role in the tolerance to environmental stress, where a balance between the input and expenditure of energy is a key requirement for survival ²⁴. However, tissue injury is usually characterized by low oxygen tension and nutrient deprivation, which limit the availability of substrates necessary for energy generation, leading to an imbalance between the cell energy demand and the supply needed to maintain homeostasis, resulting in cell death.

These limitations are the reason why the endogenous repair is often inadequate to restore normal function or to prevent disease progression over time and, consequently, they justify the increasing interest in developing exogenous strategies for tissue repair. In this way, regenerative medicine has emerged as a branch of medical science with the potential to heal tissues and organs that have

been injured by aging or disease, on the basis of regeneration principles^{53,54}. Regeneration is a natural process by which damaged tissues or organs are repaired or replaced through the activation of specific renewal mechanisms, resulting in the restoration of their natural function⁵⁵.

Therefore, regenerative medicine is defined as an interdisciplinary area of research that comprises a broad range of biomedical approaches to heal the body *via* stimulation of endogenous cells to repair damaged tissues/organs, or *via* transplantation of cells or engineered tissues to replace the diseased or injured ones^{56,57}. The area of regenerative medicine encompasses several strategies including: *i*, cell therapies; *ii*, gene therapies; and *iii*, tissue engineering (Table 1).

Table 1. Regenerative medicine strategies.

Cell Therapy	is based on the transplantation of specific types of cells or cell products to replace or repair damaged tissue.
Gene Therapy	is a technique that uses genes to treat or prevent disease. Genes can be replaced, added or turned off to help the body to fight or treat disease.
Tissue Engineering	is the combination of cells, biomaterials and biologically active molecules to develop functional tissues to restore, maintain, or improve damaged ones or whole organs.

The central focus of regenerative medicine is human cells. Among them, stem cells play a relevant role given their capability to differentiate into different cell lineages, promote the repair and regeneration of target tissue, and release an array of growth factors and immunomodulatory molecules⁵⁸.

I.2. Stem Cells

Stem cells, present in most multicellular organisms, have three specific properties: *i*, they are capable of dividing and renewing themselves for long periods; *ii*, they are unspecialized; and *iii*, they can give rise to specialized or differentiated cell types⁵⁹ (Fig. 1).

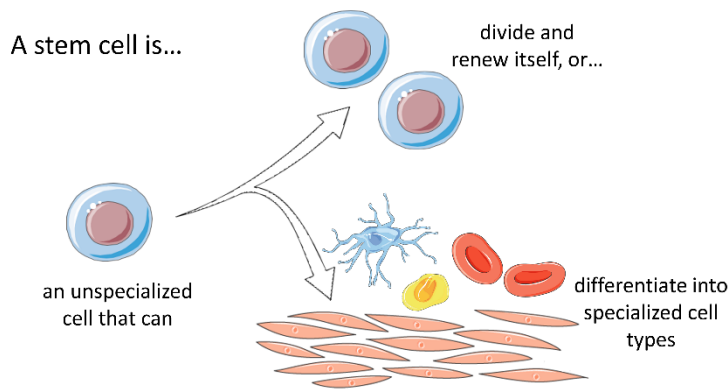


Figure 1. Stem cells properties. Modified from the image prepared by Catherine Twomey for the National Academies, Understanding Stem Cells: Overview of the Science and Issues from the National Academies, <http://www.nationalacademies.org/stemcells>.

I.2.1. Stem Cells Types

Depending on their potential to differentiate to specialized cell types, stem cells can be defined as totipotent, pluripotent or multipotent (Fig. 2).

I.2.1.1. Totipotent Stem Cells

Totipotent stem cells are the least differentiated cells, produced from the fusion of an egg and sperm cell, and are only present until morula stage of development. They can generate an entire functional organism by differentiating into both embryonic and extraembryonic tissues, including the umbilical cord and placenta⁶⁰.

I.2.1.2. Pluripotent Stem Cells

Pluripotent stem cells are one step downstream of totipotent stem cells, having been lost the potential to differentiate into extraembryonic tissues. They can give rise to cells from all three embryonic germ layers: endoderm, ectoderm and mesoderm. Embryonic stem cells (ESCs), isolated from the inner cell mass of mammalian blastocysts, are the best known type of pluripotent stem cells⁶¹⁻⁶³. Another example are the induced pluripotent stem cells (iPSCs), which were generated by reprogramming somatic cells⁶⁴.

Embryonic stem cells (ESCs)

These pluripotent stem cells are isolated from the inner cell mass of the developing blastocyst; they have the potential to produce every cell type in the human body thanks to transcription factors such as Oct4, Sox2 and Nanog⁶⁵. ESCs are also easy to collect, purify and maintain in the laboratory. However, to be used for therapies ESCs would first need to be differentiated into specialized cell types, in order to avoid the risk of creating teratomas. Moreover, the destruction of a human embryo to obtain ESCs poses a legal and moral dilemma, thus slowing down the development of ESCs-based therapies^{66,67}.

Induced pluripotent stem cells (iPSCs)

iPSCs were first generated in 2006 by Shinya Yamanaka's team at Kyoto University (Japan). They reprogrammed mouse embryonic or adult fibroblasts directly into a pluripotent state by introducing four essential factors (Oct3/4, Sox2, c-Myc, and Klf4)⁶⁴ and only one year later, in 2007, human adult fibroblasts were also effectively reprogrammed⁶⁸. These reprogrammed cells displayed similar gene expression, epigenetic profile and differentiation potential as that of ESCs in addition to several advantages. Importantly, iPSCs solved the ethical issue of ESCs because they can be generated without

I. Introduction

destructing embryos. Furthermore, the source of iPSCs can be autologous, so immunosuppression is not necessary for cell transplantation ⁶⁹. Since their discovery, human iPSCs have been widely used for disease modelling, drug discovery and cell therapy development. However, genomic instability can occur at any stage of iPSC generation, which can lead to adverse effects including tumorigenicity ^{70,71}. Therefore, to ensure iPSCs safety prior to potential clinical applications, it is crucial to characterize and classify the possible genomic aberrations acquired during reprogramming.

I.2.1.3. Multipotent Stem Cells

Multipotent stem cells are derivative of either of the three germ layers. Although they are capable of giving rise to multiple cell types, they cannot differentiate into all somatic cell types (like pluripotent stem cells). Therefore, differentiation of multipotent stem cells is restricted to a single germ lineage from which the cells initially originated ⁷² (Table 2). Most adult stem cells are multipotent stem cells.

Table 2. Types of multipotent stem cells depending on their origin.

Germ Layer	Multipotent Stem Cells
Ectoderm	Neural, Dental Pulp, Skin and Ocular Stem Cells
Mesoderm	Mesenchymal, Hematopoietic, Endothelial and Cardiac Stem Cells
Endoderm	Pulmonary, Epithelial, Gastrointestinal Tract, Pancreatic, Hepatic Stem Cells

Adult stem cells

Adult stem cells are undifferentiated cells found in adult organisms; they are capable of self-renewal and give rise to a limited number of mature cell types that divide to replenish dying cells and regenerate damaged tissues ⁷³. Initially they were defined as multipotent cells, however, years later it was observed that some cells were able to differentiate themselves to different lineages ⁷⁴. Some such mesenchymal stem cells (MSCs) are able to differentiate themselves to various cell types, such as cardiomyocytes (mesodermal), hepatocytes (endodermal) and keratinocytes (ectodermal), according to the local microenvironment ⁷⁴⁻⁷⁶.

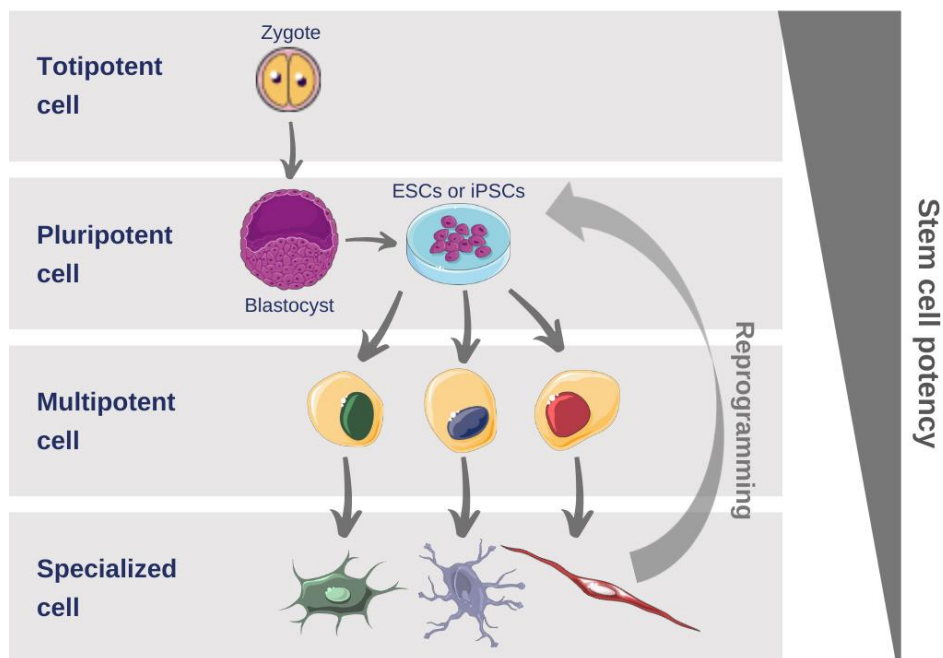


Figure 2. Differentiation potentials of stem cells. Modified from Tewary et al. ⁷⁷.

I.2.2. Stem Cell Research: Then and Now

The promise of using human stem cells for regenerative medicine began in 1956, with the first successful bone marrow transplant performed by Dr. E. Donnall Thomas in Cooperstown (New York) ⁷⁸. Years later, in 1961, Canadian researchers Till and McCulloch demonstrated the existence of multipotent stem cells and offered the first biological definition of stem cells, which included two key characteristics: self-renewal and differentiation capacity ⁷⁹. Since then, scientists have been developing new technologies to extract stem cells from mice, other animals, and then humans. In 1998, Dr. Thomson successfully removed cells from spare embryos at fertility clinics and grew them in the laboratory becoming the first scientist to isolate human ESCs ⁸⁰. Then, in 2006, researchers made another breakthrough by identifying conditions that would allow some specialized adult cells to be genetically "reprogrammed" to a stem cell-like state. This new type of stem cell is now known as iPSCs ⁸¹. Since the generation of iPSCs, stem cell field has expanded incredibly quickly. In 2010, a patient with spinal injury became the first to receive a medical treatment derived from human ESCs as part of a trial by Geron Corporation, a pioneering company for human ESCs therapies, and in 2011 the FDA approved the first MSC-based commercial product (Fig. 3). Stem cell research has now progressed dramatically and there are countless research studies published each year in scientific journals.

A BRIEF HISTORY OF STEM CELLS

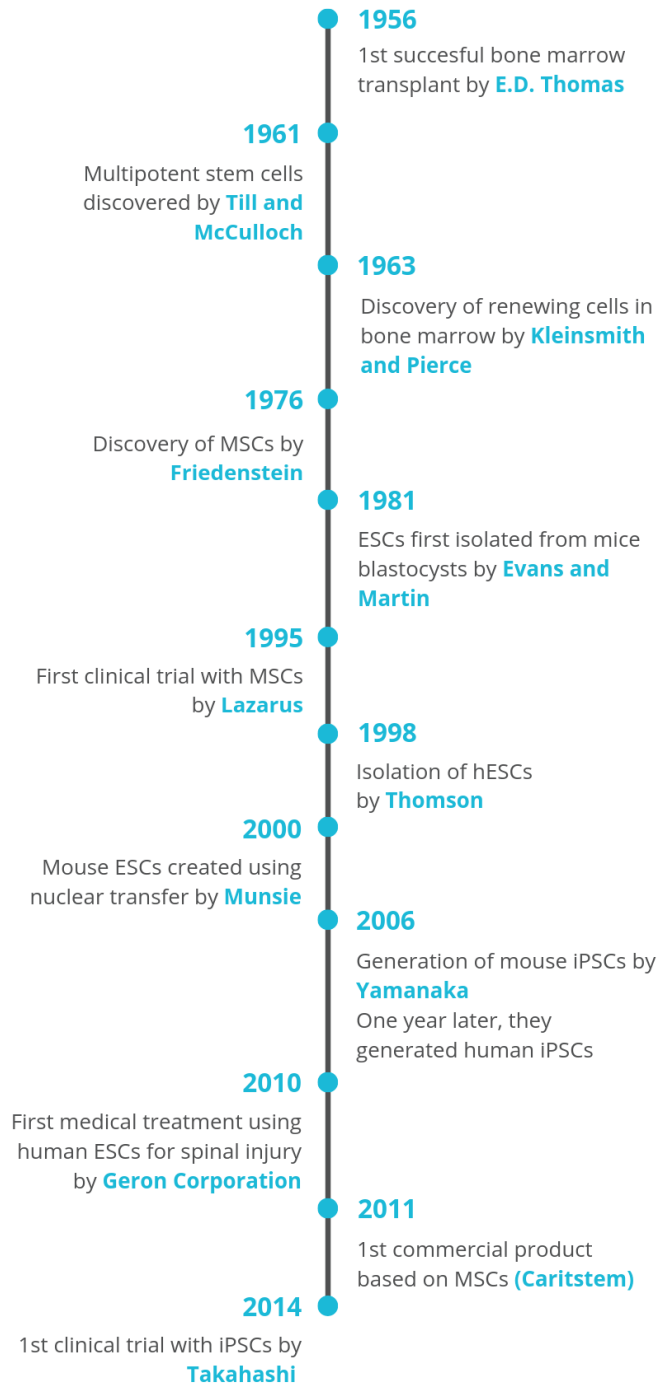


Figure 3. Schematic timeline showing the main discoveries in stem cell research.

I.3. MSCs in Regenerative Medicine

Adult stem cells are already being used to treat many conditions such as heart disease and leukemia, among others^{82,83}. Particularly, MSCs are one of the most commonly employed cell types under investigation. Over the past decade, MSCs have been considered the basis for novel therapeutic approaches for regenerative medicine. The availability and versatility of these cells, together with the fact that there are no ethical issues associated with their use, and their immunomodulatory properties, homing ability, and trophic activities^{1-3,7}, has led to their wide clinical applications in treating conditions associated with inflammation, ischemia, autoimmunity and, trauma. In fact, over 500 active clinical trials utilizing MSCs are now listed at the official database of the US National Institutes of Health (www.clinicaltrials.gov; Fig.4).



Figure 4. Map of the different MSC-based clinical trials ongoing worldwide. Data obtained from www.clinicaltrials.gov, 2019.

MSCs are used in clinical trials for treatment of a variety of diseases. The majority of the ongoing MSC-based clinical trials are focused on treating nervous system diseases (119 clinical trials) followed by cancer (80 clinical trials) and heart and blood diseases (67 clinical trials; Fig. 5). However, researchers still have a long way to go before they completely control the regulation of MSCs.

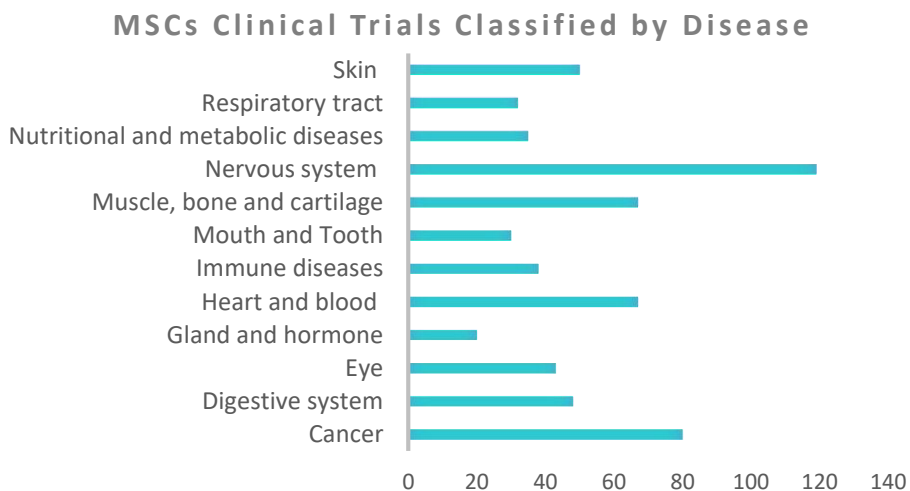


Figure 5. Ongoing MSC-based clinical trials classified by disease. Data obtained from www.clinicaltrials.gov, 2019.

After their initial discovery in bone marrow⁸⁴, MSCs have been isolated from other tissues including umbilical cord, placenta, dental pulp, and adipose tissue^{85–87}. Due to the existence of different MSCs sources and expansion methods, in 2006, the Mesenchymal and Tissue Stem Cell Committee of the International Society for Cellular Therapy (ISCT) proposed the universal minimal criteria for defining MSCs, which includes: *i*, adherence to tissue culture plastic; *ii*, being positive for CD105, CD73 and CD90, and negative for CD45, CD34, CD14 or CD11b, CD79a or CD19 and HLA-DR; and *iii*, the ability to differentiate into osteoblasts, adipocytes and chondroblasts under standard *in vitro* differentiating conditions⁸⁸.

I.3.1. Benefits

The use of human MSCs in cell-based therapy has attracted extensive interest in the field of regenerative medicine due to several superior properties for therapeutic use compared to other types of stem cells.

I.3.1.1. Homing Ability

Homing is the process of MSCs selective migration ability toward the site of injury, and subsequent differentiation into tissue-specific cell phenotypes or exertion of their local effects⁸⁹. Tissue injury microenvironment is characterized by the presence of a wide range of molecular signals, such as growth factors and chemokines that play a key role in MSCs recruitment facilitating trafficking, adhesion and infiltration of MSCs to the injured site. Since MSCs administration can be systemic or site-specific, homing can be divided into systemic and non-systemic⁹⁰. In non-systemic homing, MSCs are transplanted locally at the target tissue where they are guided to the site of injury via a chemokine gradient. In systemic homing, MSCs are administered or endogenously recruited into the circulatory system and then must undergo several steps to exit circulation and migrate to the injury site. Briefly, the process of systemic homing can be split into five steps (Fig. 6)⁹¹:

1. Tethering is facilitated by selectins expressed by endothelial cells. MSCs express CD44, which binds to the selectins, allowing the cells to begin rolling along the vascular endothelium.
2. Activation is triggered by chemokines, generally in response to inflammatory signals. The role of the activation step is to increase the affinity of integrins, which are essential for cell arrest, by inducing conformational changes in their extracellular domains.

3. Cell arrest is facilitated by integrins. MSCs express integrin $\alpha 4\beta 1$ (VLA-4), which become activated in response to chemokines like stromal cell-derived factor (SDF)-1. Following activation, the VLA-4 integrin binds to vascular cell adhesion protein (VCAM)-1 on endothelial cells.
4. Diapedesis or transmigration is accomplished by matrix remodelers. MSCs must transcellularly travel through the endothelial cell layer and basement membrane. To perform this, cells secrete matrix metalloproteinases (MMPs) to break down the endothelial basement membrane. The expression of MMPs is induced by inflammatory cytokines, which serve as a signal for migration into damaged tissue. MMPs maturation and activity are regulated by various other proteins, most prominently the tissue inhibitors of metalloproteinases (TIMPs).
5. Extravascular migration is guided by chemotactic signals released in response to tissue damage. MSCs migrate toward various signals, including the platelet-derived growth factor-AB (PDGF-AB), insulin-like growth factor (IGF)-1, and to a lesser extent, the chemokines RANTES, macrophage-derived chemokine (MDC) and SDF-1.

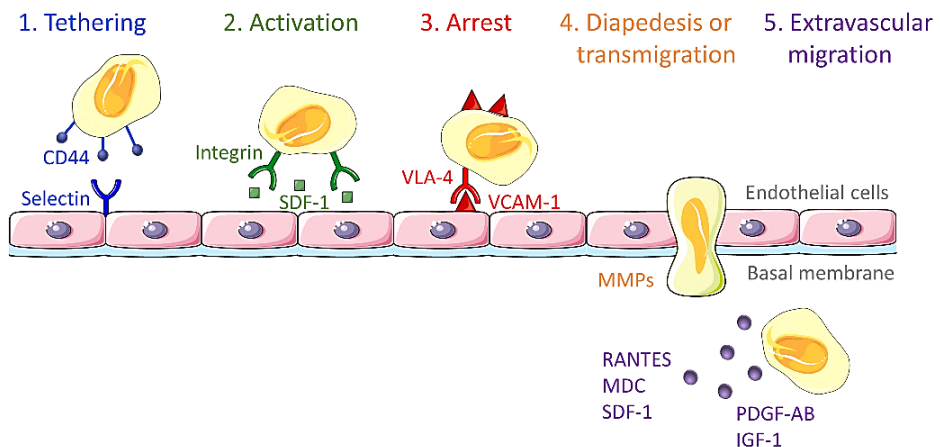


Figure 6. Mesenchymal stem cells homing mechanisms. Modified from Ullah et al. ⁹¹.

I. Introduction

A growing number of studies have documented that systemically infused MSCs can home to the site of injury and exert therapeutic effects. Cho et al. demonstrated that adipose-derived mesenchymal stem cells (ASCs) administered intravenously migrated in higher numbers into the nasal mucosa in an allergic rhinitis mouse model, compared with control mice. These results suggest that immune response to allergens may improve the ASCs recruitment environment at the allergen entry site⁹². Also, xenogeneic bone marrow (BM)-MSCs, delivered intravenously to rats following myocardial infarction (MI), were recruited to the injured myocardium through the bloodstream and improve ventricular function, whereas MSCs delivered intravenously to non-infarcted rats localized to the bone marrow⁹³.

I.3.1.2. Immunomodulatory Properties

MSCs have the ability to modulate the functions of the immune system by interacting with a wide range of immune cells, including T lymphocytes, B lymphocytes, dendritic cells, natural killer cells, neutrophil, and macrophages⁹⁴. Mechanisms of interaction were shown to rely on cell-cell contact along with the secretion of soluble immune factors such as prostaglandin E2 (PGE-2), indoleamine 2,3-dioxygenase (IDO) or nitric oxide (NO)⁹⁵. The immunomodulatory activity of MSCs is, therefore, subject to the concentrations of the inflammatory mediators present in their microenvironment. In fact, depending on the strength of activation of the immune system, the types of released inflammatory cytokines and the effects of immunosuppressants, MSCs can both promote an immune response or suppress it⁹⁶. In essence, the immunoregulatory fate of MSCs is determined by the inflammation status. Several reports have documented this immunomodulatory ability of the MSCs both *in vitro* and *in vivo*. Yañez et al. demonstrated that human ASCs inhibited the proliferation and cytokine secretion of human primary T cells in response to mitogens and allogeneic T cells⁹⁷. Similarly, Corcione et al. showed for the first

time that BM-MSCs inhibit *in vitro* B-cell proliferation, differentiation to antibody-secreting cells and chemotaxis⁹⁸. In addition, BM-MSCs blocked the differentiation of monocytes into dendritic cells and impaired their antigen-presenting ability by arresting monocytes in the G0 phase of the cell cycle, and make them unable to stimulate allogeneic T-cells⁹⁹. Furthermore, Lim et al. demonstrated, in an *in vivo* mouse model of delayed-type hypersensitivity (DTH), that infused MSCs can migrate to the draining lymph nodes and induce T cells apoptosis via NO production, attenuating DTH¹⁰⁰. The immunomodulatory properties of MSCs *in vivo* have become an exciting focus for investigators since the first successful clinical application of MSCs to treat severe acute graft-versus-host disease (GvHD) in a 9-year-old boy¹⁰¹. Patients with other severe immune-related diseases, such as systemic lupus erythematosus and Crohn's disease, have also been successfully treated with MSCs^{102,103}.

I.3.1.3. Antioxidant Properties

MSCs have antioxidant properties and, consequently, the capacity to reduce oxidative stress during inflammation. A major cellular mechanism to reduce oxidative stress is the nuclear factor E2-related factor 2 (NRF2)-antioxidant response element (ARE) signaling pathway. NRF2 is a transcription factor that regulates the expression of genes coding for antioxidant, anti-inflammatory and detoxifying proteins^{11,12}. In the absence of any stress conditions, NRF2 localizes in the cytoplasm where it interacts with the actin binding protein, Kelch-like ECH associating protein 1 (Keap1), leading to its ubiquitination and proteasomal degradation¹³. However, when signals from reactive oxygen species (ROS) target the NRF2-Keap1 complex, NRF2 dissociates from Keap1 and translocates into the nucleus inducing transcription of diverse proteins, such as heme-oxygenase (HO)-1, superoxide dismutase (SOD)-1, glutathione peroxidase (GPx)-1 and catalase (CAT), that play an important role in protecting cells against oxidative stress-induced damage¹⁴⁻¹⁶ (Fig. 7).

I. Introduction

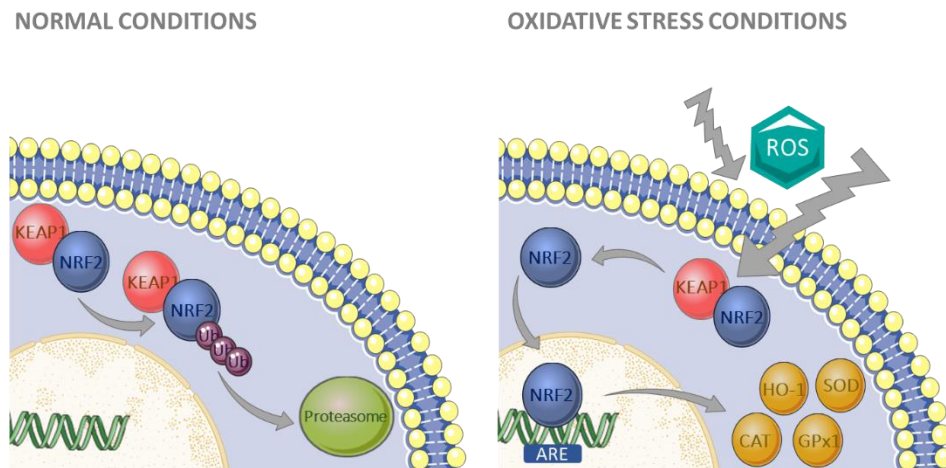


Figure 7. The NRF2-Keap1 signaling pathway. Under normal conditions, NRF2 is constantly ubiquitinated through Keap1 and degraded in the proteasome. Under stress conditions, Keap1 is inactivated, NRF2 translocates into the nucleus and promotes transcriptional activation of antioxidants and detoxification enzymes.

Several studies have demonstrated the antioxidant properties of MSCs. Da Costa et al. found that MSCs played an important role in preventing the impairment of antioxidants defenses in inflamed colon by increasing SOD levels¹⁰⁴. Additionally, BM-MSCs transplantation in diabetic mice increased the expression of HO-1 in the kidney, resulting in an improvement in renal function¹⁰⁵. Nonetheless, Yan et al. showed that GPx1-containing hUC-MSC-Exosomes reduced H₂O₂-induced damage on L02 cells and, rescued liver failure in mice¹⁰⁶.

Moreover, to better understand the effect of MSCs antioxidant properties, various investigations have been performed. Among others, Abdel-Mageed et al. showed that intravenous administration of MSCs genetically modified with extracellular SOD improves survival in irradiated mice¹⁰⁷. Likewise, Mohammadzadeh et al. demonstrated that transient overexpression of NRF2 by adenoviral vectors improved the resistance of the MSCs to an oxidative and apoptotic stimuli¹⁶.

I.3.1.4. Metabolic Plasticity

Another quality of MSCs is their metabolic plasticity. MSCs, *in vivo*, are present in a quiescent state, in which cells remained metabolically healthy but non-proliferative, with reduced levels of RNA and protein synthesis¹⁰⁸. In this state, cells appear to be primarily glycolytic, displaying low levels of mitochondrial activity²⁵. Glycolysis seems to be also the main source of energy during proliferation and self-renewal to maintain the pool of MSCs. However, when MSCs undergo differentiation, they switch from glycolysis to oxidative phosphorylation (OXPHOS), which supplies the energy for this rapid transition (Fig. 8).

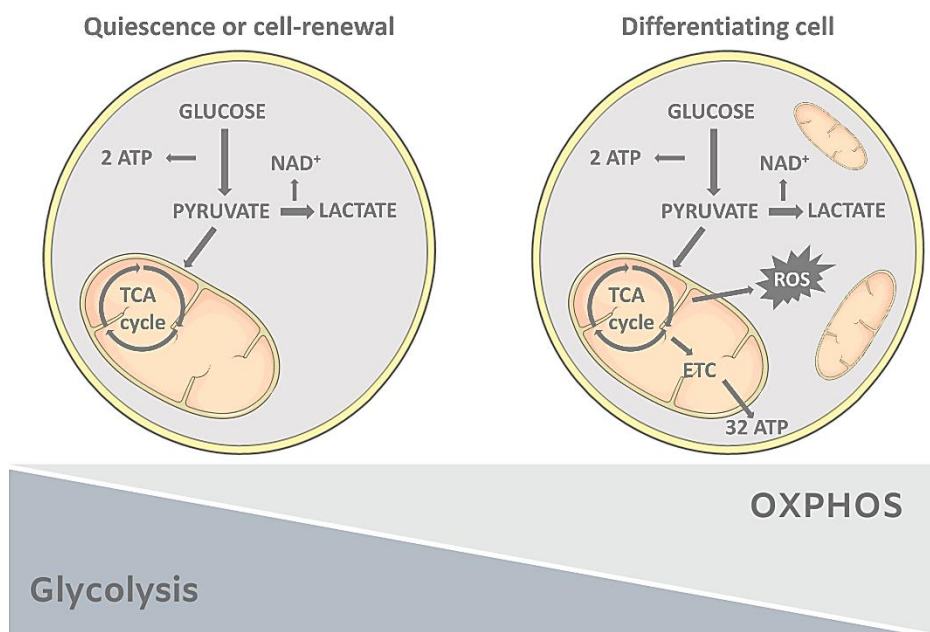


Figure 8. Overview of metabolic features contributing to MSCs maintenance and differentiation.

To enable this metabolic change from a glycolytic phenotype to oxidative phosphorylation, MSCs mitochondria undergo many changes including increase of mitochondrial mass, upregulation of metabolic enzymes in tricarboxylic acid (TCA) cycle, and increased oxygen consumption and ROS¹⁰⁹.

I. Introduction

The changes in cellular metabolism do not merely result from cell differentiation, but can also be required to allow survival under stress conditions. For instance, when subjected to permanent oxygen deprivation, MSCs attenuated cellular ATP levels, reducing mitochondrial ATP production but stimulating glycolytic ATP production, while maintaining cells viability and proliferation¹¹⁰. Furthermore, in an oxidative stress situation MSCs shifted their metabolism from oxidative phosphorylation toward glycolysis to avoid excessive and cytotoxic levels of ROS accumulation, thus ensuring their survival¹¹¹. Therefore, MSCs metabolic plasticity may provide the necessary protection from harsh microenvironments, allowing cells to accomplished their regenerative function.

I.3.1.5. Paracrine Activity

One more characteristic that supports the therapeutic importance of MSCs is their paracrine activity¹¹². Paracrine secretion by MSCs was first identified in 1996 by Haynesworth et al.¹¹³. They reported that MSCs can synthesize and secrete multiple bioactive factors that modulate the action of adjacent cells. These soluble factors include various cytokines such as transforming growth factor- β (TGF- β) and IL-10; growth factors such as vascular endothelial growth factor (VEGF), hepatocyte growth factor (HGF), brain-derived neurotrophic factor (BDNF) and IGF-1; proteins such as angiopoietin-1 (Ang-1), tumor necrosis factor-stimulated gene 6 (TSG-6), and others¹¹⁴. In addition, it has been reported that MSCs also release numerous extracellular vesicles (EVs) that contain miRNA, mRNA and proteins from their cells of origin¹¹⁵ (Fig. 9).

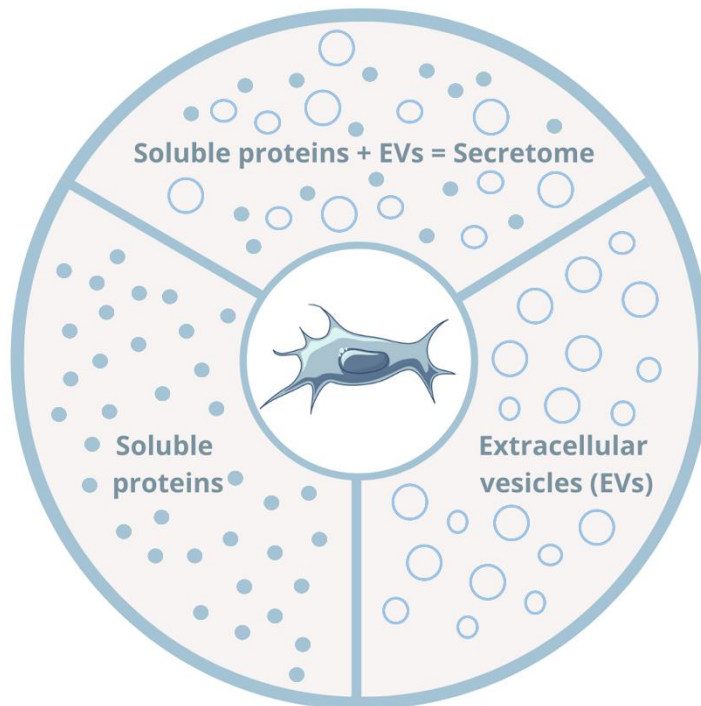


Figure 9. Overview of the MSC secretome. The secretome comprises of soluble proteins and extracellular vesicles. The proteins include biologically active factors such as cytokines, chemokines and growth factors, and the extracellular vesicles include exosomes and microvesicles. Modified from Driscoll et al. ¹¹⁶.

MSCs secretome has demonstrated several biological effects that can: *i*, increase angiogenesis, survival, migration and differentiation; *ii*, reduce apoptosis, fibrosis and oxidative stress; *iii*, restrict local inflammation, and *iv*, adjust immune responses ¹¹⁷ (Table 3). Besides, it can act either directly, by activating the target cells, or indirectly, by stimulating neighboring cells to functionally secrete active mediators ¹¹⁸.

I. Introduction

Table 3. Function of bioactive factors present in MSC-derived secretome.

Function	Bioactive Factors
Angiogenesis	VEGF, HGF, Ang-1, bFGF, IGF-1, PDGF, IL-6, MCP-1
Anti-apoptosis	VEGF, HGF, bFGF, IGF-1, TGF- β , GM-CSF, IL-6
Anti-fibrosis	MMP-2, MMP-9, TIMP-1, HGF, bFGF, Ang-1, KGF
Anti-oxidation	SCT-1, HO-1, TNF- α , IL-1 β , GDNF
Chemo attraction	SDF, HGF, IGF, VEGF, CCLs, CXLs
Proliferation	KGF, FGF-2, VEGF, IGF, PDGF, HGF
Immunomodulation	IDO, PGE2, TGF- β , HGF, TSG-6, LIF, NO, HO-1, IL-6

In addition, MSCs can dynamically change bioactive factors composition in response to various pathologies and environmental stimuli. Thus, depending on the environment or the pathology they face, MSCs generate a specific molecular expression response through the activation of different pathways ¹¹⁹. Several studies have investigated the therapeutic effects of the molecules secreted by MSCs on different disorders, including neurological diseases, liver injury, acute kidney failure and cardiovascular diseases, among others ¹¹⁷. For example, Morigi et al. co-cultured human umbilical cord mesenchymal stem cells (hUC-MSCs) with cisplatin-treated human kidney-2 cells and observed significant increases in hUC-MSCs secreted growth factors such as fibroblast growth factor (FGF), heparin-binding epidermal growth factor-like growth factor (HB-EGF), VEGF and particularly HGF, which create a regenerative environment for tubular repair. Similarly, in an *in vivo* model, they showed a strong increase in HGF with the administration of hUC-MSCs compared with untreated animals ¹²⁰.

Nevertheless, in an experimental model of ulcerative colitis, Yang et al., demonstrated that rat BM-MSCs secretome exert protective effects upon rats colon, by modulating inflammation, suppressing oxidative stress and alleviating apoptosis¹²¹. Moreover, MSC paracrine secretions ameliorated cardiac function via stimulation of neoangiogenesis and suppression of the inflammation response, in both *in vitro* and *in vivo* MI models^{6,122}.

I.3.1.6. Differentiation Capacity

As previously mentioned, MSCs can differentiate into mesodermal lineages, such as osteoblasts, adipocytes, and chondroblasts, under culture conditions containing specific growth factors and chemical agents. Although the preference is for differentiation to these lineages, there is strong experimental evidence demonstrating that MSCs can also differentiate to ectoderm and endoderm lineages¹²³⁻¹²⁵. Under certain defined inducing conditions, Wang et al. differentiated BM-MSCs and ASCs toward a hepatocyte phenotype *in vitro*, which exhibited specific hepatic biochemical functions¹²⁶. Moreover, UC-MSCs can be differentiated into neural-lineage cells and secrete numerous trophic factors that modulate neurogenesis, inflammation, angiogenesis and apoptosis¹²³. Additionally, Choi et al. demonstrated that ASCs can be differentiated into beating cardiomyocytes using direct cell-cell interaction with rat cardiomyocytes¹²⁷.

I.3.2. Limitations

Despite of the aforementioned advantages of MSCs for cell therapy purposes, there are still several challenges for their use in clinical application. A combination of different environmental stresses that MSCs face, both pre and post-transplantation, is probably the cause of many MSC-based therapies failure.

I.3.2.1. Pre- transplantation Limitations

MSCs isolation and expansion methods differ widely between laboratories leading to a variation in their regenerative potential ¹²⁸. Generally, MSCs are isolated by two different methods. On one hand, MSCs are isolated through their ability to adhere to plastic surfaces; however, this method provides heterogeneous cell populations with different lineage commitments resulting in a low purity culture ¹²⁹. On the other hand, MSCs are isolated using mechanical explant approach or proteolytic enzymes, which may impact on their biological properties, influencing their therapeutic potential ¹³⁰. Regarding MSCs expansion, the influence of proteolytic enzymes to detach cells, culture media and storage reagents are relevant aspects that should be considered. Proteolytic enzymes used for cell passaging or tissue digestion could promote extracellular matrix (ECM) protein damage, which may modify the activation of different intracellular signaling pathways. Furthermore, the addition of fetal bovine serum (FBS) to supplement culture media is a controversial issue, due to the not so well characterized components and growth factors present in the serum. Finally, in most cases, expanded MSCs have to be stored frozen until the time of transplantation and the storage condition could alter the quality of the product. For this reason, the optimal freezing and thawing temperature control, cryopreservation media, and long-term storage in liquid nitrogen should be considered ¹³⁰.

Moreover, MSCs are heterogeneous population whose biological effectiveness and phenotype may vary depending on the tissue source or donors age. The function of MSCs is known to decline with age, a process that is called senescence. This phenomenon was first described in the 1960s by Leonard Hayflick ¹³¹. The classic features characterizing the senescence phenotype of MSCs include growth arrest in the G1 phase of the cell cycle, enlarged or flattened morphology, increased expression of senescence-associated β -

galactosidase (SA- β -gal) and senescence-associated lysosomal α -L-fucosidase (SA- α -Fuc), and surface marker alteration ¹³². The process of MSC senescence depends mainly on the source of MSCs. Several authors have demonstrated that BM-MSCs become senescent at much earlier passages during subculturing compared with ASCs and UC-MSCs ^{133–135}.

MSCs can be found in many tissues and organs in the body, but in very low numbers, and must be expanded *ex vivo* in order to obtain the required amount for therapeutic applications. This progressive passaging *in vitro* to obtain the optimal concentration of cells and the culture conditions, can lead them towards a senescent state, in which proliferation, the level of certain surface antigens (CD13, CD29 and CD44) and the ability to suppress T cell proliferation decreases, whereas oxidative stress increases ^{9,136}. Moreover, senescent MSCs negatively influence neighboring cells by secreting soluble factors, termed “*senescence-associated secretory phenotype (SASP)*”, that elicit high production of proinflammatory cytokines (IL-1, IL-6 and IL-8) and resulting in tissue homeostasis impairment, which decreases MSCs therapeutic potential ¹³⁷ (Fig. 10).

In addition, ROS imbalance and the subsequent oxidative stress can also trigger or increase the process of senescence due to its contribution to DNA and protein damage, as well as mitochondrial dysfunction and secretory phenotype modification ^{136,138}. For these reasons, the analysis of *in vitro* senescence in MSC is essential for therapeutic applications. Therefore, it would be necessary to monitor the appearance of a senescent phenotype and to evaluate its functional consequences, taking into consideration their differentiation potential, immunomodulation, homing and paracrine activity ¹³⁹.

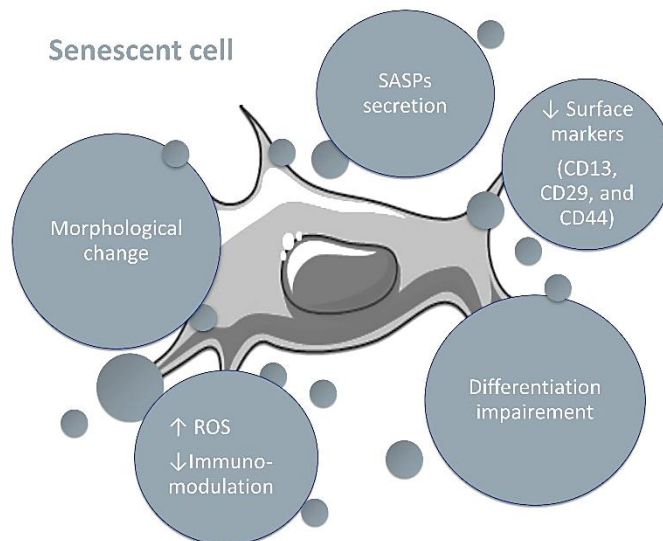


Figure 10. Overview of senescence in MSCs. MSC senescence is characterized by an irreversible cell cycle arrest, a change in morphology and an impairment in differentiation ability. In addition, senescent cells secrete SASPs, decrease the level of certain surface antigens (CD13, CD29 and CD44) and increase the levels of ROS.

I.3.2.2. Post-transplantation limitations

Another challenge MSCs face is the poor engraftment post-transplantation. Around 99% of grafted cells usually die within the first few days after administration, mainly due to the harsh microenvironment they encounter upon transplant ^{7,140}.

Given that MSC-based therapy is focused on the treatment of different diseases or trauma, administration sites often presented an inflammatory response situation characterized by oxidative stress and an increase in the release of chemokines or cytokines to the blood flow ¹⁴¹, promoting the migration of inflammatory cells such as neutrophils, monocytes, and macrophages to the injury area. These inflammatory cells produce high levels of ROS, which create an inflammatory/oxidative vicious cycle and thus metabolic dysregulation, apoptosis, as well as inactivation of the cytoprotective production of NO ^{142,143}.

Additionally, the overproduction of ROS can also be responsible for preventing cell adhesion of grafted cells, leading to anoikis¹⁴⁴. Anoikis is a form of programmed cell death induced by the loss of attachment to the ECM and neighboring cells, which initiates the apoptotic signaling cascade¹⁴⁵. Cell-cell adhesion through the ECM plays an important role in differentiation, survival, and proliferation. When MSCs are attached to ECM, the cells receive active survival signals mediated by the ECM receptors, the integrins¹⁴⁶. However, some cellular stress events such as inflammation or oxidative stress, are known to negatively affect integrin attachment and therefore, induce the death of the transplanted MSCs by anoikis^{147,148}. As aforementioned, MSCs have anti-oxidative stress properties as they can activate the NRF2-ARE signaling pathway, which makes a substantial contribution to ROS reduction. However, in pathological conditions, such as neurodegenerative diseases, MSCs antioxidant systems can be overwhelmed, leading to poor antioxidant defense⁸. Last but not least, harsh environmental signals induce dynamic changes in MSCs metabolism, which not only provides energy and substrates for cell survival and proliferation but also regulates cellular functions, such as secretory profiles and immune responses²³. To survive and keep their functions, MSCs must align their bioenergetic demand with available energy resources post-implantation. However, sometimes, metabolic plasticity is not sufficient to meet the energy demand and cells die.

I.3.3. Strategies to Overcome Limitations

Optimization of MSC culture conditions, gene modification and preconditioning are key strategies to improve MSC function *in vitro* and *in vivo*. All of these procedures can contribute to improve MSC transplantation efficacy in regenerative medicine along with a proper thawing procedure, route of delivery and dosing of MSCs to the site of injury¹²⁸.

I.3.3.1. Optimization of MSCs culture

Identification of optimal culture conditions is a prerequisite for MSC clinical applications. Traditionally, basal culture media supplemented with growth factors, proteins and enzymes was used to support cell growth during MSCs *ex vivo* expansion. One of the most commonly used supplements in MSCs culture is FBS, because it is enriched with growth factors and is poor in antibodies. However, the use of animal derived products such as FBS for the development of hMSC, especially in clinical-scale manufacturing, has been discouraged, considering the risk of zoonoses and xenogeneic immune reactions ¹⁴⁹. Consequently, alternatives to FBS have arisen, including human platelet-derivatives (HPD) and chemically-defined media (CDM) ¹⁵⁰.

Human platelet-derivatives (HPD)

HPD are attractive supplements for cell culture, since platelets alleviates the immunologic risk of FBS and contain high concentrations of physiological growth factors, such as platelet-derived growth factor (PDGF) and basic fibroblast growth factor (bFGF), which have been shown to enhance proliferation of MSC ^{149,151}. HPD may be used as autologous or 'pooled' products. Autologous products eliminate the risk of disease transmission, although their effects are highly dependent on the donor and method of platelet isolation, and large volumes are difficult to obtain. The use of autologous products may therefore be limited to applications when small numbers of MSC are needed. Alternatively, 'pooled' products can provide larger volumes of concentrates, and also reduce donor-based variations, which make them more appealing for experiments that require more standardized culture conditions ^{150,152}.

Besides the large quantities of growth factors, HPD also contains a plethora of potent substances including lysosomal enzymes, coagulation factors,

immunologic and adhesion molecules, and chemokines that are involved in important cellular processes, such as hemostasis, host defense, angiogenesis and tissue repair ¹⁵³.

Chemically-defined media (CDM)

To avoid the risks of pathogen transmission and the difficulty of standardized preparation of human serum-derived supplements, synthetic serum-free CDM have been developed. CDM is a protein-free basal medium containing low-molecular-weight components, synthetic peptides or hormones, and a few recombinant or synthetic versions of proteins. CDM is usually supplemented with recombinant human growth factors-combinations (PDGF, FGF, TGF- β , EGF, among others) that can influence cellular responses, the concentration and nature of growth factors released, and the clinical outcomes ¹⁵⁴.

Several studies have investigated the effect of these alternatives to FBS. HPD have demonstrated to be important for MSCs proliferation ¹⁵⁵⁻¹⁵⁷, differentiation ^{158,159}, cytokines secretion ^{160,161} and migration ¹⁶². Furthermore, HPD-cultured cells have already been used in the clinic. In fact, they have been used for treatment of GvHD (NCT01764100) and for lumbar intervertebral degenerative disc disease (NCT01513694). Regarding CDM, Wu et al. showed that their chemically defined medium could stimulate the proliferative and self-renewal capacity of UC-MSCs ¹⁶³. In the same way, Lee et al. stated that their CDM, termed STK2, has many advantages through which it is possible to obtain safer, superior and larger numbers of MSCs. In fact, MSCs cultured in STK2 exhibited a reduced senescence rate, small and homogenous cell size, and were more genetically stable compared to those cultured in DMEM with FBS. Further to this, secretome analysis showed that the expression of factors related to proliferation/migration, anti-inflammation and differentiation were increased in STK2 culture medium compared to control medium ¹⁶⁴. Unfortunately, many

of the commercially available chemically-defined FBS replacements or serum-free media still need improvement with regard to the performance and the cost, compared to FBS ¹⁶⁵.

I.3.3.2. Gene Modification

Genetic modification of MSCs aims to upgrade their properties, such as viability, homing, immunomodulation or growth factor production to improve their efficacy in regenerative medicine applications. MSCs can be genetically modified by viral and non-viral methods.

Viral methods can efficiently transduce MSCs with vectors such as retrovirus, lentivirus, baculovirus and adeno-associated virus (AAV), without affecting their stem cell properties ¹⁶⁶. To insert new genetic information into a host organism or alter its preexisting genetic material, viruses are generally modified in order to become replication incompetent with attenuated cytopathic effects and immunogenicity ^{167,168}. Usually, the insertion of the target gene into the host genome is random, however, nowadays can be ameliorated by cutting/inserting specific sequence using ZFN or CRISPR/Cas9 system ¹⁶⁹. Viral methods, while highly efficient, are limited by safety issues, have a relatively small transgene cargo capacity, and present difficulty in production and scale-up.

Non-viral methods of gene transfer are safer than viral ones, are able to deliver larger transgenes and are easier to scale up, but are less efficient due to their low transfection efficiency and transient gene expression. Current methods used to transfect MSC can be divided into physical methods and chemical methods. Physical methods include electroporation, nucleofection and sonoporation, whereas chemical methods include the use of lipid agents, polymeric carriers, dendrimers and inorganic nanoparticles ¹⁶⁶.

Several genetic approaches have been used to improve MSC survival and properties. For example, Mangi et al. demonstrated that Akt-engineered MSCs were more resistant to apoptosis and could enhance cardiac repair after transplantation into the ischemic rat heart ¹⁷⁰. Similarly, MSCs infected with adenovirus vector harboring the HO-1 gene (Ad-hHO-1) normalized the balance between MMPs and TIMPs, after MI, resulting in reversing myocardial extracellular remodeling and enhancing angiogenesis ^{171,172}. Furthermore, genetically engineered MSCs to overexpress NRF2 enhance their survival and resistance to oxidative stress, upregulating SOD-1, SOD-2 and HO-1 expression ¹⁶. In addition, MSCs genetically modified to overexpress HGF or VEGF ameliorated acute renal damage by reducing inflammation and apoptosis ^{173,174}. Currently, most studies of modified MSCs are pre-clinical and, although they showed enhanced therapeutic efficacy, there is no clinical data to support further applications.

I.3.3.3. Preconditioning

MSCs preconditioning is one of the main strategies to improve MSCs adaptability and thus survival in harsh microenvironments. Preconditioning is based on the biological concept of *hormesis*, which is an adaptive response of cells and organisms to stress ¹⁷⁵. Therefore, preconditioning process is the exposure of the cells to sub-lethal stressors in order to promote the expression and the secretion of some molecules that are required to reduce damage and increase survival, providing cells the capacity to respond efficiently to a higher level of the same stressor ²⁹⁻³¹ (Fig. 11). Lately, several studies have proved that preconditioned MSCs present better cell survival, increased differentiation efficacy, enhanced paracrine effects and improved homing ability into injury sites ^{29,176-178}.

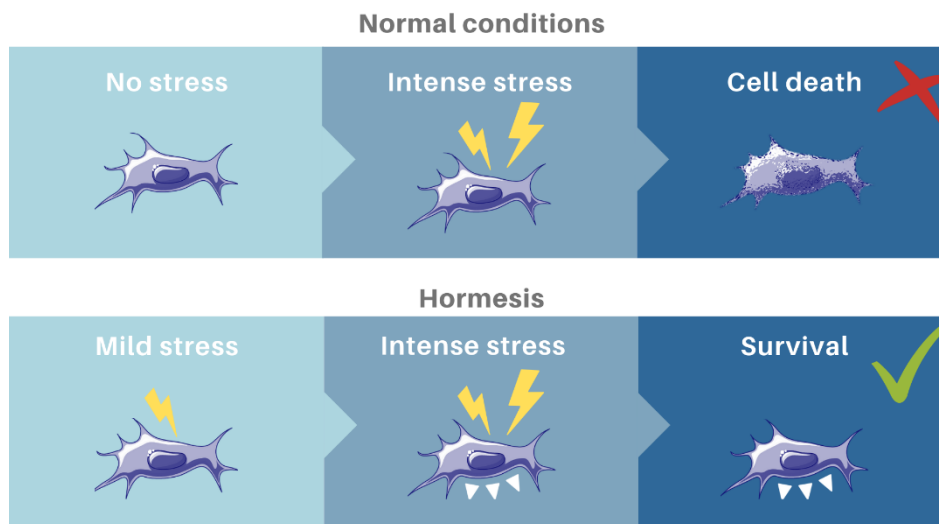


Figure 11. *Hormesis* concept. In normal conditions cells exposed to an intense stress undergo cell death. However, cells preconditioned with mild stress can become resistant to subsequent intense stresses. This process is called hormesis: an adaptive behavior that is crucial for survival in a stress environment.

Preconditioning of MSCs includes *in vitro* exposure to hypoxic conditions, deprivation of nutrients and exposure to hydrogen peroxide (H_2O_2), among others.

Hypoxic Preconditioning

Hypoxia is a condition in which the oxygen levels supplied to one or more tissues in the body are severely reduced¹⁷⁹. This condition is a crucial physiological and pathological phenomenon that regulates a wide range of cellular processes. MSCs usually reside in hypoxic niches. The two niches in the body where MSCs can be found in most abundance, the bone marrow and the adipose tissue, have an O_2 concentration between 1%-7% and 10%-15%, respectively¹⁸⁰. During the transplantation procedure, MSCs are exposed to different O_2 concentrations, considering that *ex vivo* expansion is generally conducted in a 20-21% O_2

atmosphere, and the transplant site is characterized by a hypoxic/anoxic microenvironment due to poor vascularization¹⁸¹. Therefore, it has been suggested that preconditioning with hypoxia prior to cell transplantation would allow a better cell adaptation to lower oxygen level at injury site ¹⁸². Accumulating evidence has shown that hypoxic preconditioning of MSCs promotes cell survival, proliferation, migration, angiogenesis and cell engraftment ^{28,183–189}.

Nutrient Deprivation Preconditioning

Another way of preconditioning, which is not as commonly used as hypoxic one, is the nutrient deprivation preconditioning. Under *in vitro* conditions, MSCs culture media contain amino acids, vitamins, inorganic salts, glucose and serum, which promotes their proliferation and metabolism. Nonetheless, MSCs transplanted into the injured site, encounter a microenvironment characterized by poor nutrient support. Cells obtain free energy in chemical form through the catabolism of nutrient molecules and use this energy to produce ATP from ADP + Pi. ATP is used in endergonic processes, such as the synthesis of metabolic intermediates and macromolecules, and its intracellular loss results in cell necrosis or apoptosis ^{190,191}. For this reason, a prior adaptation to a limited-nutrients situation might be helpful for increasing the survival rate of MSCs upon implantation. For example, Moya et al. demonstrated that 48 hours of serum-deprivation preconditioning protected human MSCs (hMSCs) against a harmful ischemic environment by inducing hMSCs quiescence ¹⁹². Quiescence is characterized by exit from the cell cycle, reducing the cell metabolic rate. The quiescent state is critical for MSCs in order to maintain stem cell potency and function during tissue homeostasis, and tissue repair in the event of an injury ¹⁹³.

Oxidative Stress Preconditioning

Generally, MSCs are isolated from environments without oxidative stress, hence, they lack of mechanisms strong enough to counteract excessive ROS production. For this reason, when transplanted into the site of injury, the presence of high oxidative stress damage MSCs activity, thus reducing their survival rate and limiting their clinical applications. Therefore, since one of the main reasons why MSCs die following engraftment is ROS-mediated-oxidative stress ²⁶, several studies have already focused on the beneficial effect of preconditioning cells with sub-lethal doses of H₂O₂ [1-100 μM]. For instance, preconditioned hUC-MSCs were more resistant to oxidative damage induced by high-concentration H₂O₂ exposure than their control, which showed a significantly reduced number of cells compared to the preconditioned group ¹⁹⁴. H₂O₂ preconditioning also protected rat BM-MSCs against *in vitro* apoptosis ¹⁹⁵. In the same way, it has been described that preconditioned human Wharton jelly-MSCs increase survival after exposure to toxic levels of H₂O₂ by overexpression of HIF-1α protein ¹⁹⁶. In addition, we previously have reported that H₂O₂ preconditioning provided hASCs a significantly faster recovery capacity post-thaw maintaining cell functionality ³². However, the exact mechanisms underlying oxidative stress preconditioning remain to be fully understood. In the current study, we evaluated the preconditioning effect of low doses (10 μM) of H₂O₂ on hASCs behavior, thus elucidating bioenergetic and molecular mechanisms underpinning the survival and adaptation of these cells in an oxidative stress environment, and their reparative capacity.

II. Hypothesis and Aims

The **hypothesis** underlying this work is that H₂O₂ preconditioning provides hASCs a higher resistance to oxidative stress and improves their therapeutic capacity through an enhancement in their antioxidant response and the adaptation of their energetic metabolism.

To validate our hypothesis, we proposed the following **aims**:

1. To evaluate the influence of H₂O₂ preconditioning on hASCs status.
2. To analyze the resistance of PC-hASCs to oxidative stress and compare it with that of hASCs.
3. To elucidate the molecular and bioenergetic mechanisms underlying the increase of survival and the adaptation of PC-hASCs to oxidative stress.
4. To assess the therapeutic effect of PC-hASCs and their conditioned media on a model of oligodendroglial cells exposed to oxidative stress.

III. Chapter 1

Evaluation of the influence of the preconditioning on hASC cellular status and analysis of its cytoprotective effect on hASCs subjected to oxidative stress

Over the last decades, MSCs have been broadly used in cell therapy because of their immunomodulatory and anti-inflammatory properties, and their well-documented cytoprotective and reparative effects ¹⁹⁷⁻¹⁹⁹. In addition, there is evidence that compared to other types of stem cells, hASCs present several advantages. Thus, they can be easily harvested from adipose tissue by a minimally invasive method, retained stem cell phenotypes and pluripotency at higher passages and display a greater proliferation capacity and low immunogenicity ^{4,5}. Moreover, hASCs exert a therapeutic effect on other cell types, largely due to their paracrine activity ¹ and, under stress situations, they increase this activity and condition the culture medium, releasing a large number of bioactive factors ¹⁷⁸. However, their transplantation results in a low survival rate and engraftment, mainly due to harsh environmental conditions such as nutrient deprivation, inflammation and oxidative stress ^{7,140}.

As a means to upgrade hASCs adaptability to harsh environments, thus increasing the survival rate upon implantation, cell preconditioning strategies have been proposed ^{3,26-28}. Since one of the main reasons why MSCs die following engraftment is ROS-mediated-oxidative stress, **the present *in vitro* study aimed to evaluate the influence of preconditioning with low doses of H₂O₂ on the hASCs behavior.**

III.1. Materials and methods

III.1.1. Cell culture

Human ASCs were kindly donated by Histocell S.L. (Science and Technology Park of Bizkaia, Spain). hASCs were expanded in monolayer on 636 cm² tissue culture flask (Corning, Tewksbury, MA, USA) in DMEM Glutamax™ (Dulbecco's Modified Eagle Medium, Gibco, Paisley, UK) supplemented with gentamicin (1 µl/ml, Sigma-Aldrich, St. Louis, MO, USA) and a 10% of heat-inactivated fetal bovine serum (FBS, Biochrom, Berlin, Germany), and incubated at 37 °C, in a saturated humidity atmosphere containing 5% CO₂. Culture medium was changed every other day and the cells were subcultured with trypsin-EDTA 0.05% (Gibco, Paisley, UK) after reaching 80% of confluency (Fig. 12).

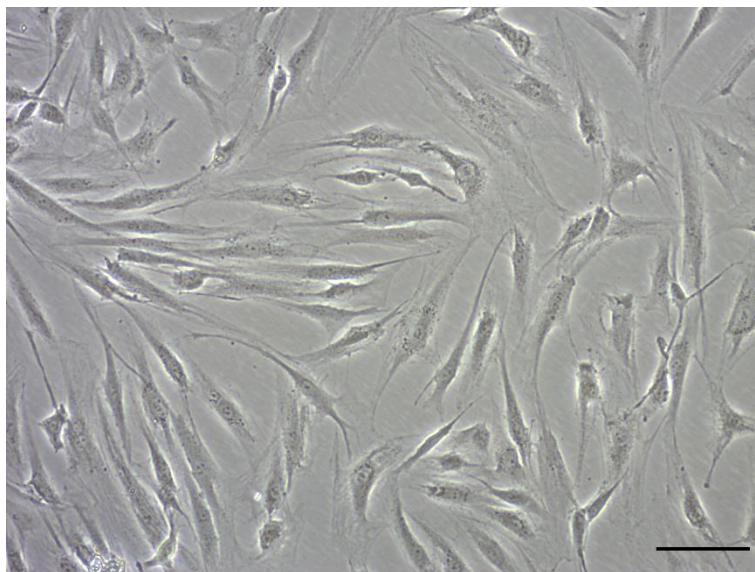


Figure 12. Phase contrast microscopy image of 80% confluent hASCs culture (scale bar: 100 µm).

For subculturing, the spent media was carefully aspirated without disturbing the monolayer and the cells were rinsed once with 1x phosphate-buffered saline (PBS, Sigma-Aldrich, St Louis, MO, USA) to eliminate traces of serum. Then, 20

ml of trypsin-EDTA 0.05% were added to the culture for 5 minutes at 37 °C and 5% CO₂ until the cell layer was dispersed. The cell suspension was centrifuged at 250 g, for 5 minutes at 4 °C. The resulting pellet was gently resuspended in DMEM Glutamax™ containing 10 % FBS, until the suspension appeared homogenous. Finally, the cells were counted using a hemocytometer and 3x10³ cells per cm² were seeded in a tissue culture flask. Cells were passaged serially when they reached confluence until passage 3 (P3).

III.1.2. hASCs H₂O₂-preconditioning

To obtain H₂O₂-preconditioned hASCs (PC-hASCs), long term exposure to low concentration of H₂O₂ (PanReac AppliChem, Barcelona, Spain) was applied (see details in HC016 patent; WO/2013/004859, 2013). Briefly, hASCs were exposed to 10 μM of H₂O₂ for 7 days with refreshment of oxidative culture media twice until the end of the preconditioning protocol. Non-preconditioned hASCs were cultured in parallel for the same number of passages. Once the preconditioning process was completed, PC-hASCs and hASCs were seeded at high density, and incubated at 37 °C in a humidified 5% CO₂ atmosphere for 18-20 hours in complete medium, until the beginning of the experiments.

III.1.3. Senescence, cell cycle analysis and proliferation rate

To determine if preconditioning affected senescence, cell cycle or proliferation, hASCs and PC-hASCs were evaluated in standard conditions (no oxidative stress induction) 18-20 hours after the preconditioning process.

III.1.3.1. Senescence Assay

Senescence was assessed with the Senescence Cells Histochemical Staining Kit (Sigma-Aldrich, St Louis, MO, USA). This assay is based on a histochemical stain for β-galactosidase activity, which is detectable in senescent cells, but not in quiescent, immortal, or tumor cells. The assay was performed according to the

manufacturer instructions. Briefly, cells cultured in 24 well plates (Sarstedt, Nümbrecht, Germany) were washed with 1x PBS, fixed for 3-5 minutes with the fixation solution at room temperature (RT), washed, and incubated overnight (o/n) at 37 °C (no CO₂) with a freshly prepared staining solution containing β -galactosidase. Following incubation, percentages of β -galactosidase positive cells (blue stained) were calculated with phase contrast microscopy (Nikon, ECLIPSE TS 100, Tokio, Japan) with the 10x objective. Results were expressed as the means \pm SD of at least three independent experiments ($n \geq 3$).

III.1.3.2. Cell cycle analysis

The cell cycle analysis of hASCs and PC-hASCs was determined by staining the DNA with a fluorescent dye (propidium iodide, PI, Life Technologies, Eugene, OR, USA) and measuring its intensity by flow cytometry (λ_{ex} 488; λ_{em} 617nm). The PI intercalates into the major groove of double-stranded DNA producing a highly fluorescent signal. Besides, the PI binds in proportion to the amount of DNA present in the cell, which allows to determine the percentage of the population in G0/G1, S, and G2/M. For this method, hASCs and PC-hASCs were harvested and fixed with 70% methanol (PanReac AppliChem, Barcelona, Spain) for 2 hours at -20 °C. Following fixation, cells were washed with 1x PBS and resuspended to a final concentration of 10⁶ cells/mL. Cell suspension was incubated with PI (5 $\mu\text{g/mL}$), and RNase A (10 $\mu\text{g/mL}$, Roche, Mannheim, Germany) to increase specificity of DNA staining, during 30 minutes at 4 °C. Stained cells, at least 1x10⁴ events/sample, were analyzed in a flow cytometer (Gallios, Beckman Coulter, Indianapolis, IN, USA). Histograms were representative of three independent experiments.

III.1.3.3. Proliferation rate assay

Proliferation rate was assessed by viable cells quantification at different time points (0, 24 and 48 hours) with PrestoBlue® (Invitrogen, Eugene, OR, USA), a resazurin-based solution that functions as a colorimetric cell viability indicator.

Cells were cultured in 96 well plates (Sarstedt, Nümbrecht, Germany) at a density of 4×10^3 cells/well in 100 μ l of complete culture medium. At each time points, PrestoBlue[®] reagent was added to the cells following manufacturer instructions. The optical density (OD) was measured at λ 570 and λ 600 nm in a spectrophotometer (Biotek, Synergy HT, Winooski, VT, USA). Results were normalized to cell number at 0 hours and expressed as the means \pm SD of at least three independent experiments performed in quintuplicates.

III.1.4. Proteomic profile analysis

Protein isolation and digestion

hASCs and PC-hASCs (5×10^6 cells/condition) were resuspended in 300 μ l of SDT lysis solution (4% sodium dodecyl; SDS, Sigma Aldrich, St. Louis, MO, USA), 100 mM dithiothreitol (DTT, Sigma Aldrich, St. Louis, MO, USA); 100 mM Tris-HCl pH 7.6) and mixed vigorously for one minute. In order to reduce the viscosity, the samples were sonicated for 3 minutes and then, incubated at 95 °C for 5 minutes. Finally, the extracts were centrifuged at 16×10^3 g for 10 minutes at 20 °C and the supernatant was transferred to a 1.5 ml Eppendorf tube.

Afterwards, protein concentrations were estimated using BCA[™] Protein Assay Kit – Reducing Agent Compatible (Thermo Fisher Scientific, Eugene, OR, USA) and digested with the FASP (Filter-Aided Sample Preparation) method²⁰⁰. Briefly, 100 μ g of proteins were mixed with 200 μ l of UA solution (8 M urea, 100 mM Tris-HCl pH 7.6) in Amicon Ultra-0.5 Centrifugal Filter Unit with Ultracel-30 membrane (EMD Millipore, Darmstadt, Germany) and centrifuged at 14×10^3 g for 15 minutes at 20 °C. This step was repeated twice. Then, the samples were incubated in the filters with 100 μ l of 50 mM iodoacetamide in UA solution at RT for 20 minutes in darkness. The filters were washed three times with 200 μ l of UA solution, followed by three washes with 50 mM ammonium bicarbonate. For the digestion, samples were incubated for 16 hours at 37 °C in 1:50 dilution

of trypsin (Roche, Mannheim, Germany) in 50 mM ammonium bicarbonate. After the incubation, the peptides were collected by centrifugation and the filter was washed with 50 μ L of 50 mM ammonium bicarbonate.

From the 100 μ g of digested protein of every sample, 25 μ g were desalted by C-18 Micro SpinColumn™ (Harvard Apparatus, Holliston, MA, USA). Ultimately, samples were desiccated in SPD121P SpeedVac (Thermo Fisher Scientific, Eugene, OR, USA), and stored at -20 °C until used.

Liquid chromatography tandem-mass spectrometry (LC-MS/MS)

The LC-MS/MS analysis was performed using a reverse-phase liquid chromatography system (EASY-nLC 1000 ultra-high pressure, Thermo Fisher Scientific, Eugene, OR, USA) interfaced with a Q Exactive mass spectrometer (Thermo Fisher Scientific, Eugene, OR, USA) in the SGIKER Proteomic Service of the UPV/EHU (Leioa, Spain).

The digested samples were resuspended in 0.1% formic acid at a concentration of 1 μ g/ μ l, sonicated for 3 minutes and centrifuged at 16×10^3 g for 10 minutes. Then, 1 μ g of the resultant supernatant was loaded onto an Acclaim PepMap100 pre-column (75 μ m x 2 cm, Thermo Fisher Scientific, Eugene, OR, USA) connected to an Acclaim PepMap RSLC analytic column (75 μ m x 25 cm, Thermo Fisher Scientific). Peptides were eluted directly to nanoES Emitter (Thermo Fisher Scientific) by a linear gradient of 4.25% to 38.25% of acetonitrile in 0.1% formic acid, for 150 minutes at a flow rate of 300 nl/min. Q Exactive mass spectrometer was operated in data dependent acquisition – DDA mode. Survey scans were acquired at a resolution of 60000 (m/z 200) and fragmentation spectra at 15000 (m/z 200). Precursors were fragmented by higher energy C-trap dissociation (HCD) with normalized collision energy of 26 eV. The maximum injection time was 100 ms for fragments and precursors acquisition and AGC (Automatic Gain Control) target values of 3×10^6 were used for MS acquisitions

and 5×10^5 for MS/MS scans. Repeat sequencing of peptide was minimized by excluding the selected peptide candidates for 30 s. Ions with one charge or ions whose charge couldn't be determined were also excluded.

Identification and quantification of proteins

All raw data files acquired were searched against the UniProt human database version 2017.02 (with 42147 sequence entries) with MaxQuant proteomics computational platform version 1.5.3.17²⁰¹ and using Andromeda search engine²⁰². For protein identification, the following parameters were used: carbamidomethylation of Cys as fixed modification; oxidation of Met, protein N-terminal acetylation and NQ deamidation as variable modifications; 8 and 20 ppm for precursor and fragment mass tolerances, respectively; 2 missed cleavages for trypsin; minimal peptide length of 7 aminoacids and 1% FDR (False Discovery Rate) for peptides and proteins. Label-free quantification intensity (LFQ intensity) was calculated with the MaxLFQ algorithm²⁰³. The obtained results were analyzed with Perseus platform (version 1.5.6.0)²⁰⁴. The contaminating proteins, those identified in the reverse database and those identified only with modified peptides, were eliminated. The missed LFQ values were replaced with the "replace missing values from normal distribution" option of Perseus and default values were used. A Student's t-test was used to determine statistically significant changes in protein expression. Proteins that showed $p < 0.05$ and a change in LFQ greater or less than 1.5 times were considered as differentially expressed proteins. Samples were obtained from 5 different experiments.

III.1.5. Oxidative stress induction

Oxidative stress conditions were achieved using a moderate (0.25 mM) or a high (0.5 mM) dose of H_2O_2 . For the different experiments, hASCs and PC-hASCs were exposed to H_2O_2 (0.25 or 0.5 mM), for 1 hour in DMEM Glutamax™ FBS free at

37 °C in a humidified 5% CO₂ atmosphere. After that period, media were replaced with fresh media FBS free.

III.1.6. PC-hASCs tolerance to H₂O₂-induced oxidative stress.

To determine if hASCs acquire tolerance to moderate and high doses of H₂O₂ by their prior exposure to a sub-lethal dose of H₂O₂, the intracellular ROS levels of hASCs and PC-hASCs, their apoptotic rate, and the percentage of cytotoxicity were analyzed.

III.1.6.1. Measurement of ROS

hASCs and PC-hASCs intracellular levels of ROS were detected using 2'-7'-dichlorofluorescein diacetate (H2-DFC-DA, Molecular Probes, Eugene OR, USA). H2-DFC-DA is a chemically reduced form of fluorescein that upon cleavage of the acetate groups by intracellular esterases and ROS, is converted to highly fluorescent 2',7'-dichlorofluorescein (DCF). H2-DFC-DA probe was added to the cells (4x10³ cells/well) at a final concentration of 10 μM, for 30 minutes at 37 °C. After this period, the fluorescent probe was removed and cells were washed with 1x PBS. Finally, hASCs and PC-hASCs were exposed to different H₂O₂ concentrations (0.25 or 0.5 mM) and intracellular ROS accumulation was measured every 10 minutes for an hour in a microplate reader (λ_{ex} 492–495; λ_{em} 517–527 nm). Results were expressed as the means ± SD of at least three independent experiments performed in quintuplicate.

III.1.6.2. Apoptosis assay

Apoptosis was analyzed by flow cytometry using Alexa Fluor 488 Annexin V/PI Dead Cell Apoptosis Kit (Thermo Fisher Scientific, Eugene, OR, USA), which measure apoptosis by detecting phosphatidyl serine expression and membrane permeability. hASCs and PC-hASCs were harvested 24 hours after moderate and high H₂O₂ exposure and stained with Alexa Fluor 488 Annexin and PI during 15 minutes at RT (1.10⁶ cells/mL). Then, stained cells were analyzed by flow

cytometry measuring the fluorescence emission at 530 nm and 575 nm using 488 nm excitation. Data was analyzed using Flowing software (Turku Centre for Biotechnology, University of Turku, Finland) and provided as the means \pm SD of three independent experiments. Histograms are representative of these experiments.

III.1.6.3. Cytotoxicity assay

Lactate dehydrogenase (LDH) is a stable cytoplasmic enzyme present in all cells, which is rapidly released into the cell culture medium upon damage of the plasma membrane. This assay, therefore, is a measure of the membrane integrity. LDH activity can be determined by a coupled enzymatic reaction: LDH oxidizes lactate to pyruvate, which reacts with tetrazolium salt INT (2-(4-iodophenyl)-3-(4-nitrophenyl)-5-phenyl-2H-tetrazolium chloride) to form formazan. The increase in the amount of formazan produced in culture supernatant directly correlates to the increase in the number of damaged cells.

For this assay, 4×10^3 cells were seeded in a 96-well plate. LDH assay was performed according to manufacturer's protocol (Cytotoxicity Detection Kit, Roche, Mannheim, Germany). Briefly, 24 and 48 hours after moderate or high oxidant application, cytotoxicity was assessed measuring LDH release from damaged cells into culture media. The kit reaction mixture was added to each well (1:2 dilution) and the plate was incubated in darkness and at RT, for 30 minutes. Finally, the absorbance was measured in a microplate reader at a λ 490 nm. The relative cell LDH release (% cytotoxicity) was calculated as follows:

$$\text{Cytotoxicity (\%)} = \frac{OD \text{ treated samples} - OD \text{ low control}}{OD \text{ high control} - OD \text{ low control}} \times 100$$

where OD low control is the absorbance obtained for untreated cells (spontaneous LDH release), and OD high control is the absorbance obtained for positive control (1% v/v Triton X-100, Sigma-Aldrich, St Louis, MO, USA), defined

as the 100% LDH release (maximum LDH release). Results were expressed as the means \pm SD of at least three different assays ($n \geq 4$).

III.1.7. Statistical analysis

The number of samples analyzed was described in each experiment. All data are shown as mean \pm SD. Statistical analysis was performed using GraphPad Prism statistical software (version 5.0; GraphPad Software). Significance was assessed using analysis of variance followed by Bonferroni's post hoc test and t-tests, as appropriate. Statistical differences were considered significant where $p < 0.05$. All the images shown in this thesis represent the data obtained, at least, in three independent experiments with similar results.

III.2. Results

III.2.1. Preconditioning does not alter morphology, senescence, cell cycle or proliferation rate

To confirm that H₂O₂-preconditioning did not alter morphology, the degree of senescence, cell cycle or proliferation rate, hASCs and PC-hASCs were analyzed by contrast-phase microscopy, senescence assay, flow cytometry and cell viability assay, respectively.

hASCs and PC-hASCs exhibited a similar fibroblast-like, spindle-shaped morphology when observed under phase-contrast inverted microscope (Fig. 13).

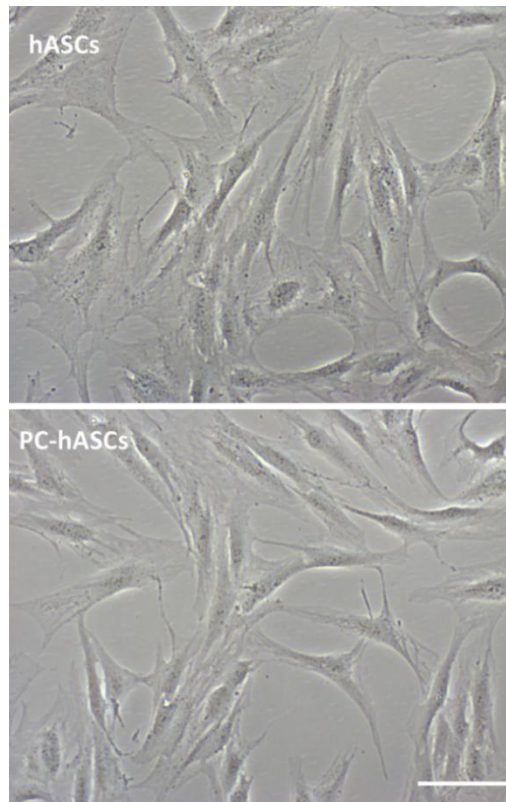


Figure 13. Representative images of 80% confluent hASCs and PC-hASCs morphology by contrast phase microscope. Scale: 100 μ m.

Regarding senescence, cells were subjected to X-GAL staining and examined by contrast phase microscopy (Fig. 14A). After quantification of the X-GAL stained cells, no significant differences were detected between hASCs (26%) and preconditioned cells (23,2%; Fig. 14B).

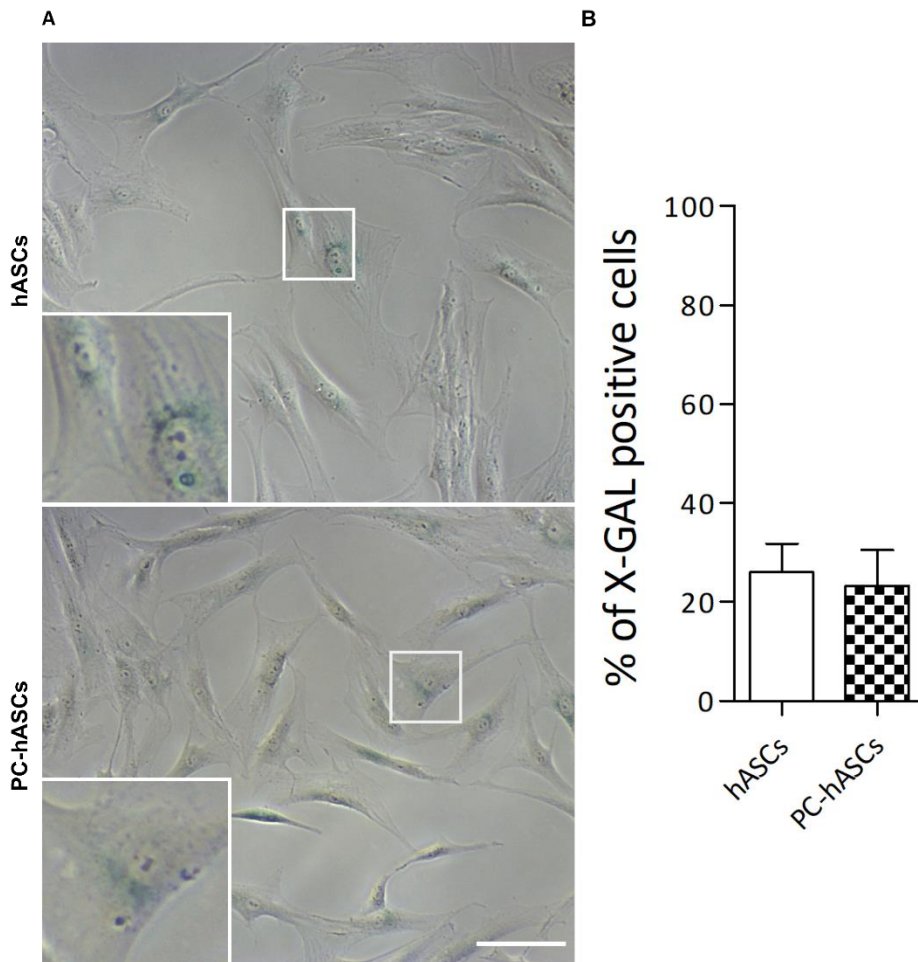


Figure 14. (A) Representative images of hASCs and PC-hASCs dyed with X-GAL staining (senescent cells are dyed in blue, scale bar: 100 μ m) and (B) their quantification. Data are expressed as mean \pm SD. * $p < 0.05$.

As shown in Figure 15A, at 24 hours of culture, PC-hASCs also presented the same percentage of cells (11.4%) undergoing proliferating G2/M phases as hASCs (11.7%). Consistent with cell cycle analysis, hASCs and PC-hASCs

proliferation rate neither showed significant differences at 24 and 48 hours (Fig. 15B).

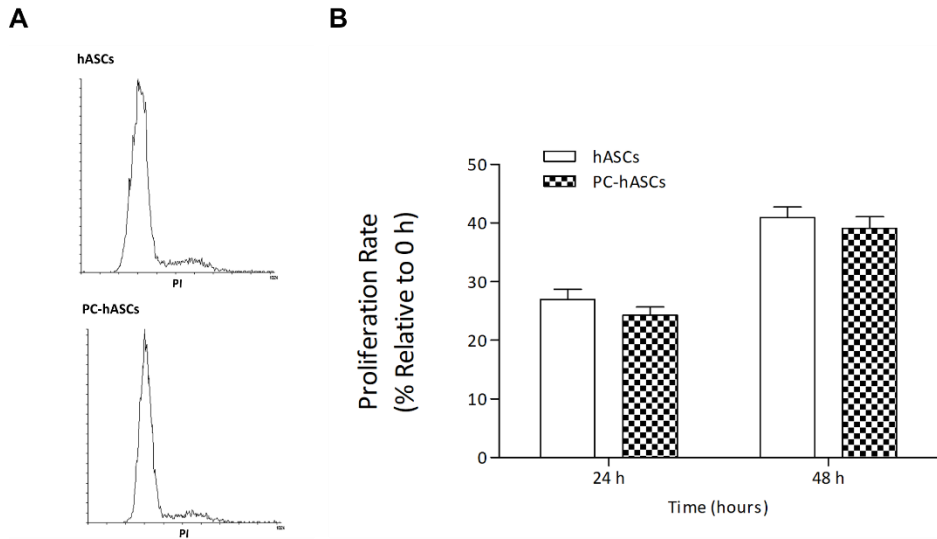


Figure 15. (A) Flow cytometry analysis for cell-cycle distribution (B) Evaluation of the proliferation rate of hASCs and PC-hASCs under standard conditions. Experiments were, at least, performed in triplicate. Data are expressed as mean \pm SD. * $p < 0.05$.

Among the 40 overexpressed proteins, 19 proteins were overexpressed in hASCs and 21 in PC-hASCs (Table 4).

Table 4. List of overexpressed proteins in hASCs or PC-hASCs and their functions.

hASCs		PC-hASCs	
Protein	UniProt ID	Protein	UniProt ID
CNN3 ⁸	Q15417	CDR2 ¹	Q01850
COMMD1 ^{3,7}	Q8N668	CBX1 ⁸	P83916
CDK13 ⁴	Q14004	H2AFY2 ⁸	Q9P0M6
DCAF8 ⁸	Q5TAQ9	ALDH1L1 ^{1,2}	O75891
ELP2 ⁸	Q6IA86	SMURF2 ¹	Q9HAU4
MFN2 ¹	O95140	ETFDH ^{1,3}	Q16134
NOL6 ⁸	Q9H6R4	FAR1 ¹	Q8WVX9
PXN ⁶	P49023	GID8 ⁴	Q9NWU2
PITHD1 ⁸	Q9GZP4	IRS1 ^{1,4}	P35568
FUCA2 ¹	Q9BTY2	LYPLAL1 ¹	Q5VWZ2
RECK ^{2,5}	O95980	MCFD2 ⁸	Q8NI22
STK25 ^{2,3,5}	O00506	BIN1 ¹	O00499
STAMBP ^{2,4}	O95630	NUDT19 ¹	A8MXV4
TJP2 ⁶	Q9UDY2	FAP ^{5,6}	Q12884
TCEAL6 ⁸	Q6IPX3	PSMB6 ⁷	P28072
VPS11 ¹	Q9H270	FAM114A2 ⁸	Q9NRY5
SORCS2 ³	Q96PQ0	PBDC1 ¹	Q9BVG4
CEBPZ ⁸	Q03701	DHX16 ⁸	O60231
TIMM9 ¹	Q9Y5J7	RRP15 ⁸	Q9Y3B9
		SLC39A14 ⁸	Q15043
		COX7A2L ¹	O14548

1: Metabolism, 2: Cell Signaling, 3: Oxidative Stress, 4: Proliferation, 5: Migration, 6: Adhesion, 7: Inflammation and 8: Others.

These proteins play important roles in different cellular processes (Fig. 17). In fact, PXN or Paxillin is involved in cell adhesion to ECM, reversion-inducing cysteine-rich protein with Kazal motifs (RECK) overexpression has an inhibitory effect on hMSCs migration and insulin receptor substrate 1 (IRS1) is implicated in cell proliferation as well as in transmitting signals from the insulin and insulin-like growth factor-1 (IGF-1) receptors to PI3K/AKT and ERK MAP kinase pathways. Furthermore, COMM domain-containing protein 1 (COMMD1) overexpression has shown to inhibit nuclear factor (NF)- κ B, hypoxia inducible factor (HIF)-mediated gene expression and SOD-1, and cytochrome c oxidase subunit 7A-related protein, mitochondrial (COX7A2L), electron transfer flavoprotein-ubiquinone oxidoreductase (ETFDH) and mitofusin 2 (MFN2) are associated with mitochondrial metabolism. In the overall, almost 50% of the differentially expressed proteins are related to metabolism, signaling pathways and oxidative stress.

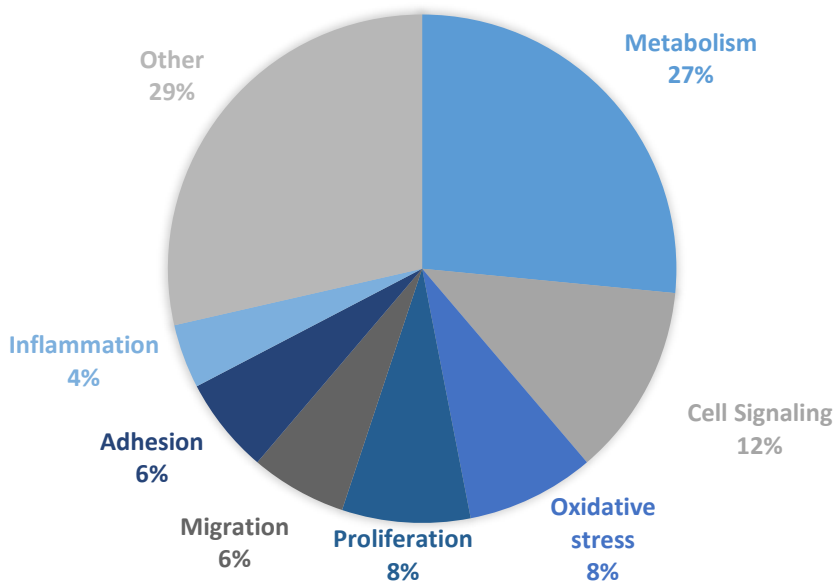


Figure 17. Graphical representation of the percentage of differentially expressed proteins according to their function.

III.2.3. Preconditioning protects cells against oxidative stress

To evaluate the cytoprotective effect of the H₂O₂-preconditioning, cells were exposed to 0.25 or 0.5 mM H₂O₂ for 1 hour. During this period, we evaluated ROS levels and observed that, although ROS increase in a time and dose dependent manner in both, hASCs and PC-hASCs, PC-hASCs showed a significant lower values at 30 and 60 minutes when exposed to 0.25 mM H₂O₂ and also at 60 minutes in the case of 0.5 mM H₂O₂ exposure (Fig. 18).

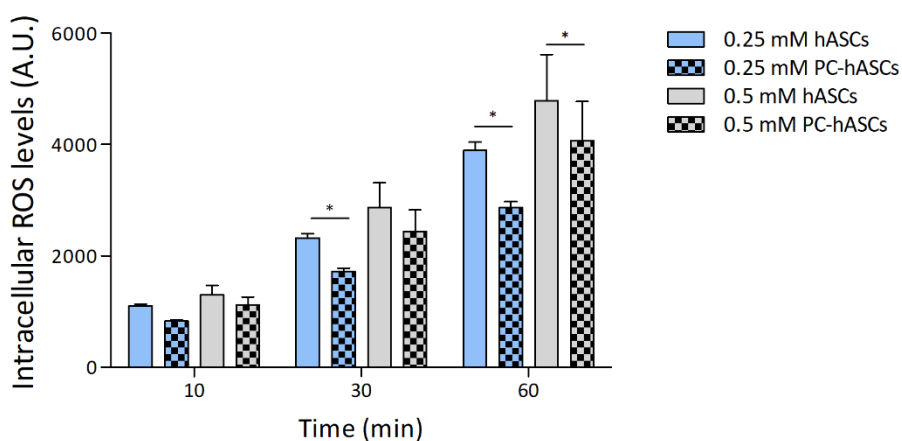


Figure 18. Intracellular ROS levels of hASCs and PC-hASCs during the oxidative stress insult. ROS generation was induced by H₂O₂ (0.25 or 0.5 mM) and measured for 1 hour every 10 minutes. At least three different experiments were performed ($n \geq 5$). Data are expressed as mean \pm SD. * $p < 0.05$.

To evaluate the apoptotic rate, 24 hours after the oxidative stress exposure, cells were stained with Alexa Fluor 488 Annexin and PI. As demonstrated in figure 19A, H₂O₂ exposed PC-hASC culture showed a significant decrease in percentage of apoptotic cells compared to oxidized hASC culture. Particularly, a 2.4-fold reduction was achieved in the case of cultures exposed to 0.25 mM H₂O₂ (hASCs: $8.3 \pm 1.2\%$ and PC-hASCs: $3.5 \pm 0.4\%$) and a 1.4-fold in those exposed to 0.5 mM H₂O₂ (hASCs: $9.9 \pm 0.4\%$ and PC-hASCs: $7.0 \pm 0.6\%$) (Fig. 19B).

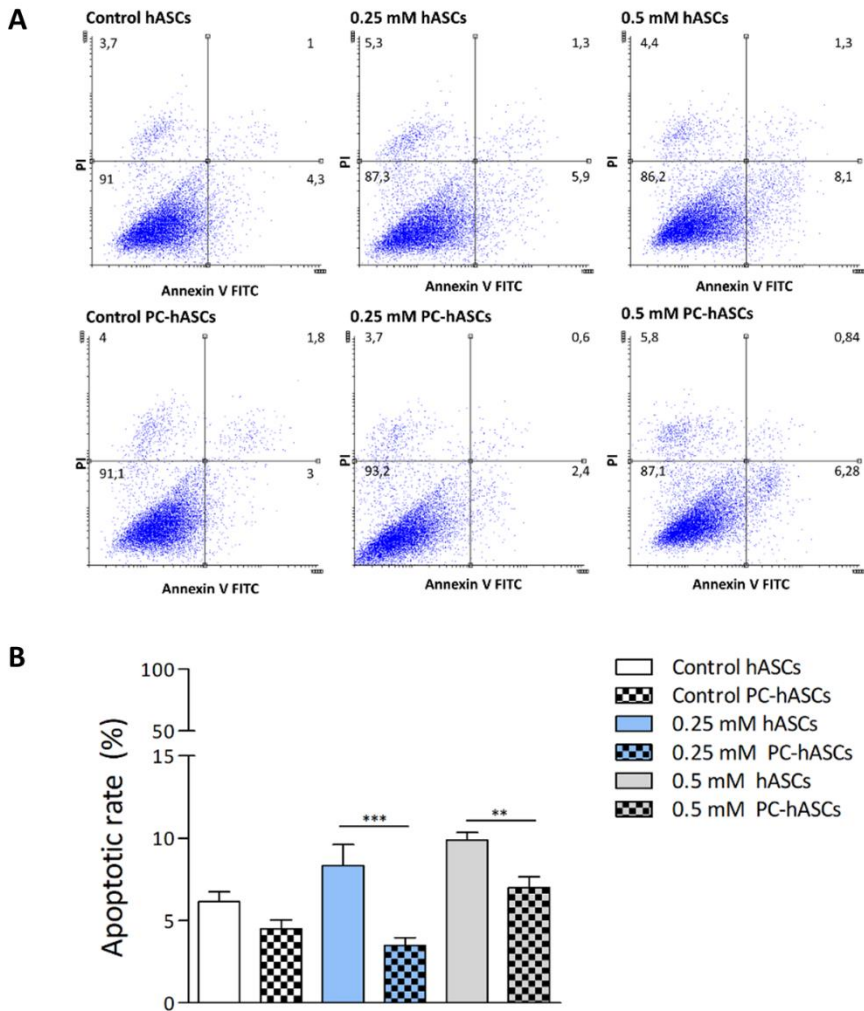


Figure 19. Analysis of hASCs and PC-hASCs undergoing early and late apoptosis. (A). Annexin V/PI assay was performed by flow cytometry. Annexin V⁻/PI⁻ represents live cells; Annexin V⁺/PI⁻ or Annexin V⁺/PI⁺ represents early or late apoptosis phase respectively; Annexin V⁻/PI⁺ reflects necrosis. (B) Quantification of cells undergoing early and late apoptosis. Experiments were performed in triplicate. Data are expressed as mean \pm SD. * $p < 0.05$.

Moreover, to evaluate the cytotoxic effect of H₂O₂ on hASCs and PC-hASCs LDH assay was performed after 24 and 48 hours of the oxidative insult. The results showed that preconditioning significantly decreased H₂O₂-induced cytotoxicity

in PC-hASCs. Thus, compared to hASCs at 24 hours, PC-hASCs exposed to 0.25 mM or 0.5 mM showed a 1.7 and 1.9-fold decrease in the cytotoxicity percentage, respectively (Fig. 20). At 48 hours, the reduction in LDH release when compared to hASCs was maintained. In fact, PC-hASCs exposed to 0.25 mM or 0.5 mM showed a 2.0- and 1.8-fold decrease in the cytotoxicity percentage, respectively.

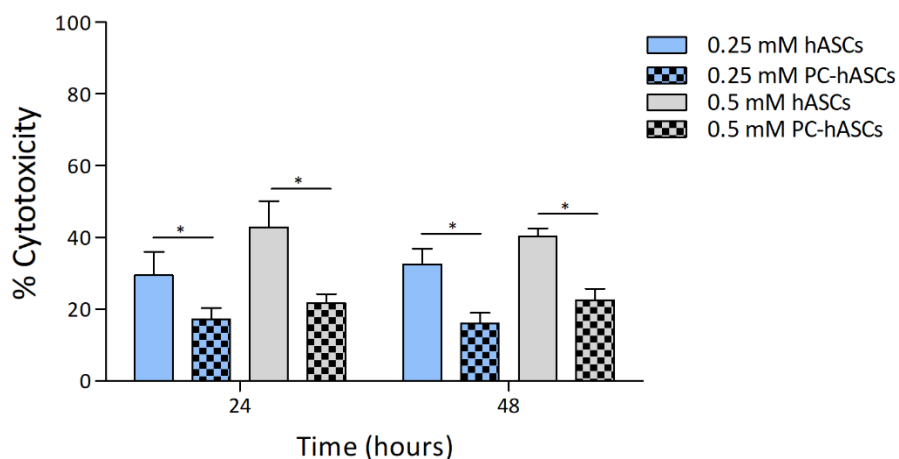


Figure 20. Determination of H_2O_2 cytotoxic effect on hASCs and PC-hASCs. LDH release was quantified at 24 and 48 hours post-stimulus (0.25 or 0.5 mM H_2O_2). At least three different experiments were performed ($n \geq 5$). Data are expressed as mean \pm SD. * $p < 0.05$.

In this chapter, we have shown that preconditioning does not affect morphology, senescence, cell cycle or the proliferative rate of hASCs. However, we have observed a slight change in the expression of certain proteins. Among these differentially expressed proteins, 27% participate in metabolism, 12% in cellular signaling and 8% are related to oxidative stress, which led us to focus our attention on hASCs and PC-hASCs metabolic and molecular mechanisms underlying the survival and adaptation of these cells to oxidative stress.

Besides, by subjecting the cells to two different doses of oxidation, we observed that the PC-hASCs withstand stress conditions better than hASCs. After the analysis of obtained results we determine that the dose of 0.25 mM H₂O₂ is the experimental condition in which the differences between hASCs and PC-hASCs are better appreciated, and considering that this concentration is similar to that observed in inflammatory processes^{33,217}, from this point we used that concentration for the remaining experiments.

IV. Chapter 2

Elucidation of the molecular and bioenergetic mechanisms underlying the survival and adaptation of PC-hASCs to oxidative stress

As previously described, the functionality of hASCs may be affected by the oxidative/inflammatory environment present into damaged tissue where they are transplanted, reducing their therapeutic activity. In the previous chapter, we have shown that preconditioning with low doses of H₂O₂ induce a resistance to oxidative stress on hASCs. Besides, through proteomic analysis, we observed that this preconditioning, under normal conditions, modulated the expression of certain proteins related to inflammation, oxidative stress or metabolism. **Then, in this chapter, we focused on elucidating the molecular and bioenergetic mechanisms underlying the survival and adaptation of PC-hASCs under oxidative stress.**

IV.2. Materials and methods

IV.1.1. Cell culture

In this part of the experimentation we also used hASCs as described in the section IV.1.1.

IV.1.2. Western blot analysis

To determine the expression of proteins of interest, a western blot analysis was conducted. hASCs and PC-hASCs exposed to a moderate dose of H₂O₂ were lysed in 1x Laemmli buffer (Sigma-Aldrich, St. Louis, MO, USA) and sonicated to obtain a homogeneous sample. Whole cell preparations and nuclear extracts were obtained employing an adaptation of a high-quality biochemical fractionation protocol ²⁰⁵. Briefly, cells were pelleted and resuspended in cytoplasmic extraction buffer (20 mM Tris, pH 7.6, 0.1 mM EDTA, 2 mM MgCl₂·6H₂O, 0.5 mM Na₃VO₄) to induce hypotonic swelling. To release cytoplasmic proteins, Nonidet P-40 (Igepal, Sigma-Aldrich, St. Louis, MO, USA) was added to a final concentration of 1%. The cytoplasmic extract was separated by centrifugation (500 g for 3 minutes, at 4 °C) and the pellet containing nuclei was resuspended in the 1% Nonidet P-40 cytoplasmic extraction buffer and centrifuged at 4 °C and 500 g for 3 minutes; this washing step was repeated one more time in order to obtain a pure nuclei pellet. Protein quantification was performed using trichloroacetic acid (TCA, Fluka Biochemika, Steinheim, Germany) precipitation and bovine serum albumin (BSA, Sigma-Aldrich, St Louis, MO, USA) as the standard curve.

Whole cell lysates, cytoplasmic and nuclear extracts were boiled for 5 minutes to allow denaturation. Then, denatured samples were loaded onto 10% SDS-PAGE gels and resolved by electrophoresis using a SDS running buffer (25 mM Tris, 200 mM glycine, 0.1% SDS (w/v), pH 8.3) at 90 V for 90 minutes in a Mini-

Protean® 3 Cell (BioRad, Segrate MI, Italy). Resolved proteins were transferred onto nitrocellulose membrane (GE Healthcare, Life Sciences, Freiburg, Germany) at 380 mA for 180 minutes at 4 °C using a SDS transfer buffer (25 mM Tris, 200 mM glycine, 0.1% SDS (w/v), 20% methanol, pH 8.3). Subsequently, nitrocellulose membranes were stained with Ponceau S solution (Sigma-Aldrich, St Louis, MO, USA) to allow visibility of resolved proteins. Membranes were washed with TBS-T (20 mM Tris, 500 mM NaCl, 0.1% Tween-20 (v/v), pH 7.5) to remove the Ponceau and then blocked with 5% skimmed milk in TBS-T for 1 hour. Subsequently, membranes were incubated o/n at 4 °C with the primary antibodies listed below (Table 5). After washing with TBS-T, membranes were incubated with the corresponding secondary antibody for 1 hour at RT (Table 5). Finally, membranes were visualized using SuperSignal West Pico PLUS Chemiluminiscent Substrate (ThermoFisher, Waltham, MA, USA). Images were acquired with the gel documentation system, G: Box Chemi HR16 (Syngene, Frederick, MD, USA) and densitometry was performed with the ImageJ software (NIH, Bethesda, MD, USA). Densitometry values were then normalized to that of their corresponding loading controls. PC-hASCs data were relativized to hASCs and provided as the average (mean \pm SD) of at least three different experiments.

Table 5. List of western blot antibodies used in the PC-hASCs analysis.

Primary Antibodies	Source	Dilution
NRF2	GeneTex GTX103322	1:500
SOD-1	GeneTex GTX100554	1:1000
HO-1	GeneTex GTX101147	1:1000
GPx1	GeneTex GTX116040	1:1000
CAT	GeneTex GTX110704	1:1000
NF- κ B (p65)	GeneTex GTX107678	1:1000
COX-2	Abcam Ab21704	1:1000

Primary Antibodies	Source	Dilution
IL-1 β	R&D Systems AF-201-SP	1:1000
HIF-1 α	BD Biosciences 610959	1:250
Phospho-Akt (Ser 473)	Cell Signalling 9271	1:1000
Akt	Cell Signalling 9272	1:1000
Phospho-p44/42 MAPK (ERK 1/2)	Cell Signalling 9101	1:1000
p44/42 MAPK (ERK 1/2)	Cell Signalling 9102	1:1000
β -Actin	EMD Millipore ABT264	1:5000
Lamin A+C	GeneTex GTX101127	1:5000
GAPDH	EMD Millipore ABS16	1:10000
Secondary Antibodies	Source	Dilution
Goat anti-Rabbit IgG	Thermo Fisher 65-6140	1:1000
Rabbit anti-Mouse IgG	Thermo Fisher 31813	1:1000
Donkey anti-goat IgG	Bethyl Laboratories A50-101P	1:1000

IV.1.3. Assessment of mitochondrial stress

To evaluate mitochondrial stress, MitoTracker[®]Red CMXRos probe (Invitrogen, Eugene, OR, USA), a derivative of X-rosamine, was used. This probe labelled mitochondria depending on the membrane potential ($\Delta\psi_m$) and gives information of mitochondria morphology and stress. For this experiment, cells were seeded in 96 well plates or μ -Slide 8 well (Ibidi GmbH, Martinsried, Germany); 24 hours after the H₂O₂ exposure period, they were incubated with 100 mM MitoTracker[®] probe for 30 minutes at 37 °C. For mitochondria visualization, samples were examined under a Zeiss LSM880 Airyscan confocal microscope (Carl Zeiss Inc, Chicago, IL, USA) using 40x objective. For $\Delta\psi_m$ quantification, the fluorescence intensity of living cells was measured in a

microplate reader (λ_{ex} 579; λ_{em} 599 nm). Results were given as the mean \pm SD of three independent assays ($n \geq 3$).

IV.1.4. Cellular bioenergetic evaluation

To determine if the preconditioning altered the bioenergetic profile of hASCs, XF Cell Mito Stress Test, XF Glycolytic Rate Assay and XF Real-Time ATP Rate Assay were performed using a Seahorse XFe96 Extracellular Flux Analyzer (Agilent Technologies, Santa Clara, CA, USA) following manufacturer instructions. PC-hASCs and hASCs were plated in a XF96 cell culture microplate and 24 hours after the oxidative stress insult, cells were assayed for both oxygen consumption rate (OCR) and extracellular acidification rate (ECAR) in XF DMEM Base Medium without phenol red, supplemented with 10 mM glucose, 2 mM glutamine, 1 mM pyruvate, 5 mM HEPES, pH 7.4. For each assay, OCR and ECAR were measured before (basal conditions) and after sequential injections of different metabolic stressors (Table 6).

Table 6. List of different metabolic stressors used in the energetic metabolism analysis of PC-hASCs.

Metabolic Stressor	Function	Dose
Oligomycin	ATP synthase inhibitor	1.5 μ M
Carbonyl cyanide 4-(trifluoromethoxy) phenylhydrazone (FCCP)	Uncoupling agent that collapses the proton gradient and disrupts the mitochondrial membrane potential	0.5 μ M
Mix of rotenone and antimycin A (Rot/AA)	Respiratory chain inhibitor	0.5 μ M
2-Deoxy-D-glucose (2-DG)	Glycolytic inhibitor	50 mM

IV.1.4.1. Mitochondrial respiration

Mitochondrial respiration is the set of metabolic reactions and processes requiring oxygen that takes place in mitochondria to convert the energy stored in macronutrients to ATP. In order to measure the mitochondrial respiration of hASCs and PC-hASCs we used the Seahorse XF Cell Mito Stress Test Kit, that uses modulators of cellular respiration (Oligomycin, FCCP, Rot/AA) that specifically target components of the electron transport chain (ETC) to reveal key parameters of metabolic function. After basal rates were recorded over three measurement periods, the compounds were serially injected to measure basal respiration, maximal respiration, ATP-linked respiration and coupling efficiency. The first compound injected was oligomycin. Oligomycin is an ATP synthase (complex V) inhibitor that decreases electron flow through the ETC, leading to a decrease in OCR, which is linked to cellular ATP production. Next, FCCP, an uncoupling agent that collapses the proton gradient and disrupts the mitochondrial membrane potential, was injected. As a result, electron flow through the ETC was uninhibited, and oxygen consumption by complex IV reached the maximum. The FCCP-stimulated OCR was then used to calculate spare respiratory capacity, defined as the difference between maximal respiration and basal respiration. Spare respiratory capacity is a measure of the ability of the cell to respond to increased energy demand or under stress. Finally, the third injection was a mixture of rotenone, a complex I inhibitor, and antimycin A, a complex III inhibitor. This combination shut down mitochondrial respiration and enabled the calculation of non-mitochondrial respiration driven by processes outside the mitochondria. Figure 21 illustrates the injection sequence of these compounds and the parameters that can be obtained with this assay.

Seahorse XF Cell Mito Stress Test Profile Mitochondrial Respiration

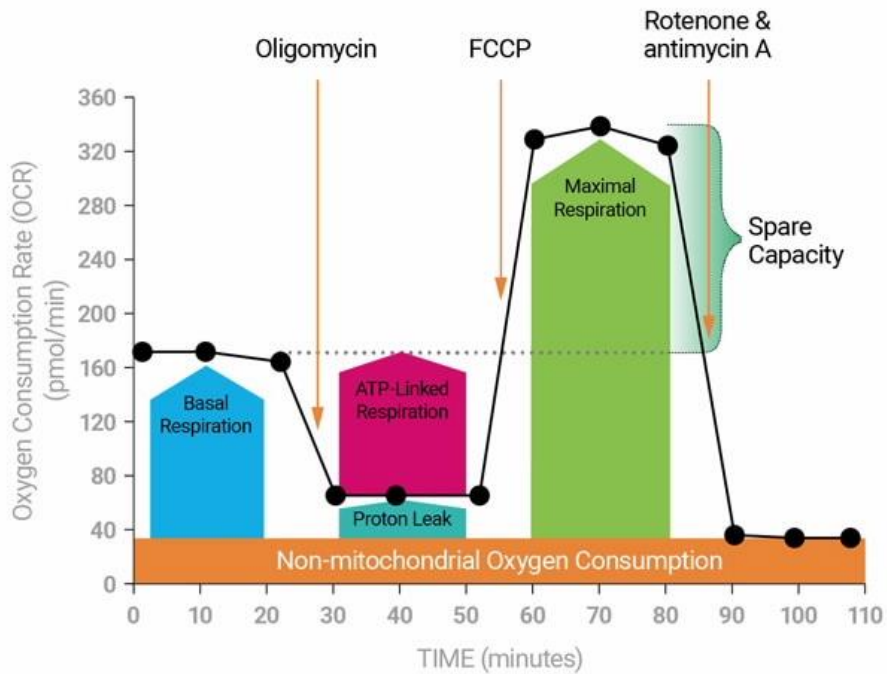


Figure 21. Agilent Seahorse XF Cell Mito Stress Test profile, showing the key parameters of mitochondrial function. https://www.agilent.com/cs/publishingimages/Cell_Mito_Profile.jpg

IV.1.4.1. Glycolysis

Glucose in cells is converted to pyruvate, and then converted to lactate in the cytoplasm, or to CO_2 and water in the mitochondria. The conversion of glucose to lactate results in a net production and extrusion of protons to the extracellular medium, which is detected by the XF Analyzer as ECAR. However, despite the strong correlation of ECAR with glycolytic activity, there are other sources of acidification (mainly mitochondrial-derived CO_2 ; Fig. 22).

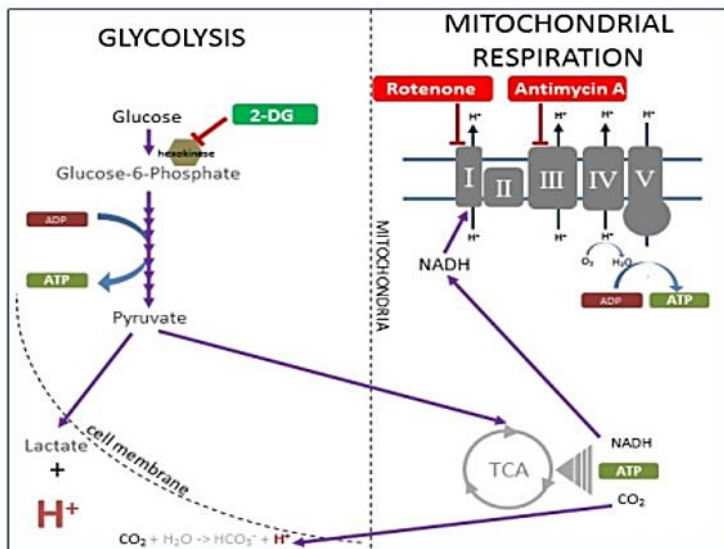


Figure 22. Principle of the Agilent Seahorse XF Glycolytic rate assay. <https://www.agilent.com/cs/promotions/images/glycolysis-rate-measure.png>

The Agilent Seahorse XF Glycolytic Rate Assay utilizes both ECAR and OCR measurements to account for CO₂ contribution to extracellular acidification, and thus obtain the Glycolytic Proton Efflux Rate (glycoPER). This parameter is the rate of protons extruded to the extracellular medium during glycolysis and is equivalent to the amount of lactate produced during glycolysis.

In order to quantify the glycoPER, the XF Glycolytic Rate Assay injected three metabolic compounds (Rot/AA and 2-DG) after the three basal measurements. The mitochondrial respiration was inhibited by Rot/AA. By inhibiting respiration, the rate of proton efflux from respiration was calculated and removed from the total proton efflux rate (PER) giving the glycoPER. Furthermore, to confirm pathway specificity 2-DG was injected. 2-DG is a glucose analog which inhibits glycolysis through competitive binding of glucose hexokinase, the first enzyme in the glycolytic pathway. The resulting decrease in the PER confirmed that the PER produced prior to the injection is primarily due to glycolysis (Fig. 23).

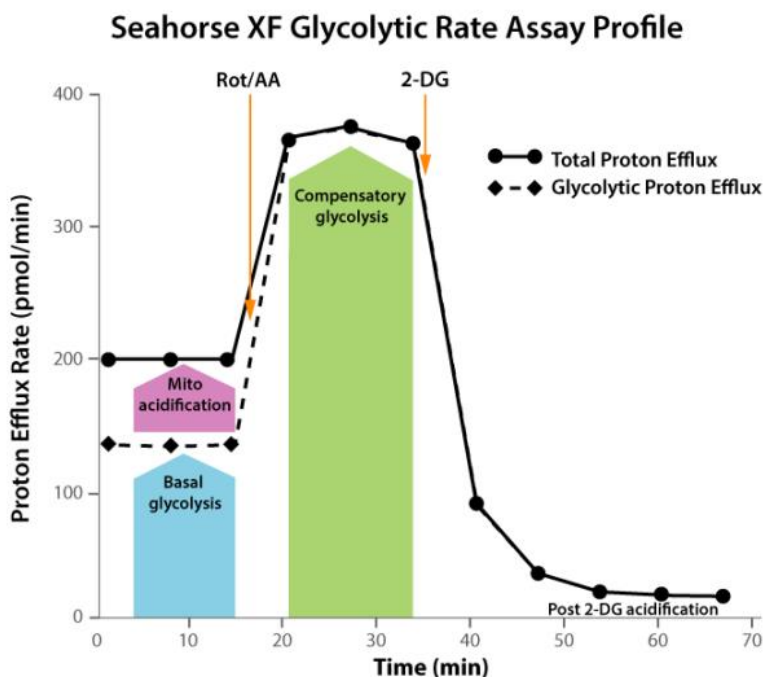


Figure 23. Agilent Seahorse XF Glycolytic rate assay profile. Proton efflux from live cells comprises both glycolytic and mitochondrial-derived acidification. Inhibition of mitochondrial function by Rot/AA enables calculation of mitochondrial-associated acidification to Total Proton Efflux Rate (PER) results in Glycolytic Proton Efflux Rate (glycoPER).

<https://www.agilent.com/cs/publishingimages/seahorse-xf-glycolytic-rate-assay-kit-square.jpg>

IV.1.4.1. ATP production

Finally, to determine the total rate of cellular ATP production as well as the fractional contribution from mitochondrial respiration and glycolysis we performed the XF Real-Time ATP Rate Assay (1.5 μM oligomycin and 0.5 μM of Rot/AA). As previously mentioned, injection of oligomycin resulted in an inhibition of mitochondrial ATP synthesis that led to a decrease in OCR, allowing mitochondrial ATP production rates to be quantified. Complete inhibition of mitochondrial respiration with Rot/AA enabled calculation of mitochondrial-associated acidification, allowing calculation of glycolytic ATP production. Lastly, the total cellular ATP Production Rate was the sum of the mitochondrial and glycolytic ATP production rates (Fig. 24).

Agilent Seahorse XF Real-Time ATP Rate Assay

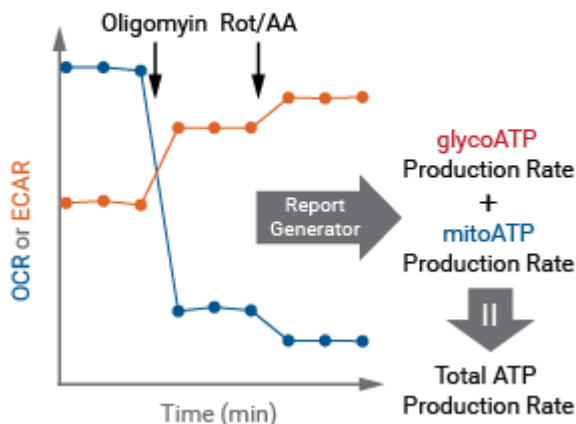


Figure 24. Agilent Seahorse XF Real-Time ATP rate assay. This assay removes contributions from non-ATP production related signals through sequential injection of energy pathway modulators (oligomycin and Rot/AA). <https://www.agilent.com/cs/promotions/images/atp-figure6.png>

The results obtained were normalized to the number of cells and analyzed by Wave Desktop Software 2.6 (Agilent Technologies, Cedar Creek, TX, USA). All assays ($n \geq 3$) were performed at least three times and plotted as means \pm SD.

IV.1.5. Statistical analysis

The number of samples analyzed was described in each experiment. All data are shown as mean \pm SD. Statistical analysis was performed using GraphPad Prism statistical software (version 5.0; GraphPad Software). Significance was assessed using analysis of variance followed by Bonferroni's post hoc test and t-tests, as appropriate. Statistical differences were considered significant where $p < 0.05$. All the images shown in this thesis represent the data obtained, at least, in three independent experiments with similar results.

IV.2. Results

IV.2.1. Preconditioning promotes the antioxidant response and reduces the pro-inflammatory proteins expression

To analyze the antioxidant effect of the preconditioning, NRF2 and relevant antioxidant enzymes (HO-1, SOD-1, GPx-1 and CAT) expression was studied by western blot immediately after the H₂O₂ insult. The results revealed that there were no differences between non-oxidized controls. After the exposure of hASCs and PC-hASCs to 0.25 mM H₂O₂ an increase in nuclear NRF2 expression was produced (1.52 and 1.97-fold higher, respectively), being this increment 1.3-fold higher in PC-hASCs compared to hASCs (Fig. 25).

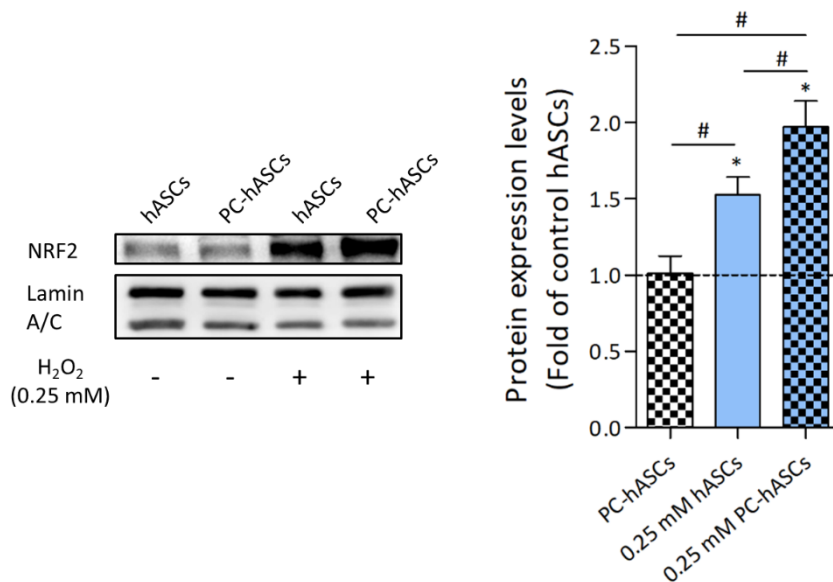


Figure 25. Expression and quantification of nuclear NRF2 in hASCs and PC-hASCs exposed to oxidative stress. Cells were treated with 0.25 mM H₂O₂ for 1 hour, and lysed just after the insult. Values were normalized to their corresponding loading control. At least three different experiments were performed. Data were relativized to control hASCs (dotted line) and expressed as mean \pm SD. * $p < 0.05$, compared with control hASCs, # $p < 0.05$.

Remarkably, preconditioned cells also exhibited an enhancement in antioxidant enzymes expression. In fact, compared to oxidized hASCs, PC-hASCs exposed to 0.25 mM H₂O₂ showed a 1.3-fold increase in the expression of HO-1 and CAT, 1.4-fold increase in the expression of SOD-1 and 1.7-fold increase in the expression of GPx-1. Furthermore, expression of SOD-1 and GPx-1 were increased in control PC-hASCs (1.26 and 1.3-fold increase, respectively) when compared to hASCs (Fig. 26).

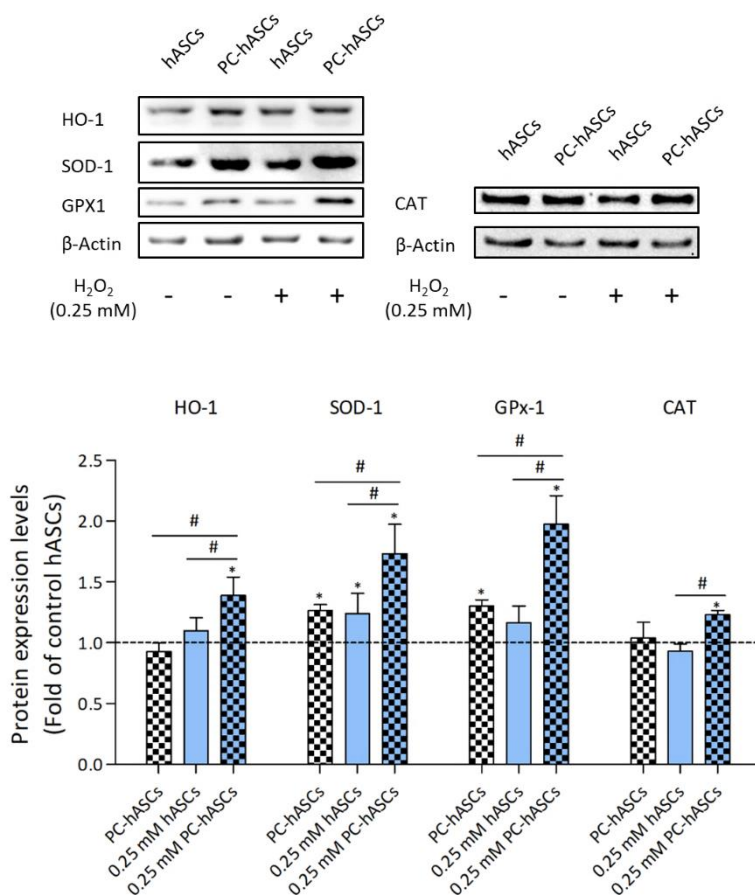


Figure 26. Expression and quantification of HO-1, SOD-1, GPx1 and CAT in hASCs and PC-hASCs exposed to oxidative stress. Cells were treated with 0.25 mM H₂O₂ for 1 hour, and lysed just after the insult. Values were normalized to their corresponding loading control. At least three different experiments were performed. Data were relativized to control hASCs (dotted line) and expressed as mean ± SD. *p < 0.05, compared with control hASCs, #p < 0.05.

To evaluate how preconditioning affected the expression of inflammatory proteins, we measured by western blot the expression of NF- κ B and proinflammatory molecules COX-2 and IL-1 β .

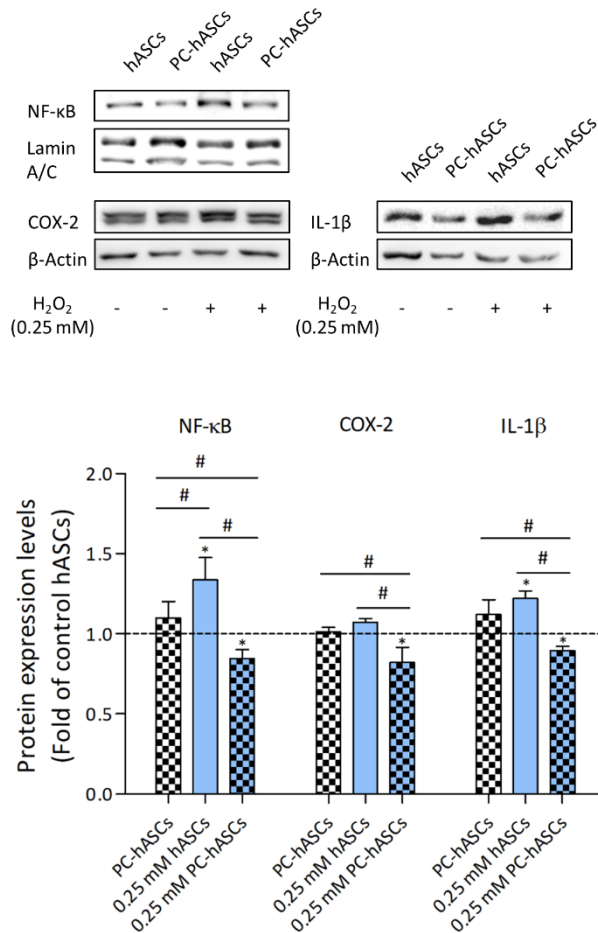


Figure 27. Expression and quantification of NF- κ B, COX-2 and IL-1 β in hASCs and PC-hASCs exposed to oxidative stress. Cells were treated with 0.25 mM H₂O₂ for 1 hour, and lysed 24 hours after the insult. Values were normalized to their corresponding loading control. At least three different experiments were performed. Data were relativized to control hASCs (dotted line) and expressed as mean \pm SD. *p < 0.05, compared with control hASCs, #p < 0.05.

IV. Chapter 2

The results showed that preconditioning attenuated the expression of all these proteins when cells were subjected to oxidative stress. As shown in Figure 27, whereas no differences were observed between control groups, 24 hours after 0.25 mM H₂O₂ exposure, PC-hASCs exhibited a significant lower expression in NF-κB, COX-2 and IL-1β than hASCs (1.6, 1.3 and 1.4-fold decrease, respectively).

Additionally, the effect of preconditioning on ERK and AKT was evaluated by western blot. When the cells were cultivated in standard conditions there were no differences in the expression of p-ERK or p-AKT. Under stress conditions, a down-expression of p-ERK was observed in both, PC-hASCs and hASCs (4 and 2.4-fold decrease, respectively), whereas p-AKT was overexpressed (1.21 and 1.26-fold increase, respectively; Fig.28).

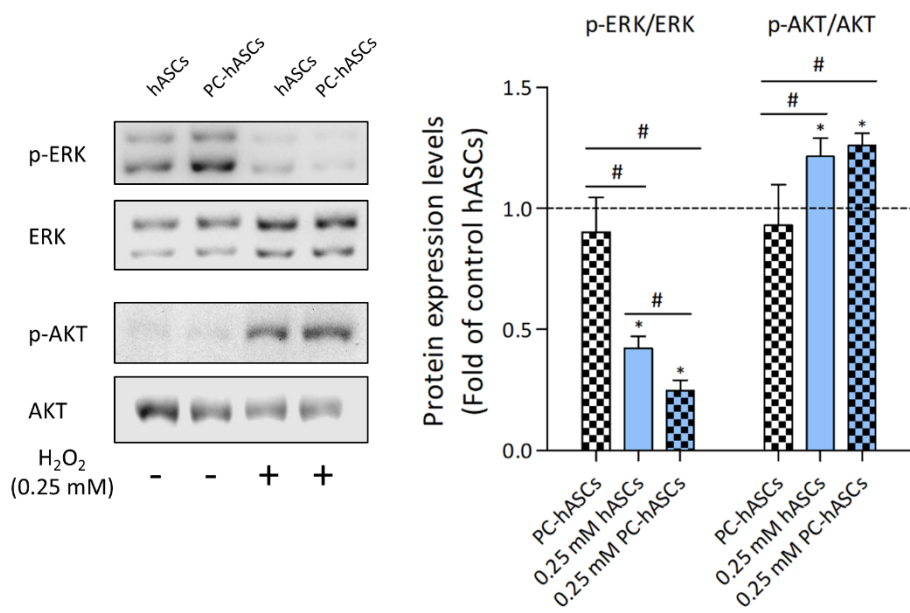


Figure 28. Expression and quantification of p-ERK and p-AKT. hASCs and PC-hASCs were exposed to 0.25 mM H₂O₂ for 1 hour, and lysed 24 hours after the insult. At least three different experiments were performed. Data were relativized to control hASCs (dotted line), and expressed as mean ± SD. *p < 0.05, compared with control hASCs, #p < 0.05.

IV.2.1. Preconditioning alters cells metabolism

IV.2.1.1. Mitochondrial respiration

We evaluated if the preconditioning had any impact on OXPHOS or glycolytic metabolism of hASCs in standard conditions and in response to oxidative stress. Firstly, to determine mitochondrial stress, mitochondrial morphology and $\Delta\psi_m$ were analyzed with MitoTracker®Red CMXRos probe. In figure 29, we observed that mitochondria of control hASCs and PC-hASCs presented a similar elongated and tubular shape.

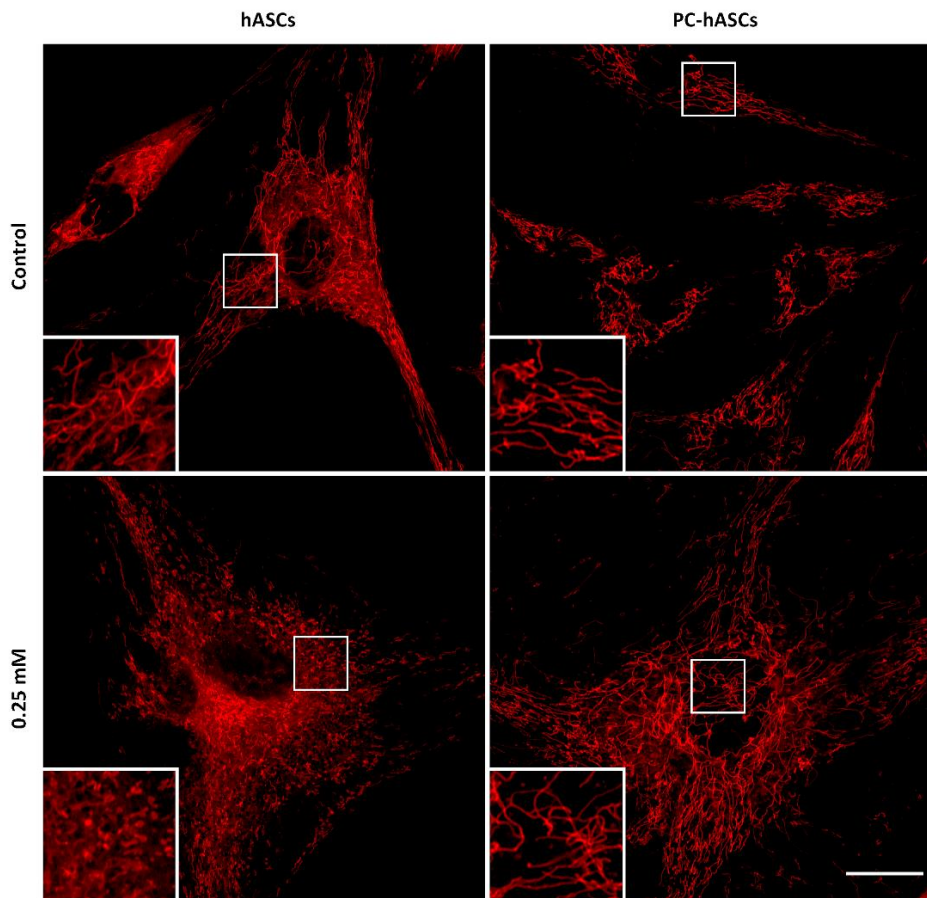


Figure 29. Mitochondrial morphology. Confocal microscopy images of PC-hASCs and hASCs under standard and oxidative stress situation; cells labeled live with MitoTracker Red CMXRos. Scale bar: 30 μm .

However, when cells were exposed to 0.25 mM H₂O₂, the morphology of hASCs and PC-hASCs mitochondria differed. PC-hASCs mitochondria had the same tubular shape as the controls, whereas hASCs looked fragmented (Fig. 29). Besides, PC-hASCs seemed to increased mitochondrial mass and developed a strongly interconnected network that distributed uniformly through the cytoplasm, suggesting potentiation of fusion processes. In regard to $\Delta\psi_m$, control hASCs and PC-hASCs showed no significant differences; however, when the cells were subjected to a moderate oxidative stress insult, PC-hASCs exhibited a higher $\Delta\psi_m$ than their corresponding control (16 ± 1.2 % increase) and oxidized non-preconditioned cells (14 ± 1.2 % increase), which correlates with the confocal images (Fig. 30).

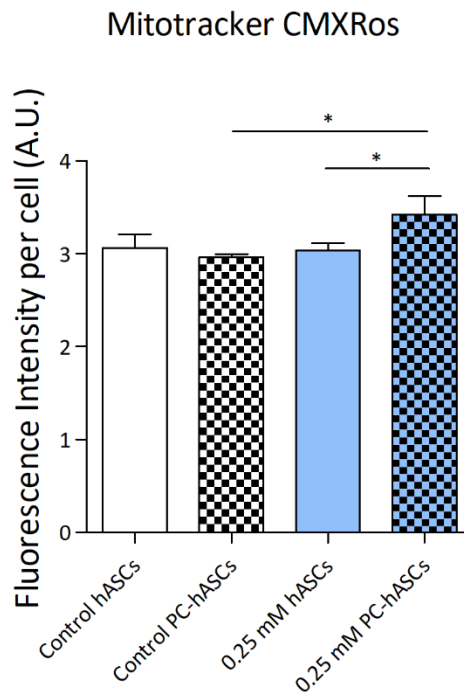


Figure 30. $\Delta\psi_m$ quantification. hASCs and PC-hASCs under standard and oxidative stress situation were labeled live with MitoTracker Red CMXRos and fluorescence was quantified. At least three different experiments were performed and results were expressed as mean \pm SD. * $p < 0.05$.

To examine mitochondrial function, the XF Cell Mito Stress Test was used. First of all, and to discard mitochondrial dysfunction, the coupling efficiency was evaluated. The coupling efficiency varies with ATP demand, but it is usually fairly high (70-90%). This index is very sensitive to changes in all bioenergetic modules, so is likely to change in any dysfunction. In this case, both cell types in basal and in oxidative conditions exhibited more than a 70% of coupling efficiency and there were no significant differences among them (Fig. 31). This result discarded mitochondrial dysfunction.

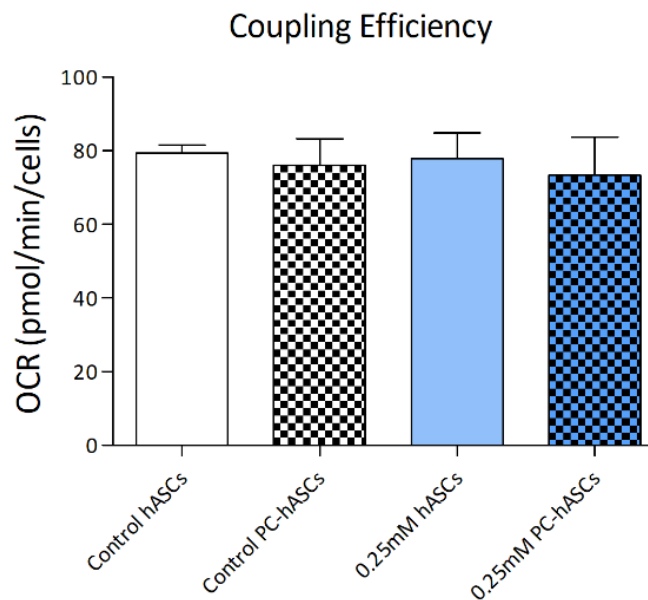


Figure 31. Coupling efficiency. Mitochondrial respiration parameters were assessed in hASCs and PC-hASCs following sequential injections of oligomycin, FCCP, and a ROT/AA under control conditions or after 0.25 mM H₂O₂ exposure. At least three different experiments were performed and results were expressed as mean ± SD. *p < 0.05.

After 0.25 mM H₂O₂ exposure, and compared to hASCs, preconditioned cells displayed a significant augmentation both, in basal mitochondrial oxygen consumption (1.8-fold increase; Fig. 32A) and in maximal respiratory capacity (1.4-fold increase; Fig. 32B).

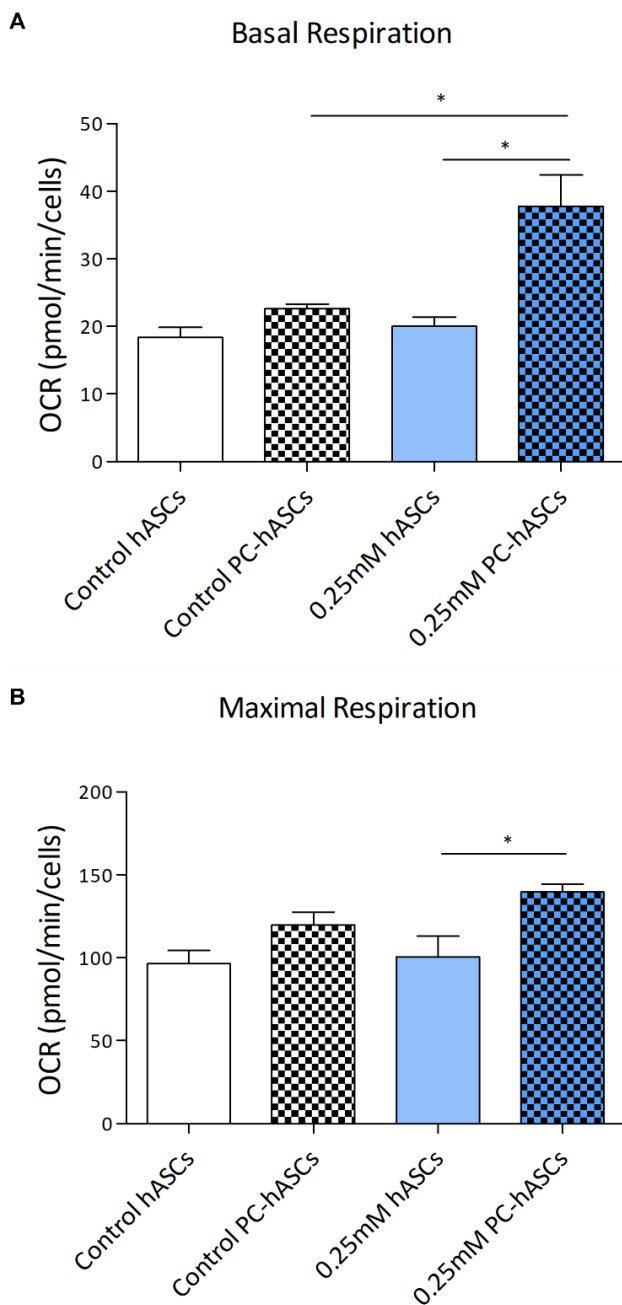


Figure 32. Mitochondrial respiration parameters. Mitochondrial respiration was assessed in hASCs and PC-hASCs following sequential injections of oligomycin, FCCP, and a ROT/AA under control conditions or after 0.25 mM H₂O₂ exposure. (A) Basal respiration, (B) Maximal respiration. At least three different experiments were performed and results were expressed as mean ± SD. *p < 0.05.

Moreover, when exposing cells to oligomycin, an inhibitor of the ATP synthase, we also detected an increase in ATP-linked respiration for PC-hASCs (1.3-fold) and for PC-hASCs exposed to 0.25 mM H₂O₂ (1.25-fold), comparing with non-preconditioned ones (Fig. 33), indicating that preconditioned cells have an enhanced energy capacity to respond to stress.

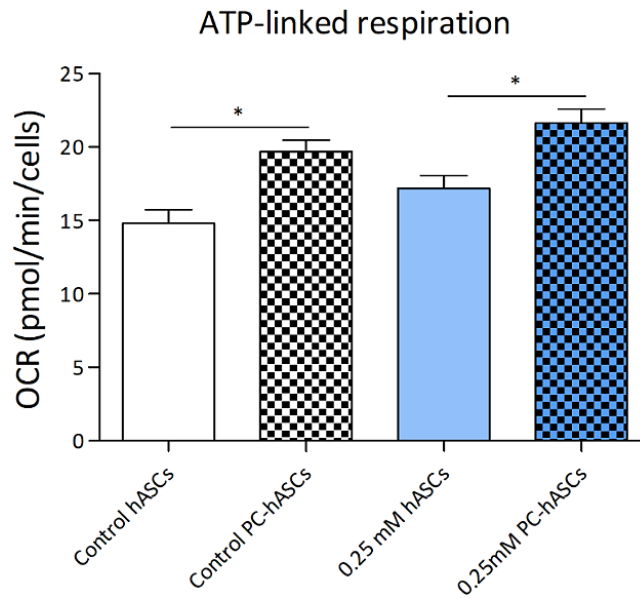


Figure 33. ATP-linked respiration. Mitochondrial respiration parameters were assessed in hASCs and PC-hASCs following sequential injections of oligomycin, FCCP, and a ROT/AA under control conditions or after 0.25 mM H₂O₂ exposure. At least three different experiments were performed and results were expressed as mean \pm SD. * $p < 0.05$.

IV.2.1.2. Glycolysis

In figure 34, we measured the PER from glycolysis percentage. This metric is the rate of protons extruded to the extracellular medium during glycolysis and is equivalent to the amount of lactate produced during glycolysis. Cells analyzed by XF Glycolytic Rate Assay showed that both, hASCs and PC-hASCs, stimulated or not with oxidative stress, were predominantly glycolytic, considering that more than a 90% of the total rate of extracellular acidification comes from glycolysis (Fig. 34).

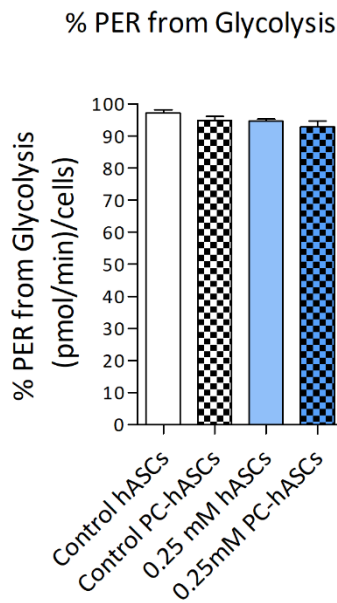


Figure 34. Percentage of PER from glycolysis. Both, hASCs and PC-hASCs present a glycolytic phenotype suggested by % PER (proton efflux rate, the number of protons exported by cells into the assay medium over time) from glycolysis. At least three different experiments were performed. Data were expressed as mean \pm SD. * $p < 0.05$.

When subjected to 0.25 mM H₂O₂, a decrease in glycolytic activity was detected in both cell types compared to their corresponding control cells; however, compared to hASCs, preconditioned cells showed a higher glycolytic phenotype as indicated by higher basal glycolysis and higher compensatory glycolysis (Fig. 35).

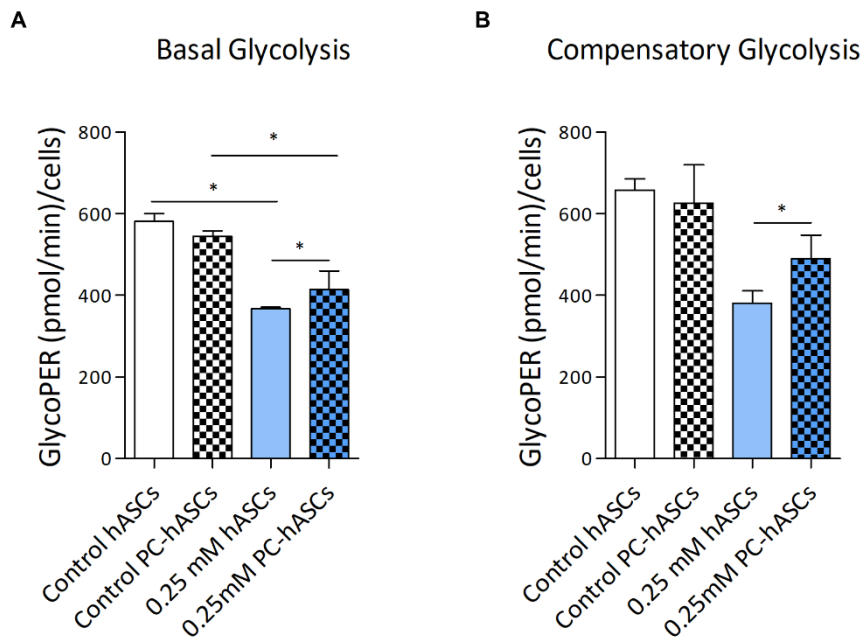


Figure 35. Glycolysis parameters. Glycolysis was assessed in hASCs and PC-hASCs following sequential injections of ROT/AA and 2-DG under control conditions or after 0.25 mM H₂O₂ exposure. (A) Basal glycolysis and (B) Compensatory glycolysis. At least three different experiments were performed. Data were expressed as mean \pm SD. * $p < 0.05$.

Considering the increase in oxidized PC-hASCs compared to non-preconditioned cells, we investigated underlying mechanisms that might be activated to counteract oxidative stress and enhance glycolysis in PC-hASCs. In this sense, HIF-1 α is known to be a key factor that codes for proteins related to glycolytic energy metabolism. When analyzing this protein by western blot we observed an overexpression in PC-hASCs exposed to H₂O₂, which was a 1.25-fold higher than HIF-1 α expression level of H₂O₂ incubated hASCs (Fig. 36).

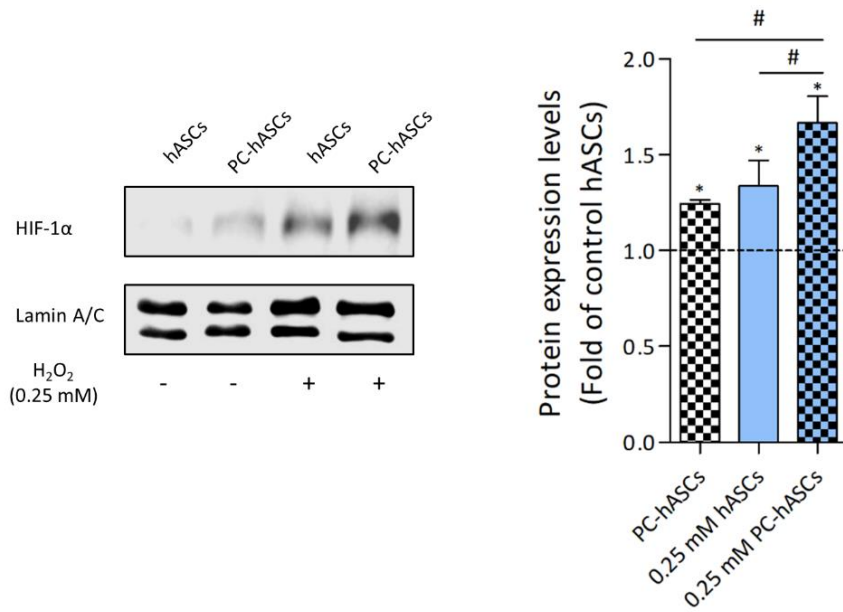


Figure 36. Expression and quantification of HIF-1 α . hASCs and PC-hASCs were exposed to 0.25 mM H₂O₂ for 1 hour, and lysed 24 hours after the insult. At least three different experiments were performed. Data were relativized to control hASCs (dotted line), and expressed as mean \pm SD. *p < 0.05, compared with control hASCs, #p < 0.05.

IV.2.1.3. ATP production

In addition, we analyzed the total rate of cellular ATP production as well as the fractional contribution from glycolysis and oxidative phosphorylation, simultaneously. Figure 37 revealed that oxidative stress decrease significantly ATP production, being this drop more acute on hASCs (decrease of $17 \pm 1\%$) than on PC-hASCs (decrease of $9.8 \pm 0.5\%$).

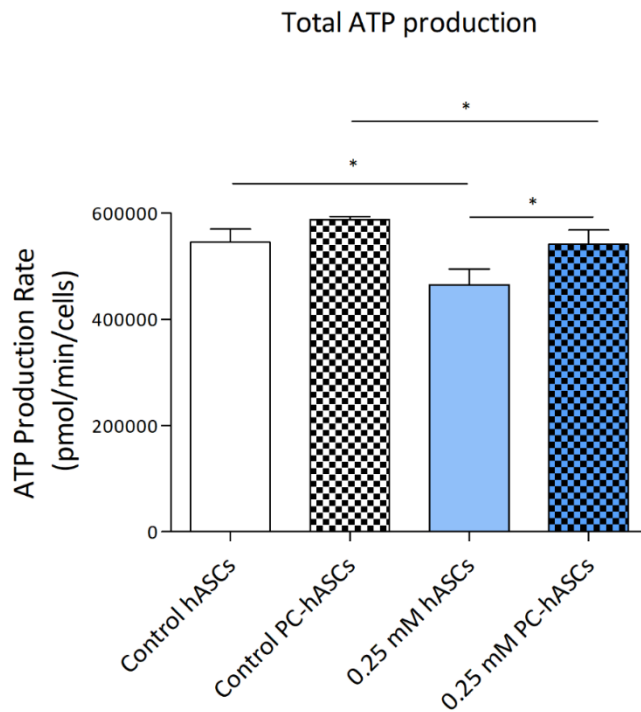


Figure 37. Total ATP production rate. Seahorse XF Real-Time ATP Rate Assay was performed in hASCs and PC-hASCs under control conditions or after 0.25 mM H₂O₂ exposure to quantify the ATP production. At least three different experiments were performed and data were expressed as mean \pm SD. * $p < 0.05$.

Similar results were obtained when analyzed the glycolytic ATP production (reduction of $17.5 \pm 0.9\%$ and $10.1 \pm 1\%$, respectively) which, as expected, was the main source of ATP for hASCs and PC-hASCs (Fig. 38).

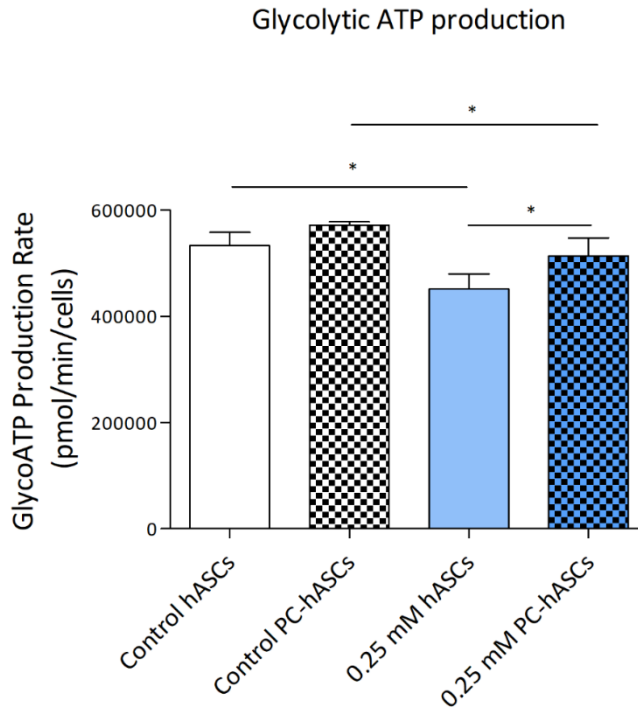


Figure 38. Glycolytic ATP production rate. Seahorse XF Real-Time ATP Rate Assay was performed in hASCs and PC-hASCs under control conditions or after 0.25 mM H₂O₂ exposure to quantify the ATP production. At least three different experiments were performed and data were expressed as mean \pm SD. *p < 0.05.

Finally, mitochondrial ATP production (which conformed around a 5% of the total ATP) was $19.2 \pm 1\%$ higher in PC-hASCs than in hASCs, and this increase became more remarkable when the cells were subjected to moderate oxidative stress (increase of $32.3 \pm 2\%$). Thus, whereas no significant differences were registered between control and H₂O₂ exposed hASCs, an increase of $22.9 \pm 2.3\%$ was detected in 0.25 mM H₂O₂ exposed PC-hASCs compared to their corresponding control (Fig. 39).

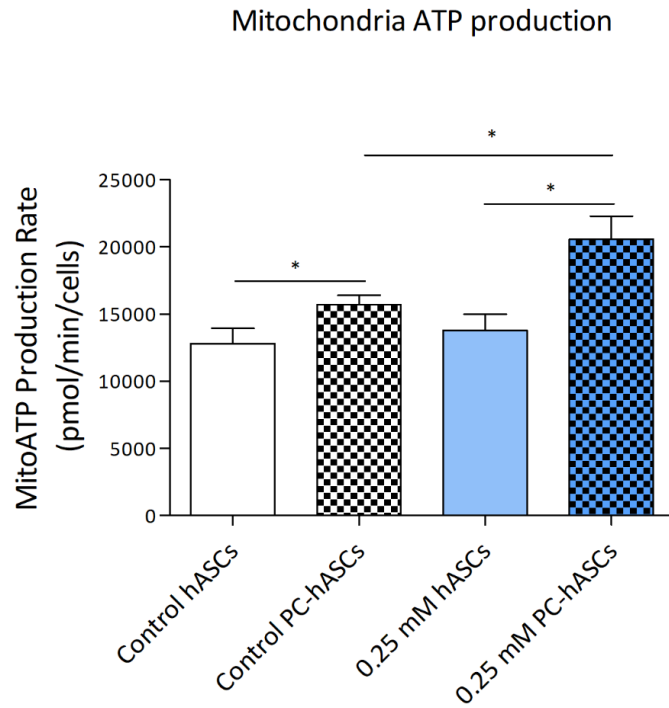


Figure 39. Mitochondrial respiration ATP production rate. Seahorse XF Real-Time ATP Rate Assay was performed in hASCs and PC-hASCs under control conditions or after 0.25 mM H₂O₂ exposure to quantify the ATP production. At least three different experiments were performed and data were expressed as mean \pm SD. *p < 0.05.

In this chapter, we have demonstrated that preconditioning enhances the antioxidant response of the hASCs, attenuates their expression of pro-inflammatory molecules and modulates the metabolism facilitating the adaptation to oxidative stress.

Taking all this into consideration, our next objective was to assess whether preconditioning is not only beneficial for the survival and adaptation of hASCs in stressful environments, but also an advantage when repairing damaged cells, thus promoting their reparative properties.

V. Chapter 3

Assessment of the effect of PC-hASCs and their CM on
an oxidative stress induced cellular damage model

Oxidative stress, associated with neuroinflammation, is a key process involved in the pathophysiology of neurodegenerative diseases such as Alzheimer's, Parkinson's or amyotrophic lateral sclerosis^{206,207}. Although oxidative stress affects any cell type of the organism, the high oxygen consumption and the limited antioxidant capacity of nervous tissue makes neurons and glia especially vulnerable to increased ROS levels²⁰⁸. In particular, oligodendrocytes, the myelin producing cells of the central nervous system (CNS), are remarkably vulnerable to oxidative stress due to their high metabolic rate and their low concentration of glutathione²⁰⁹. In a state of oxidative stress, oligodendrocytes may undergo irreversible damage of proteins, lipids and DNA, mitochondrial dysfunction, cell degeneration and death²¹⁰. These damages could be attenuated thanks to cell therapy.

Today, the use of MSCs is a potential therapeutic tool for neurodegenerative diseases. This therapeutic proposal is based on the immunomodulatory and neuroprotective/repair activity of MSCs, due to their antioxidant capacity and the release of anti-inflammatory cytokines, neurotrophic growth factors and components of the ECM^{211,212}. Although it is possible to obtain MSCs from different cell niches, it has been shown that the secretion of neurotrophic growth factors is greater in hASCs than in those derived from bone marrow (hBM-MSCs)²¹³, which may be due to the paracrine connection that exists between adipose tissue and the CNS²¹⁴. However, as previously stated, like other types of MSCs, hASCs have a low percentage of survival after transplantation at the site of injury⁷. To address this problem, we preconditioned the cells so that they resist harmful environmental factors, such as oxidative stress^{26,27}, in an attempt to improve their intrinsic antioxidant capacity and maintain their cytoprotective/repair properties.

Herein, we established an *in vitro* model of oxidative stress induced damage in oligodendrocyte-like cells and co-cultured them with PC-hASCs and their

conditioned media, in order to evaluate the therapeutic role of PC-hASCs and their derivatives.

V.2. Materials and methods

V.2.1. Cell culture

V.2.1.1. Human adipose-derived stem cells

In this part of the experimentation we also used hASCs as described in the section IV.1.1.

V.2.1.2. Human oligodendrogloma (HOG)

Human oligodendrogloma (HOG) was kindly donated by Dr. Glyn Dawson (University of Chicago, IL, USA). HOG is a clonal cell line derived from a surgically removed human oligodendrogloma, that in culture show a flat and epithelioid-like morphology that had limited resemblance with primary cultured oligodendrocytes (Fig. 40).

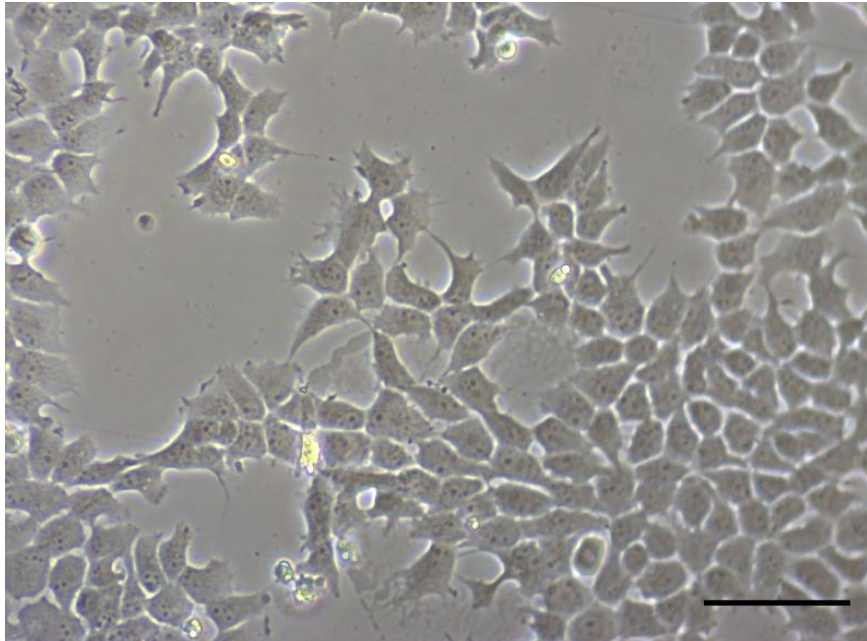


Figure 40. Phase contrast microscopy image of 80% confluent HOG cell line culture (scale bar: 100 μm).

HOG cells do not express the astrocyte marker glial fibrillary acidic protein (GFAP), but express several oligodendrocyte markers such as A2B5, myelin basic protein (MBP) and 2', 3'-cyclic nucleotide 3'-phosphodiesterase (CNPase) activity⁴³. These cells were maintained in DMEM (Dulbecco's Modified Eagle Medium, Gibco, Paisley, UK) supplemented with gentamicin (1 µl/ml), L-glutamine (Gibco, Paisley, UK), sodium pyruvate (Gibco, Paisley, UK) and a 10% of heat-inactivated FBS, and incubated at 37 °C in a saturated humidity atmosphere containing 5% CO₂. Cells were used until passage 15.

V.2.2. HOG differentiation

In this study, we differentiated HOG cell line to oligodendrocyte-like cells (HOGd). For their differentiation, the culture vessels were coated with poly-D-lysine (PDL, Sigma-Aldrich, St Louis, MO, USA) and HOG cell line was cultured at a 2.2×10^4 cells/cm² in complete media for 24 hours. Then, complete media was replaced by differentiation media (DM) containing high glucose (4.5 g/l) DMEM with N2 supplement, a chemically-defined, serum-free supplement based on Bottenstein's N-1 formulation (Life Technologies, Eugene, OR, USA), 30 nM triiodothyronine (T3, Sigma-Aldrich, St Louis, MO, USA) and 0.05% FBS, and cells were cultured for 9 days with three media refreshments (Fig. 41).

CHRONOGRAM OF HOG CELL LINE DIFFERENTIATION

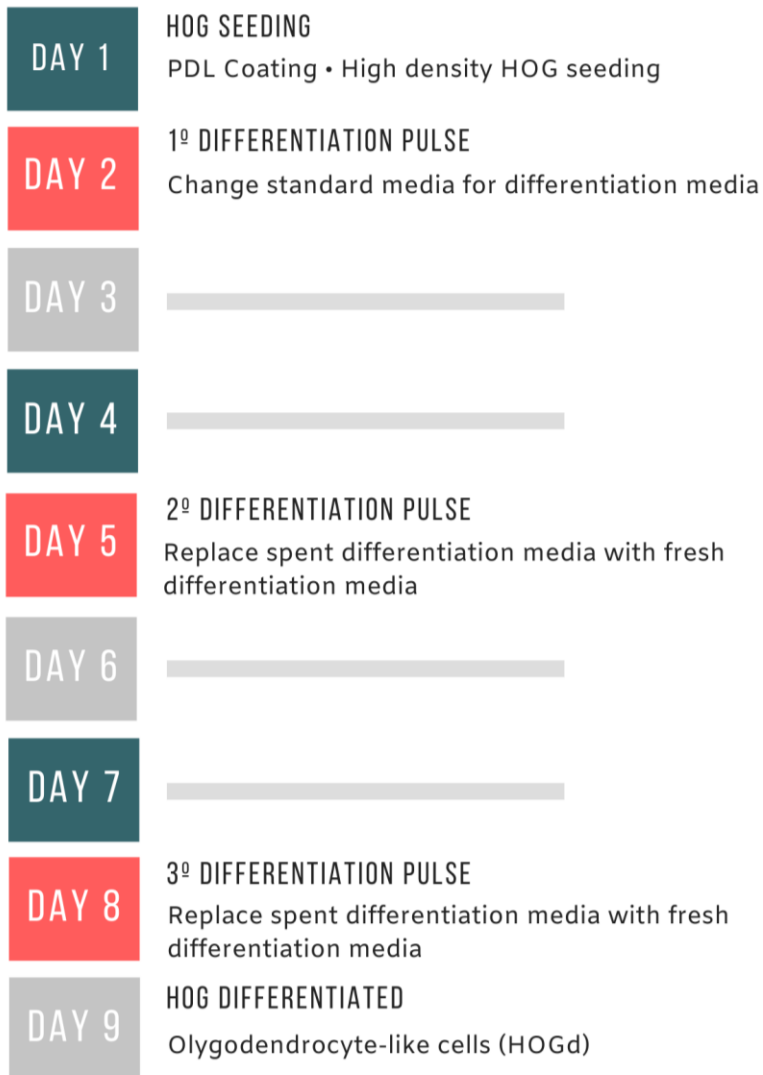


Figure 41. Chronogram of HOG cell line differentiation.

V.2.3. Immunofluorescence assay

For assessing HOG cells differentiation, an immunofluorescence assay to detect oligodendrocytes specific markers (MBP, CNPase and myelin oligodendrocyte glycoprotein, MOG) were performed. For this experiment, cells were seeded and differentiated in μ -Slide 8 well (Ibidi GmbH, Martinsried, Germany). Cells were fixed with 4% paraformaldehyde (PFA, PanReac AppliChem, Barcelona, Spain) for 15 minutes at RT and then incubated with PBS, containing 3% BSA and 0.1% Triton X-100, for 30 minutes at RT to permeabilize the cells and block non-specific protein-protein interactions. Subsequently, cells were incubated with primary antibodies o/n at 4°C. After washing three times with 1x PBS, cells were incubated with a secondary antibody for 1 hour at RT in the dark. Nuclei were counterstained with Hoechst 33342 (Abcam, Cambridge, UK). Finally, cells were washed three more times and observed under a Zeiss LSM800 confocal microscope (Carl Zeiss Inc, Chicago, IL, USA) using x20 objective. Antibodies used are listed below (Table 7).

Table 7. List of antibodies used in the immunofluorescence assay.

Primary Antibodies	Source	Dilution
MBP	GeneTex GTX133108	1:100
CNPase	GeneTex GTX103954	1:100
MOG	GeneTex GTX106283	1:100
Secondary Antibodies	Source	Dilution
Goat anti-Rabbit IgG Alexa 488	Invitrogen # A-11008	1:2000

V.2.4. Oxidative stress induction and co-culture

Oxidative stress conditions were achieved using a dose of 0.25 mM H₂O₂ according to previous experiments performed in our group²¹⁵. For the different experiments, HOG cells were seeded onto 24 (Sarstedt, Nümbrecht, Germany) or 6 well plates (Corning, Tewksbury, MA, USA). Once they reached 80% confluency, HOG cells were differentiated and then exposed to a 0.25 mM H₂O₂ insult for 1 hour in DMEM FBS free at 37 °C, in a humidified 5% CO₂ atmosphere. After that period, media were replaced with fresh DMEM FBS free. Subsequently, damaged HOGd (oxHOGd) were cultured with: *i*, hASCs or PC-hASCs conditioned media (CM); *ii*, hASCs or PC-hASCs; and *iii*, hASCs or PC-hASCs subjected to oxidative stress.

To obtain hASCs or PC-hASCs CM, cells were grown in T175 (Sarstedt, Nümbrecht, Germany) or T636 (Corning, Tewksbury, MA, USA) tissue culture flasks to 80% confluence, washed three times with 1x PBS and incubated for 48 hours in DMEM Glutamax™ FBS free. Then, the CM was centrifuged for 5 minutes at 250 g, filtered with a 0.2 µm filter (Filtropur S 0.2, Sarstedt, Nümbrecht, Germany) and stored at -20°C until used (Fig. 42).

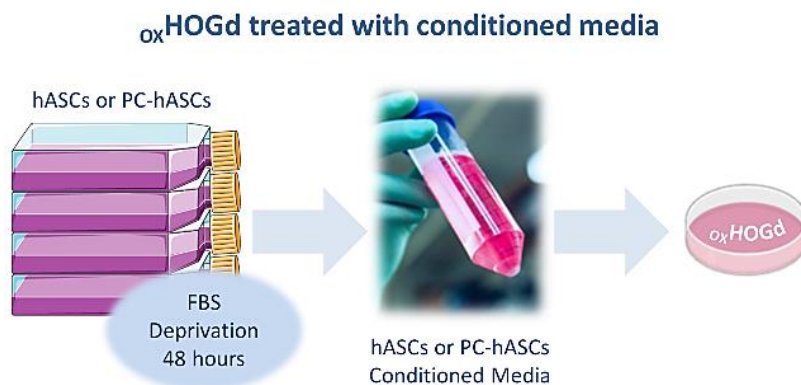


Figure 42. Visual representation of hASCs or PC-hASCs CM obtaining for oxHOGd treatment.

For the indirect co-cultures, hASCs or PC-hASCs were seeded onto cell culture inserts with 3 μm pore size (Nunc™, Life Technologies, Eugene, OR, USA) in 24 or 6 well plates at a concentration of 3×10^4 cells/ cm^2 . Cells were incubated in DMEM Glutamax™ with 10% FBS at 37 °C in a saturated humidity atmosphere containing 5% CO_2 to allow cell adhesion (2-4 hours). Once adhered to the insert, complete media was removed and hASCs or PC-hASCs were indirectly co-cultured with o_xHOGd . hASCs and PC-hASCs were co-cultured in normal conditions or after 1 hour 0.25 mM H_2O_2 oxidative stress insult (Fig. 43).

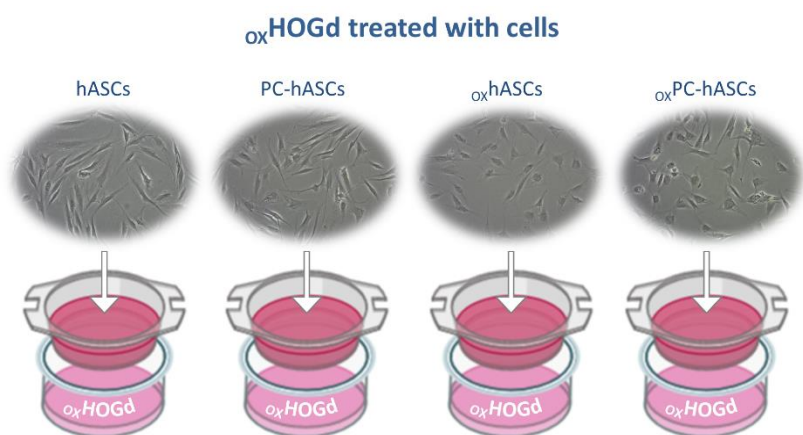


Figure 43. Visual representation of hASCs or PC-hASCs co-cultured with o_xHOGd , with or without oxidative stress induction.

V.2.5. Proliferation assay

Proliferation of o_xHOGd was assessed by viable cells quantification at 24 and 48 hours with PrestoBlue®, a resazurin-based solution that functions as a colorimetric cell viability indicator. At each time points, treated o_xHOGd cultured in 24 well plates were incubated with PrestoBlue® reagent following manufacturer instructions. The optical density (OD) was measured at λ 570 in a spectrophotometer. Results were relativized to control (HOGd) and expressed as the means \pm SD of at least three independent experiments performed in triplicates.

V.2.6. Measurement of ROS

$_{ox}HOGd$ intracellular levels of ROS were detected using H2-DFC-DA probe at 24 and 48 hours after the treatment. H2-DFC-DA is a chemically reduced form of fluorescein that upon cleavage of the acetate groups by intracellular esterases and ROS, is converted to highly fluorescent DCF. This probe was added to the cells at a final concentration of 10 μM , for 30 minutes at 37 °C. After this period, the fluorescent probe was removed and cells were washed with 1x PBS. Finally, intracellular ROS accumulation was measured in a microplate reader (λ_{ex} 492–495; λ_{em} 517–527 nm). Results were relativized to control ($_{ox}HOGd$) and represented as the means \pm SD of at least three independent experiments performed in triplicates.

V.2.7. Total antioxidant capacity assay

The Total Antioxidant Capacity Assay Kit (Abcam, Cambridge, UK) was used to determine the capability to counteract ROS of $_{ox}HOGd$ cultured alone or with *i*, hASCs or PC-hASCs conditioned media (CM), *ii*, hASCs or PC-hASCs, or *iii*, hASCs or PC-hASCs subjected to oxidative stress. The kit analyzes the concentration of small molecule antioxidants and proteins in the culture media. Briefly, after 24 hours of treatment, Trolox standard curve (4 – 20 nmol/well) was prepared and media of the different culture conditions were collected and diluted 1:2 in ddH₂O. Diluted fresh samples (100 μl) were mixed with Cu²⁺ working solution (100 μl) in a 96 well plate and incubated at RT for 90 minutes protected from light. Afterwards, the OD was measured at λ 570 nm in a spectrophotometer. Concentration of Trolox (nmol/ μl or mM) in the test samples is calculated as:

$$\text{Sample Total Antioxidant Capacity} = \frac{T_s}{S_v} \times D$$

where Ts is the total antioxidant capacity amount in the sample well calculated from standard curve (nmol), Sv is the sample volume added in the sample wells (μ l) and D is the sample dilution factor. Results were relativized to control (HOGd) and provided as the average of three different experiments (mean \pm SD) performed in duplicate.

V.2.8. Western blot analysis

To determine the expression of proteins of interest, cells were seeded onto 6 well plates or onto the inserts. After the HOG differentiation or 24 hours after the culture with *i*, hASCs CM or PC-hASCs CM; *ii*, hASCs or PC-hASCs; and *iii*, hASCs or PC-hASCs subjected to oxidative stress, cells were lysed in 1x Laemmli buffer (Sigma-Aldrich, St. Louis, MO, USA) and homogenized by sonication. Protein was quantified using a turbidimetric method based on TCA. Then, quantified protein lysates were boiled for 5 minutes for their denaturation. Denatured samples were loaded onto 10% SDS-PAGE gels and resolved by electrophoresis, using a SDS running buffer (25 mM Tris, 0.2 mM glycine, 0.1% SDS (w/v)) at 90 V, for 90 minutes in a Mini-Protean[®] 3 Cell. Resolved proteins were transferred onto nitrocellulose membrane at 380 mA, for 180 minutes at 4°C. Subsequently, nitrocellulose membranes were stained with Ponceau S solution to allow visibility of resolved proteins. Ponceau S solution was removed from the membranes by washing them with TBS-T (20 mM Tris, pH 7.5, 500 mM NaCl, 0.1% Triton X-100 (v/v)). Afterwards, membranes were blocked for 1 hour at RT in blocking buffer (5% skimmed milk in TBS-T) and then, were incubated overnight on a shaker at 4°C, with the corresponding primary antibody diluted in blocking buffer. Subsequently, membranes were washed 3 times with TBS-T for 10 minutes, incubated with secondary antibody for 1 hour at RT in blocking buffer and washed as before. Finally, membranes were visualized using SuperSignal West Pico PLUS Chemiluminiscent Substrate. Images were acquired

with the gel documentation system, G: Box Chemi and densitometry was performed with the ImageJ software. Densitometry values were then normalized to that of their corresponding loading controls. Resulting data were relativized to each control and results were provided as the average of at least three different experiments (mean \pm SD). Antibodies used are listed below (Table 8).

Table 8. List of antibodies used in the western blot analysis.

Primary Antibodies	Source	Dilution
MBP	GeneTex GTX133108	1:500
CNPase	GeneTex GTX103954	1:1000
MOG	GeneTex GTX106283	1:500
NRF2	GeneTex GTX103322	1:1000
HO-1	GeneTex GTX101147	1:1000
SOD-1	GeneTex GTX100554	1:1000
CAT	GeneTex GTX110704	1:1000
β -Actin	EMD Millipore ABT264	1:5000
Secondary Antibodies	Source	Dilution
Goat anti-Rabbit IgG	Thermo Fisher 65-6140	1:1000

V.2.9. Migration assay

To determine the migration ability of hASCs (subjected to oxidative stress or not) towards $oxHOGd$, cells which crossed the inserts pores were stained with crystal violet (Sigma-Aldrich, St Louis, MO, USA) at 24 and 48 hours after the oxidative stress insult. Co-culture plates were kept in the incubator up to 48 hours at 37 °C and 5% CO_2 to allow migration. At 24 and 48 hours, inserts were washed once with 1x PBS, and cells on the inner part of the insert membrane were removed

with a cotton swab. Migrated cells, located on the outer part of the insert, were fixed with 4% PFA, washed once in 1x PBS, and stained with crystal violet solution (1% crystal violet in 2% ethanol) for 2-5 minutes. The inserts were washed twice with dH₂O to remove unbound crystal violet and then air-dried. The migrated cells were observed and imaged (five fields per insert) under a microscope. For quantification, acetic acid (PanReac AppliChem, Barcelona, Spain) was diluted to 33% (v/v) with ddH₂O. The bound crystal violet was eluted by adding 400 μ L of 33% acetic acid into each insert and shaking for 10 minutes at RT. The eluent from the lower chamber was transferred to a 96 well plate and the absorbance at λ 590 nm was measured using a plate reader. Results were expressed as the means \pm SD of at least three independent experiments performed in triplicates.

V.2.10. Statistical analysis

The number of samples analyzed was described in each experiment. All data are shown as mean \pm SD. Statistical analysis was performed using GraphPad Prism statistical software (version 5.0; GraphPad Software). Significance was assessed using analysis of variance followed by Bonferroni's post hoc test and t-tests, as appropriate. Statistical differences were considered significant where $p < 0.05$. All the images shown in this thesis represent the data obtained, at least, in three independent experiments with similar results.

V.3. Results

V.3.1. HOG cells differentiation

In this study, we differentiated HOG cells to oligodendrocyte-like cells (HOGd). For their differentiation, HOG cell line was cultured in high glucose (4.5 g/l) DMEM with N2 supplement, 30 nM triiodothyronine (T3) and 0.05% FBS for 8 days. Differentiation was assessed by analyzing their morphology and by quantifying MBP, CNPase and MOG expression by an immunofluorescence assay and western blot analysis. The HOGd showed a different morphology than HOG cells; they exhibited extended branched processes and short membrane extensions (Fig. 44).

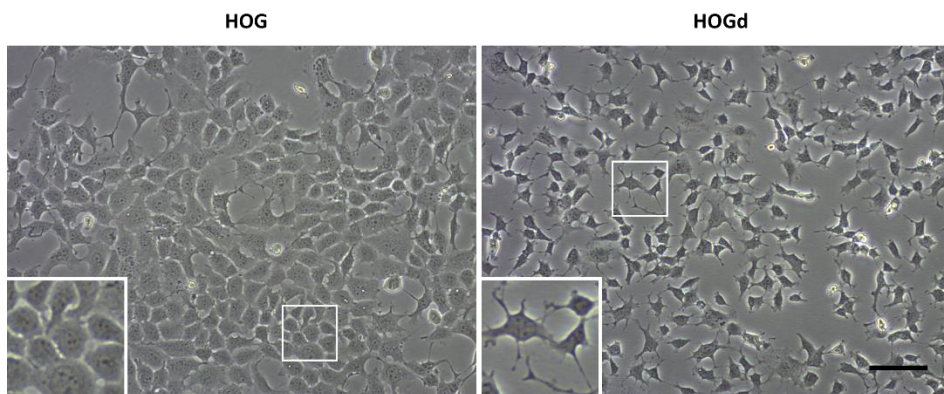


Figure 44. HOG cell line differentiation. Phase contrast images of HOG and HOGd cells. Differentiated cells showed short ramified processes. Scale bar: 100 μ m.

In addition to the differences in morphology, HOGd also showed higher expression of MBP, CNPase and MOG than HOG (Fig 45). MBP, the major structural component of myelin, was localized to the cytoplasmic surface of the plasma membrane as well as in the nucleus. CNPase, a membrane-associated enzyme in the myelin sheath, was also located in the cytoplasmic surface of the plasma membrane. Finally, MOG, a glycoprotein important in myelination, was located around the nucleus, maybe because it is synthesized in the endoplasmic

reticulum. The higher expression of these proteins showed by immunofluorescence was confirmed by western blot analysis.

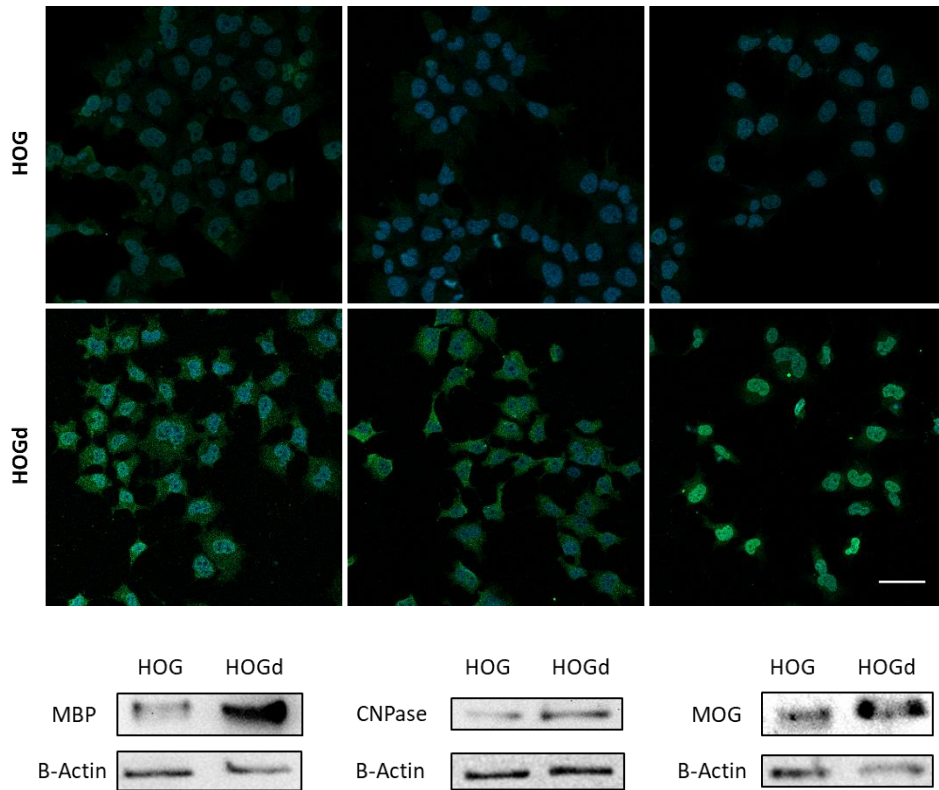


Figure 45. HOG cell line differentiation. Representative images of the expression of MBP, CNPase and MOG evaluated by immunofluorescence (scale bar: 50 μ m) and western blot. At least three different experiments were performed.

V.3.2. o_xHOGd repair

Once the HOG cells were differentiated, they were exposed to 0.25 mM H_2O_2 for 1 hour (Fig. X). After the oxidation, damaged HOGd (o_xHOGd) were cultured with: *i*, hASCs CM or PC-hASCs CM; *ii*, hASCs or PC-hASCs; and *iii*, hASCs or PC-hASCs subjected to oxidative stress, in order to analyze their cytoprotective effect. When exposed to 0.25 mM H_2O_2 , HOGd reduced their proliferation rate and increased intracellular ROS levels (Fig. 46).

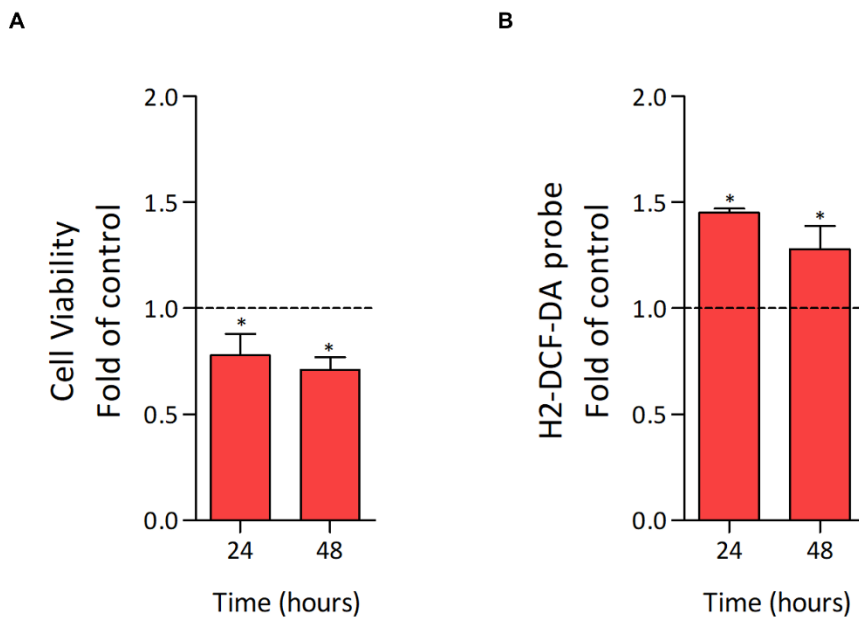


Figure 46. Effect of oxidative induction on o_xHOGd . (A) Cell viability, and (B) intracellular ROS levels after 24 and 48 hours of the H_2O_2 insult. Data are expressed as mean \pm SD and relativized to control (HOGd, dotted line). * $p < 0.05$, compared with o_xHOGd .

When cultured with hASCs CM or PC-hASCs CM, o_xHOGd viability reached the control values at 24 and 48 hours. The same occurred when o_xHOGd were co-cultured with hASCs or PC-hASCs at 24 hours, whereas at 48 hours the cell viability exceeded that of the control, being significantly higher when co-cultured with PC-hASCs (1.2-fold increase). Lastly, the effect of hASCs or PC-hASCs subjected to oxidative stress on o_xHOGd was evaluated. At 24 hours,

o_x HOGd viability was similar to that of the control, while at 48 hours o_x HOGd significantly proliferate more than the control (1.23 and 1.41-fold increase, respectively). Moreover, PC-hASCs subjected to oxidative stress significantly enhance o_x HOGd proliferation when compared to hASCs subjected to oxidative stress (1.15-fold increase; Fig. 47).

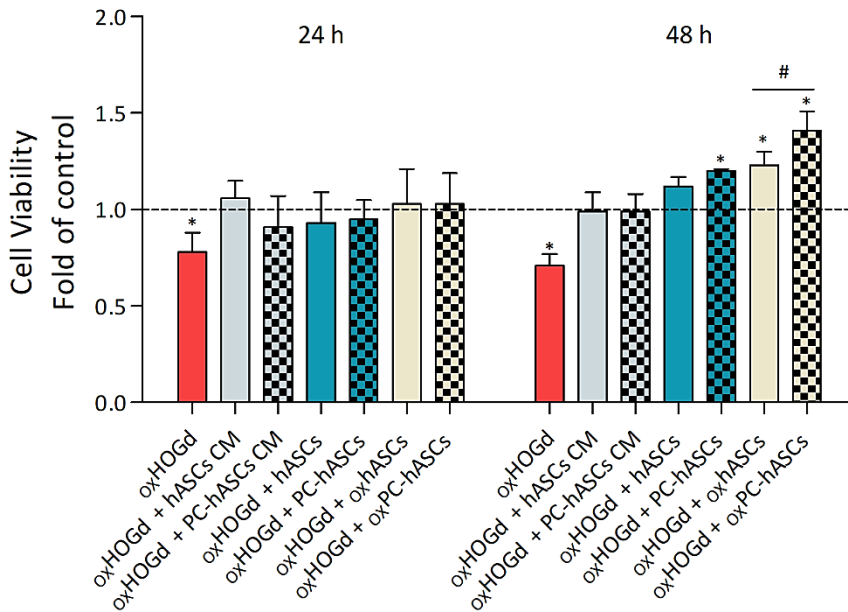


Figure 47. Reparative effect of hASCs and their derivatives on the o_x HOGd. The viability of o_x HOGd was measured at different time points (24 and 48 hours), alone or cultured with: *i*, hASCs CM or PC-hASCs CM; *ii*, hASCs or PC-hASCs; and *iii*, hASCs or PC-hASCs subjected to oxidative stress. Four different experiments were performed (n=3). Results were relativized to control (HOGd, dotted line) and expressed as mean \pm SD. *p < 0.05, compared with o_x HOGd, #p < 0.05.

Regarding intracellular ROS levels, o_x HOGd cultured with hASCs CM or PC-hASCs CM, reduced their intracellular ROS levels reaching to the control values at 48 hours. When co-cultured with hASCs or PC-hASCs, at 24 hours, the intracellular levels of ROS in o_x HOGd remained above control, while at 48 hours, a significant

reduction was observed respect to the control (1.17 and 1.25-fold decrease, respectively). Finally, oxHOGd co-cultured with hASCs or PC-hASCs subjected to oxidative stress was analyzed. On one hand, oxHOGd co-cultured with hASCs subjected to oxidative stress remained above the control at 24 hours and at 48 they reached the control. On the other hand, oxHOGd co-cultured with PC-hASCs subjected to oxidative stress reached the control values at 24 hours and reduced the intracellular ROS levels with respect to control at 48 hours (1.31-fold decrease). In fact, PC-hASCs subjected to oxidative stress significantly reduce the ROS levels when compared to hASCs subjected to oxidative stress, a 14% at 24 hours and a 24% at 48 hours (Fig. 48).

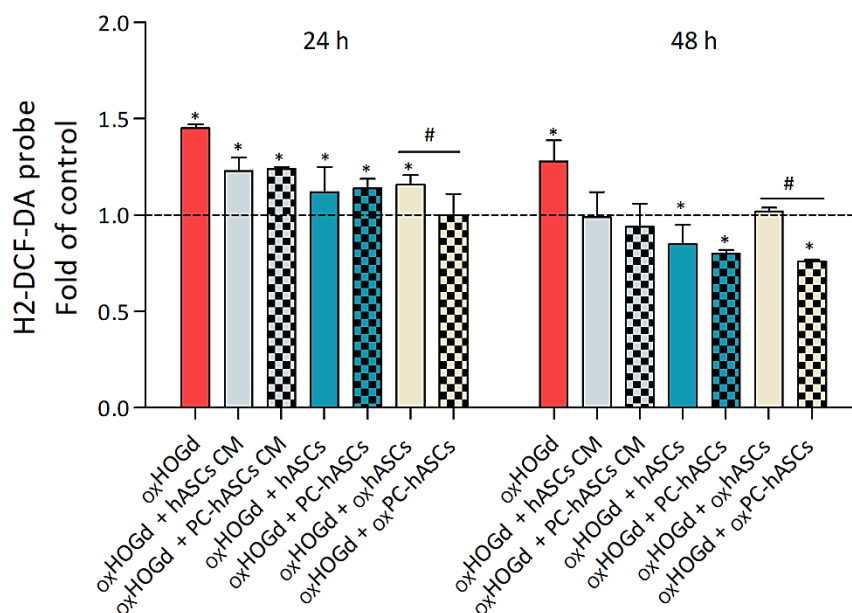


Figure 48. Reparative effect of hASCs and their derivatives on the oxHOGd . Intracellular ROS levels of oxHOGd were measured at different time points (24 and 48 h), alone or cultured with: *i*, hASCs CM or PC-hASCs CM; *ii*, hASCs or PC-hASCs; and *iii*, hASCs or PC-hASCs subjected to oxidative stress. Four different experiments were performed ($n=3$). Results were relativized to control (HOGd, dotted line) and expressed as mean \pm SD. * $p < 0.05$, compared with oxHOGd , # $p < 0.05$.

V.3.3. Antioxidant capacity

Once evaluated the reparative effect of hASCs and their derivatives on the oxHOGd , the antioxidant capacity of both cell types was analyzed. For the analysis of secretion of small molecule antioxidants and proteins in the culture media of oxHOGd alone or cultured with: *i*, hASCs CM or PC-hASCs CM; *ii*, hASCs or PC-hASCs; and *iii*, hASCs or PC-hASCs subjected to oxidative stress, the Total Antioxidant Capacity Assay Kit was used at 24 hours after the H_2O_2 insult. Results showed that oxHOGd alone secreted less antioxidant molecules to the media than the control (1.16-fold decrease), and the media of oxHOGd cultured with hASCs CM or PC-hASCs CM showed values similar to those of the control. When oxHOGd were co-cultured with hASCs or PC-hASCs, the media exhibited an antioxidant molecules concentration higher to that of the control although not significant; the same occurred when co-cultured oxHOGd with hASCs subjected to oxidative stress, whereas the co-culture of oxHOGd with PC-hASCs subjected to oxidative stress secreted a significantly higher amount of antioxidant molecules to the media (1.27-fold higher than the control and 1.15-fold higher than the co-culture of oxHOGd with hASCs subjected to oxidative stress; Fig. 49).

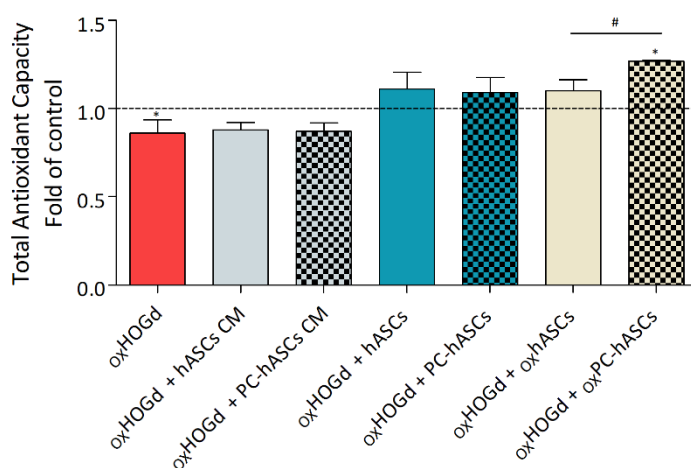


Figure 49. Total antioxidant capacity (TAC) of the culture media. oxHOGd secretion of small molecule antioxidants and proteins in the culture media was measured with the Total Antioxidant

Capacity Assay Kit at 24 hours, alone or cultured with: *i*, hASCs CM or PC-hASCs CM; *ii*, hASCs or PC-hASCs; and *iii*, hASCs or PC-hASCs subjected to oxidative stress. Four different experiments were performed ($n=3$). Results were relativized to control (HOGd, dotted line) and expressed as mean \pm SD. * $p < 0.05$, compared with $\text{oxHOGd} + \text{hASCs}$, # $p < 0.05$.

Since the analysis of the total antioxidant capacity did not distinguish between the antioxidant response of HOGs or ASCs, protein analysis of both cells types was performed separately, determining the expression of different antioxidant proteins by western blot. In first place, the expression of NRF2, HO-1, SOD-1 and CAT in HOGd under the different conditions was analyzed (Fig. 50).

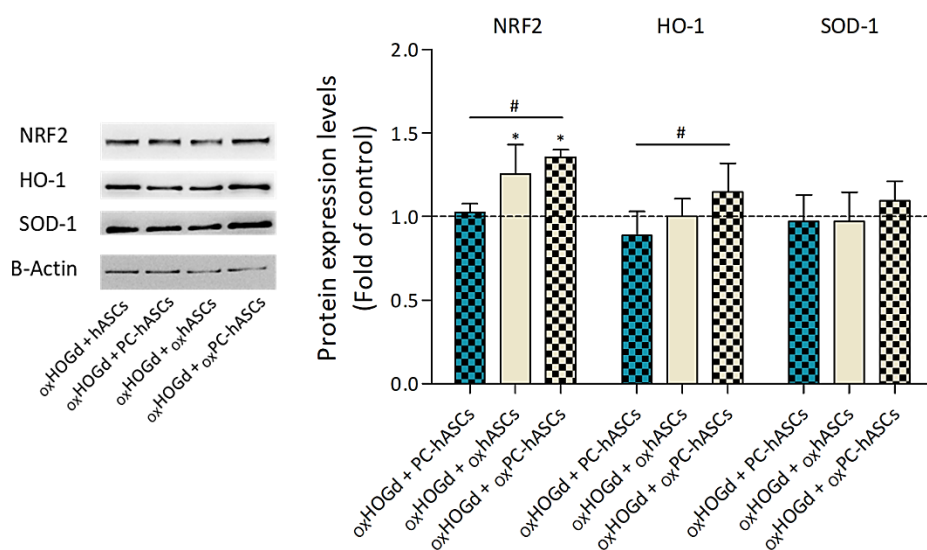


Figure 50. Expression and quantification of NRF2, HO-1 and SOD-1 in oxHOGd . HOGd were exposed to 0.25 mM H_2O_2 for 1 hour, cultured with: *i*, hASCs or PC-hASCs; and *ii*, hASCs or PC-hASCs subjected to oxidative stress, and lysed 24 hours after the insult. At least three different experiments were performed. Data were relativized to control ($\text{oxHOGd} + \text{hASCs}$, dotted line), and expressed as mean \pm SD. * $p < 0.05$, compared with $\text{oxHOGd} + \text{hASCs}$, # $p < 0.05$.

The results revealed that when co-cultured with hASCs or PC-hASCs, oxHOGd exhibited a similar expression of NRF2, HO-1 and SOD-1. In regard to oxHOGd co-cultured with hASCs or PC-hASCs subjected to oxidative stress, a significant

enhance in NRF2 expression was observed (1.25 and 1.35-fold increase, respectively), although there were no significant differences between them. Concerning HO-1 and SOD-1, no significant augmentation was found, but a slight increase is noticed in the cells co-cultured with PC-hASCs subjected to oxidative stress (Fig.50). CAT was not expressed in HOGd under any of the culture conditions.

After evaluating the antioxidant proteins expression in oxHOGd under the different conditions, NRF2, CAT, HO-1 and SOD-1 expression were assessed in hASCs, PC-hASCs and hASCs and PC-hASCs subjected to oxidative stress co-cultured with oxHOGd .

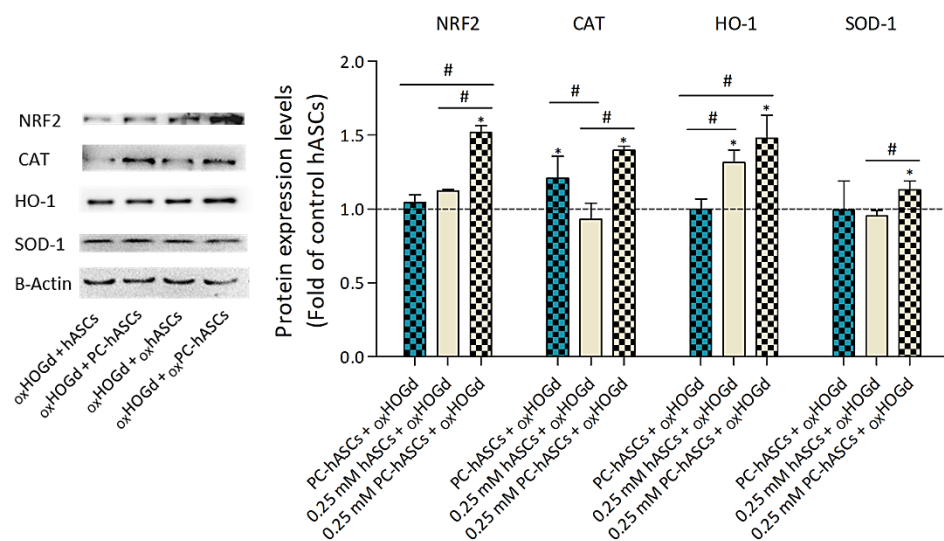


Figure 51. Expression and quantification of NRF2, CAT, HO-1 and SOD-1 in hASCs. hASCs, PC-hASCs and hASCs and PC-hASCs subjected to oxidative stress co-cultured with oxHOGd were lysed 24 hours after the insult. At least three different experiments were performed. Data were relativized to control (oxHOGd + hASCs, dotted line), and expressed as mean \pm SD. * $p < 0.05$, compared with oxHOGd + hASCs, # $p < 0.05$.

After 24 hours of co-culture, the expression of NRF2 in hASCs and PC-hASCs was almost the same, whereas when hASCs and PC-hASCs were subjected to 0.25 mM H₂O₂ an increase in nuclear Nrf2 expression was produced (1.12 and 1.51-fold higher, respectively), being this increment 1.35-fold higher in PC-hASCs compared to hASCs. In contrast to what was observed in the HOGd, CAT did express in the hASCs samples. In fact, it was significantly overexpressed in both, PC-hASCs and PC-hASCs subjected to oxidative stress when compared to hASCs (1.2 and 1.4-fold increase, respectively). In the case of HO-1, hASCs and PC-hASCs exhibited a similar expression, that was increased when the cells were subjected to oxidative stress (1.31 and 1.47-fold increase, respectively). Last but not least, SOD-1 expression was also similar in hASCs and PC-hASCs. When exposed to oxidative stress, the expression of SOD-1 increased in PC-hASCs (1.31-fold increase), whereas the expression in hASCs remained similar to control (Fig. 51).

V.3.4. Homing ability

One aspect of the reparative activity of hASCs is their ability to migrate towards the site of injury (homing). To determine whether the preconditioning promotes migration of hASCs and thus their therapeutic capacity, cells were cocultured in transwells with oxHOGd . Results showed that at 24 hours, hASCs and PC-hASCs subjected to oxidative stress or not, have already crossed the transwells pores towards the oxHOGd seeded below (Fig.52). When subjected to oxidative stress, both hASCs and PC-hASCs reduced their homing ability compared with the nonoxidizing cells (4.9 ± 0.6 and $5.9 \pm 0.5\%$, respectively). However, whether subjected to oxidative stress or not, PC-hASCs migrated more than hASCs (4.6 ± 0.7 and $5.6 \pm 0.6\%$, respectively; Fig. 54).

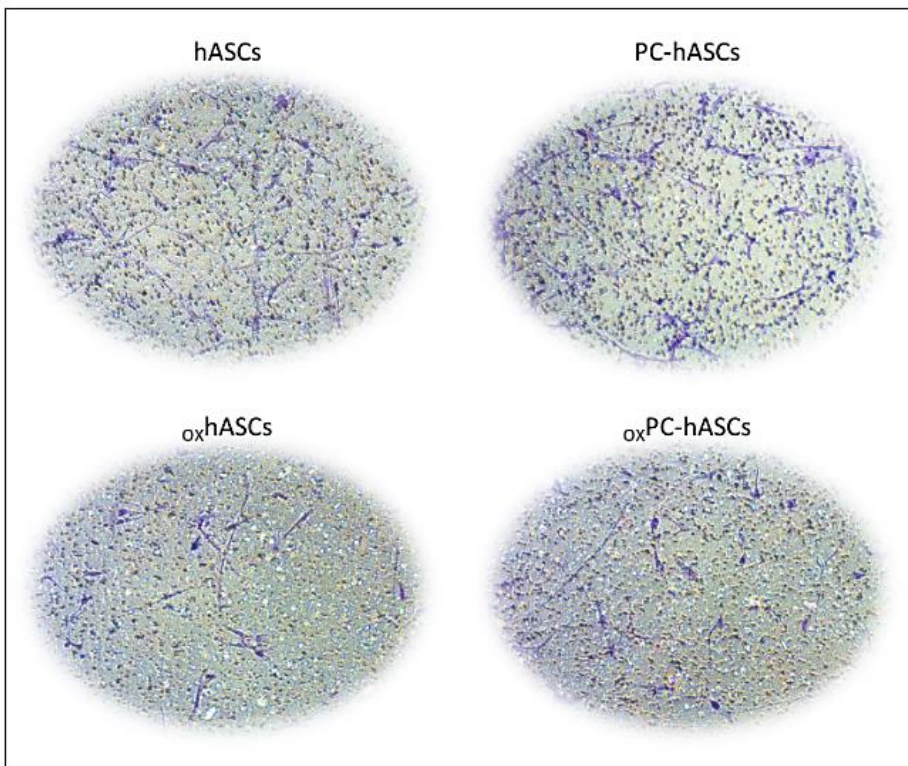


Figure 52. Migration ability of hASCs, PC-hASCs, and hASCs and PC-hASCs subjected to oxidative stress towards oxHOGd at 24 hours after the co-culture. Representative images of phase contrast microscopy (x10 objective). At least three different experiments were performed.

Similar results were obtained at 48 hours after the coculture, as shown in figure 53, hASCs and PC-hASCs seemed to respond faster to the chemoattractant molecules released by the $_{ox}$ HOGd when they have not been exposed to H_2O_2 . Also, as at 24 hours, the PC-hASCs demonstrated to migrate more than the hASCs, both in standard and oxidative stress conditions (9.4 ± 0.6 and $9.0 \pm 0.6\%$, respectively; Fig. 54).

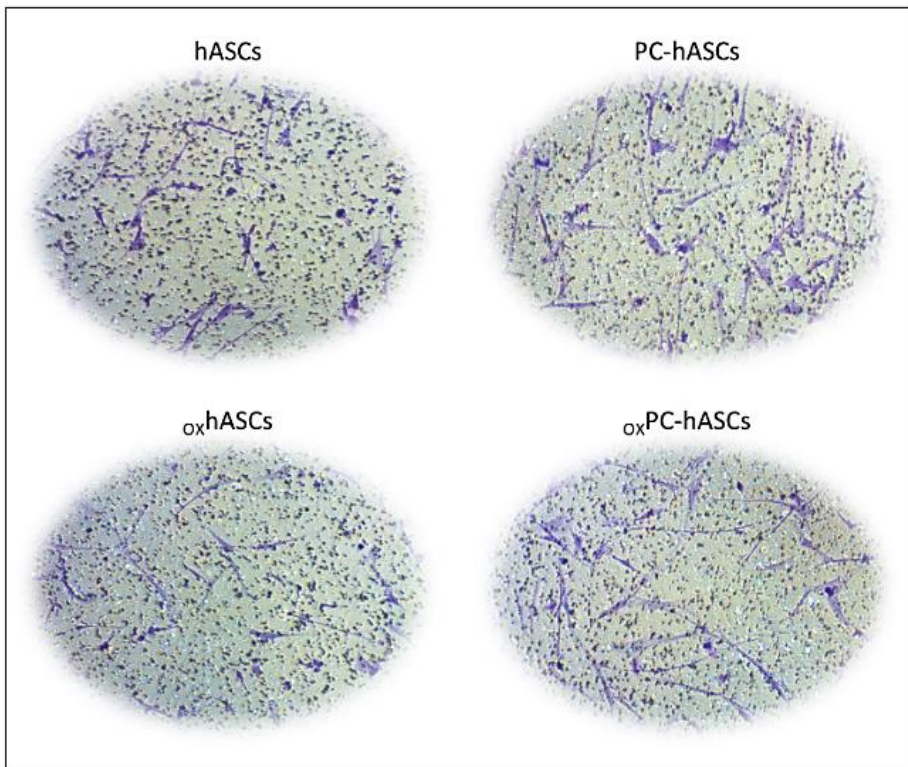


Figure 53. Migration ability of hASCs, PC-hASCs, and hASCs and PC-hASCs subjected to oxidative stress migration towards $_{ox}$ HOGd at 48 hours after the co-culture. Representative images of phase contrast microscopy (x10 objective). At least three different experiments were performed.

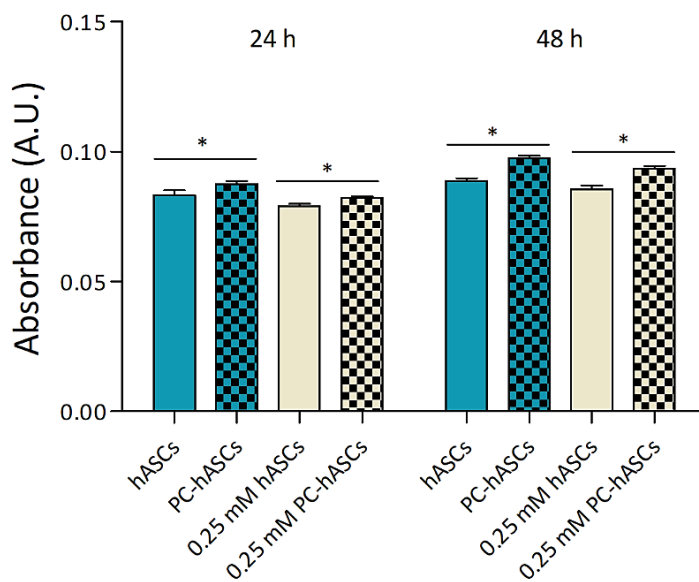


Figure 54. Quantification of hASCs, PC-hASCs and hASCs and PC-hASCs subjected to oxidative stress migration towards $oxHOGd$ at 24 and 48 hours after the co-culture. At least three different experiments were performed. Data are expressed as mean \pm SD. * $p < 0.05$.

VI. Discussion

MSCs therapeutic efficacy is limited due to the low percentage of cell survival and subsequently, their poor engraftment at the site of injury⁷. For this reason, MSCs preconditioning has emerged as one of the main strategies to tackle this situation and improve their therapeutic effectiveness³. Since one of the main reasons why MSCs die following engraftment is ROS-mediated-oxidative stress²⁶, several studies have already focused on the beneficial effect of preconditioning cells with sub-lethal doses of H₂O₂ [1-100 μM]. H₂O₂ is a reactive oxygen species that is present in inflammatory processes, where it acts as a second messenger activating different metabolic pathways involved in tissue repair. However, at high concentrations, it becomes detrimental as it easily transforms through the Fenton reaction into ·OH, a highly reactive molecule. For this reason and its great ability to diffuse freely through cell membranes, H₂O₂ has been used widely as an agent inducing oxidative stress in various investigations involving MSCs. Taking this into consideration, Li et al. preconditioned human UC-MSCs with low doses of H₂O₂ and demonstrated an enhanced oxidative stress resistance¹⁹⁴. H₂O₂ preconditioning also demonstrated to protect rat BM-MSCs against *in vitro* apoptosis¹⁹⁵. In the same way, it has been described that preconditioned human Wharton jelly-MSCs increase survival after exposure to toxic levels of H₂O₂ by overexpression of hypoxia-inducible factor (HIF)-1α¹⁹⁶. In addition, we previously have reported that H₂O₂ preconditioning provided hASCs a significantly faster recovery capacity post-thaw and an enhanced capacity to respond to oxidative stress and nutrient deprivation³². Besides, these cells have demonstrated to exert neuroprotective effects in a rat model of acute spinal cord injury²¹⁶. However, the exact mechanisms underlying MSCs preconditioning remain to be fully understood. In the current study, we evaluated the preconditioning effect of low doses (10 μM) of H₂O₂ on hASCs behavior, thus elucidating molecular and bioenergetic mechanisms underpinning the survival and adaptation of these cells in an oxidative stress environment and their therapeutic effect. Firstly, this

VI. Discussion

work demonstrates that preconditioning does not affect cell parameters such as morphology, senescence, cell cycle or proliferation, which indicated that PC-hASCs did not differ from hASCs behavior under normal conditions. However, there are differences in the proteomic profile as around 1% of the proteins are differentially expressed. Although this is not a big change, these differentially expressed proteins play important roles in various cellular processes, such as metabolism, cell signaling or oxidative stress response, which shed light on which mechanisms may be affected by the H₂O₂ preconditioning.

Secondly, we were interested in studying the response of these cells to oxidative stress, since it is one of the main stressors in the tissue damage site. Therefore, in this study, we administered H₂O₂ directly in the culture medium at two different concentrations (0.25 or 0.5 mM) to induce oxidative stress in the cells. The H₂O₂ remained in contact with the cells for 1 hour, during which ROS levels increased in a time- and dose-dependent manner. However, ROS levels in PC-hASCs were significantly lower than in hASCs, which together with the fact that apoptosis rate and the percentage of cytotoxicity were reduced compared to non-preconditioned cells indicates that PC-hASCs tolerated better the exposure to different concentrations of H₂O₂ than hASCs. This resistance to H₂O₂ was more evident when cells were subjected to a concentration of 0.25 mM, and considering that this concentration is similar to that observed in inflammatory processes^{33,217}, from this point we used this concentration for the remaining experiments.

The resistance of these cells to oxidative stress, and therefore their increase in survival, is probably due to the activation of different signaling pathways. Given the fact that our studies are based on an oxidative stress model, we focused our attention on NRF2-ARE signaling pathway, a major cellular mechanism to reduce oxidative stress. NRF2 is a transcription factor that regulates the expression of genes coding for antioxidant, anti-inflammatory, and detoxifying proteins, and

it has been extensively studied that its modulation influenced the survival, apoptosis and ROS production in MSCs²¹⁸⁻²²⁰. MSCs are known to have constitutive expression of enzymes required to manage oxidative stress²²¹ and our results showed that this expression can be enhanced with H₂O₂ preconditioning. When compared with non-preconditioned hASCs, PC-hASCs exhibited a higher expression of NRF2 and antioxidant enzymes related to this transcription factor (HO-1, SOD-1, GPx-1, and CAT) upon oxidative stimulation. Although an increase in the expression of all the antioxidant enzymes studied was observed, the increase in GPx1 expression was the most prominent. GPX-1 is a selenoprotein that catalyzes the reduction of H₂O₂ to water using GSH as a reductant²²², which could indicate that preconditioned cells stimulated with H₂O₂ have a higher concentration of GSH. Altogether, these results suggested that the antioxidant status of PC-hASCs is probably responsible for the increase in cell survival capacity against oxidative stress. This increase in the antioxidant response is also related to an attenuation of the proinflammatory response. In fact, we have seen that the overexpression of NRF2 occasioned by the H₂O₂ preconditioning may be responsible for the down-regulation of NF-κB signaling pathway observed in PC-hASCs, which is consistent with previous reports. Hence, Lin et al. pre-stimulated NRF2 in primary peritoneal macrophages and observed a reduction of the production of COX-2, TNFα, iNOS (inducible nitric oxide synthase) and IL-1β in response to lipopolysaccharide (LPS)²²³. Similarly, the NRF2-mediated increase of HO-1 expression inhibited NF-κB activity in pre-stimulated PC3 cells²²⁴ and consistently, mouse embryo fibroblasts (MEFs) from NF-κB-p65-knock-out mice showed a reduced mRNA and protein levels of NRF2 as well as the protein levels of HO-1²²⁵. Therefore, our results imply that PC-hASCs might regulate H₂O₂ induced inflammatory responses and oxidative stress *via* attenuating the activation of NF-κB and the proinflammatory molecules COX-2 and IL-1β and promoting the expression of NRF2, and consequently, the transcription of antioxidant and detoxification enzymes. Additionally, the

VI. Discussion

expression of p-AKT and p-ERK was evaluated to determine if they were related to the PC-hASCs increased survival as they are known to react to oxidative stress^{34–36}. Our results showed that oxidative stress increased p-AKT expression in both, hASCs and PC-hASCs. This increase in the AKT phosphorylation could be related to the up-regulation of anti-apoptotic proteins³⁷, however, no differences between hASCs and PC-hASCs were observed. Regarding p-ERK, we observed a decrease upon H₂O₂ stimulation. This reduction in ERK phosphorylation was more noticeable in preconditioned cells, which may be attributed to the increase in their antioxidant response. It has been demonstrated that oxidative stress induces ERK phosphorylation leading to the activation of NF- κ B³⁸, however, the increased antioxidant response of PC-hASCs may attenuate the expression of p-ERK, under oxidative stress conditions, and thus reduce the expression of NF- κ B. Nonetheless, further studies need to be performed to confirm this hypothesis.

To support this enhanced antioxidant response against oxidative stress, cells need to adapt their cellular metabolism. Metabolism not only provide energy for cell survival and proliferation, but also play an important role in cell signaling and adaptation to the immediate environment²³. Although the beneficial effects of H₂O₂ preconditioning in MSCs have already been described, to our knowledge, this is the first report that evaluates how it affected the bioenergetic adaptation of hASCs in an oxidative stress situation. In this work, we studied the two major metabolic pathways, mitochondrial respiration and glycolysis, under standard and oxidative conditions. MSCs have a mixed metabolism, utilizing both glycolysis and oxidative phosphorylation for ATP generation, relying mainly in the glycolytic pathway^{39–41}. The current study confirmed these previous observations, as around a 95% of the total ATP production of these cells resulted from glycolysis. It seems that MSCs prefer to produce energy by glycolysis to avoid the production of ROS by mitochondrial respiration²²⁶. When subjected

to oxidative stress, ATP production decreased significantly in both, PC-hASCs and hASCs, being this drop more acute on hASCs (decrease of 17%) than on PC-hASCs (decrease of 10%). When analyzing both pathways separately, we observed that after the H₂O₂ insult, PC-hASCs exhibited a 1.8-fold increase in basal respiration and 1.4-fold increase in maximal respiration when compared to oxidized hASCs. Although ROS are generated by various organelles, mitochondria are the main source of cellular oxidants, and therefore, the principal site for the potential overproduction of ROS⁴². Under oxidative stress conditions, hASCs seem to limit mitochondrial activity in an attempt to reduce intracellular ROS levels, whereas PC-hASCs increase such mitochondrial activity as they count with a higher concentration of antioxidants that can counteract ROS. This evidence has been further supported by PC-hASCs mitochondria morphology that presented a more mature and elongated shape, typical of active mitochondria, which correlates with a higher respiration rate, and higher MMP values. Besides, PC-hASCs seemed to increased mitochondrial mass and developed a strongly interconnected network uniformly distributed through the cytoplasm, suggesting potentiation of fusion processes, probably to enhance the ATP production. However, OXPHOS metabolic pathway comprises only around 5% of MSCs metabolism, so the study of glycolysis was necessary to understand the effect of preconditioning on energy metabolism.

After the oxidative stress insult, we observed that basal glycolysis was significantly decreased. This reduction was more noticeable in hASCs, which led us to investigate underlying mechanisms that might be activated to counteract oxidative stress and enhance glycolysis in PC-hASCs. HIF-1 α is known to be a key factor that codes for proteins related to glycolytic energy metabolism, not only under hypoxia but also under normoxia conditions^{227,228}. Recent studies have shown that HIF-1 α silencing decreases cellular glycolytic capacity, independently of mitochondrial respiration²²⁹. Additionally, Del Rey et al.,

VI. Discussion

observed an increase in apoptotic markers and a significant reduction of cell viability after HIF-1 α knockdown under normal O₂ conditions ²³⁰, which provide strong evidence that HIF-1 α has an important role in cell proliferation and survival processes. Moreover, some studies have pointed out the importance of aerobic glycolysis in normal proliferating cells as a mechanism for minimizing oxidative stress ²³¹ considering that pyruvate, generated by glycolytic metabolism, can be an efficient scavenger of ROS and therefore can protect cells from oxidative stress ²³². Regarding the aforementioned and that HIF-1 α can be activated by ROS under normoxia ^{233,234}, we analyzed the HIF-1 α expression and detected an enhancement in PC-hASCs compared to hASCs, both under stress conditions. This result suggests that preconditioning activates HIF-1 α , thus increasing basal glycolysis upon oxidative stimuli, probably as a mechanism to reduce intracellular ROS levels. Nevertheless, further analysis will be necessary to identify the specific pathways regulated by HIF-1 α .

Besides demonstrating the role of preconditioning in hASCs adaptation to stress along with two of the mechanisms mediating this action, namely, their antioxidant activity and metabolic plasticity, we explored whether preconditioned cells or their derivatives (CM) exhibited enhanced therapeutic properties on an oxidative stress induced-damage model. Particularly and taking into account the relationship between hASCs and nervous tissue ²¹³, for this study we use an oligodendroglial model.

Oxidative stress plays a fundamental role in the pathophysiology of neurodegenerative disorders such as multiple sclerosis, Alzheimer's disease or stroke. It induces demyelination and neurodegeneration by direct oxidation of lipids, proteins, and DNA, as well as by the induction of mitochondrial damage and subsequent alteration of energy metabolism. It affects different cells of the CNS, but oligodendrocytes, glial cells with great impact on brain development and neuronal function, are most vulnerable mainly due to their low antioxidant

defenses²³⁵. Over the years, many neuroprotective agents have been tested to protect cells against oxidative stress and prevent the neuronal loss, but clinical trials aiming to ameliorate brain injury have failed or been only partially successful²³⁶. Recently, cell therapy with MSCs has emerged as one of the most promising strategies for the treatment of neurodegenerative diseases. Their great antioxidant capacity¹⁰⁴, homing ability⁹² and paracrine effects¹¹² make them good candidates for treating CNS pathologies associated with oxidative stress. Previous studies have demonstrated that MSCs have a protective effect on CNS^{237–239}. In fact, it has been shown that the secretion of neurotrophic growth factors is greater in hASCs than in hBM-MSCs²¹³, which may be due to the paracrine connection that exists between adipose tissue and the CNS²¹⁴. However, MSCs poor survival after transplantation is still a disadvantage and for this reason, many studies are focused on using MSCs secretome^{240,241}. MSCs are known to synthesize and secrete multiple bioactive factors that modulate the action of adjacent cells increasing angiogenesis, survival, migration, and differentiation; reducing apoptosis, fibrosis, and oxidative stress; restricting local inflammation; and adjusting immune responses^{6,117,122}. Nonetheless, the fact that MSCs can dynamically change bioactive factors composition in response to various pathologies and environmental stimuli must be taken into consideration, because depending on the environment or the pathology they face, MSCs generate a specific molecular expression response through the activation of different pathways¹¹⁹. Therefore, here we have investigated the therapeutic role of PC-hASCs CM and PC-hASCs themselves to overcome the deleterious effect of oxidative stress in an oligodendroglial population.

To do this, we selected the HOG cell line, in which differentiation towards oligodendrocyte-like cells (HOGd) was induced by culturing the cells with high glucose DMEM, N2 supplement, 30 nM T3, and 0.05% FBS, for 8 days. Although primary cultures of human oligodendrocytes have been used in different

VI. Discussion

studies, these studies are hampered by the limited availability of viable human brain tissue⁴³. For this reason, it was necessary to develop a study model that allowed an unlimited supply of cells with characteristics similar to those of human oligodendrocytes. The protocol for the differentiation of HOG cells to oligodendrocyte-like cells worked well, HOGd exhibited extended branched processes and short membrane extensions, a decrease in proliferative activity, and an increase in the expression of oligodendrocyte markers, MBP, CNPase and MOG, which were consistent with already published reports^{43–46}. Once the differentiation protocol was established and a stable culture of HOGd was obtained, the effect of oxidative stress on these cells was studied. Here, we used as an oxidative stress induction model the administration of a single dose of 0.25 mM H₂O₂, for 1 hour. This model has allowed us to analyze, in the first place, the effect of oxidation on cell viability and proliferation, as well as on the intracellular levels of ROS. As expected, the H₂O₂ insult caused a decrease in cell viability, which was in accordance with the significant increase observed in intracellular ROS levels. Secondly, once the effect of oxidation on HOGd was evaluated, the therapeutic role of PC-hASCs, both through their CM and indirect co-culture, was assessed to overcome the deleterious effect of oxidative stress in the oligodendroglial population. In the first case, in the presence of CM of both hASCs or PC-hASCs, the population of HOGd subjected to oxidative stress regained its viability to levels similar to those of control cells, and at 48 hours, the intracellular ROS levels were significantly reduced. This effect was more pronounced when oxHOGd were indirectly co-cultured with hASCs or PC-hASCs. As a matter of fact, at 48 hours, intracellular ROS levels of oxHOGd were significantly reduced and cell viability exceed that of the control. Other authors have obtained similar results with MSCs obtained from other tissues, indicating that MSCs exerted a proliferative stimulus on other cell populations undergoing oxidative stress²⁴². Although the two strategies, CM and indirect co-culture, displayed reparative effects on oxHOGd, cells co-culture resulted in a better

restoration of oxHOGd functions than CM. This may suggest that the presence of oxHOGd is needed to stimulate MSCs to produce the required/specific factors for oxHOGd recovery. Supporting this, Fitzpatrick et al. showed that culture of hepatocytes (HCs) in medium previously conditioned by co-culturing HCs and MSCs demonstrated improved cell functionality, whereas HCs cultured in medium conditioned by MSCs alone showed no effect ²⁴³. Finally, among the different co-cultures, the oxHOGd co-cultured with PC-hASCs also subjected to oxidative stress showed a better recovery by further enhancing the viability (1.4-fold of control) and reducing ROS levels (1.3-fold of control). As previously demonstrated, the 0.25 mM H_2O_2 insult stimulated PC-hASCs antioxidant response, which seems to be beneficial for oxHOGd recovery.

Additionally, considering the lowering of ROS levels in oxHOGd , we analyzed the concentration of small molecule antioxidants and proteins in the culture media of the oxHOGd alone or co-cultured with *i*, hASCs CM or PC-hASCs CM, *ii*, hASCs or PC-hASCs, or *iii*, hASCs or PC-hASCs subjected to oxidative stress. The results revealed that after 24 hours, the co-culture of oxHOGd with PC-hASCs subjected to oxidative stress secreted a significantly higher amount of antioxidant molecules to the media, which was consistent with the previously observed decrease of the intracellular ROS levels. However, these results cannot confirm if the secretion of antioxidant molecules was due to oxHOGd or hASCs, so we analyzed the protein expression of several antioxidant proteins in the different cell populations.

Firstly, the expression of NRF2, HO-1, SOD-1 and CAT in oxHOGd co-cultured with hASCs or PC-hASCs subjected or not to oxidative stress was assessed. Only significant differences were observed in the NRF2 expression of the oxHOGd co-cultured with both hASCs and PC-hASCs subjected to oxidative stress (1.25 and 1.35-fold increase, respectively). Although not significant, a slight increase in HO-1 expression of oxHOGd co-cultured with oxidized PC-hASCs was also

VI. Discussion

observed. This increase is probably linked to the enhancement in NRF2 expression, since NRF2 is recognized as a pivotal regulator of HO-1 induction in the nervous system. NRF2-dependent activation of HO-1 is usually linked to a protective adaptation of neurons and glial cells, whereas the NRF2-independent activation of HO-1 seems to exert neurotoxic effects. This is probably due to the ability of NRF2 to also promote the transcription of other antioxidant and protective molecules²⁴⁴. Since the oxHOGd co-cultured with the PC-hASCs were the ones that showed the most evident recovery 24 hours after the insult with H_2O_2 , it is conceivable that it was related to the activation of the NRF2/HO-1 signaling pathway. In accordance with this, other authors have already reported the NRF2/HO-1 signaling pathway role in reducing cytotoxicity and oxidative stress induced by LPS in oligodendrocytes²⁴⁵. Moreover, SOD-1 expression was also slightly increased in oxHOGd co-cultured with oxidized PC-hASCs, which is in agreement with the NRF2 outcome, as several authors relate their expression to that of NRF2¹⁶, and with the ROS reductions, since mature oligodendrocytes overexpressing SOD-1 have proved to be more resistant to oxidative stress, enhancing their survival²⁴⁶. Ultimately, CAT was not expressed in oxHOGd under any of the culture conditions, which is in line with data obtained by Baud et al., who stated that rat oligodendrocytes subjected to a 1 hour insult of H_2O_2 inactivated the catalase activity²⁴⁷.

Regarding the MSC co-cultured with the oxHOGd , a significant increase in the expression levels of NRF2, HO-1, and SOD-1 in the PC-hASCs subjected to oxidative stress was observed. This result is in line with that obtained by analyzing the total antioxidant capacity of the media from oxHOGd co-cultured with oxidized PC-hASCs and is similar to the observed expression of the antioxidant enzymes in oxHOGd , which suggests that the exposure to soluble factors secreted by activated PC-hASCs upregulates the expression of antioxidant enzymes in oxHOGd . According to this, several authors have already

linked the increase in the expression of antioxidant enzymes of MSCs with the recovery of damaged tissue. For example, Li et al. reported that overexpression of antioxidants, specifically HO-1, could enhance the protection of MSC on retinal cells ²⁴⁸.

Additionally, in contrast to what was observed in the oxHOGd , CAT did express in the MSCs samples. In fact, it was significantly overexpressed in both, PC-hASCs and PC-hASCs subjected to oxidative stress when compared to hASCs (1.2 and 1.4-fold increase, respectively). Since the increase in CAT expression in PC-hASCs, in both standard or oxidative stress conditions, coincided with the decrease in intracellular ROS levels in oxHOGd , we can hypothesize that CAT played an important role in reducing ROS levels in oxHOGd because it is an efficient scavenger of H_2O_2 when it is present in high concentrations ²⁴⁹.

Altogether, these results suggest that overexpression of NRF2, HO-1, SOD-1, and CAT in PC-hASCs enhanced the recovery of oxHOGd by reducing ROS levels and subsequently increasing oxHOGd viability. In line with aforementioned, these data show that the adaptation to oxidative stress is a fundamental advantage for hASCs, since it makes them able to survive and maintain their functionality after being subjected to an H_2O_2 insult, and therefore enhances their therapeutic capacity.

Finally, we evaluated the ability of the MSCs to migrate or home towards oxHOGd . Cell homing into the target tissue is one aspect of the cytoprotection activity of MSCs; along with the multipotent differentiation and paracrine capabilities, is considered one of the main properties of MSCs in regenerative medicine ⁸⁹. To determine the responsiveness of PC-hASCs to chemotactic signals from oxHOGd , we utilized an indirect co-culture manner by transwell, and after 24 or 48 hours the MSCs that crossed the pores of the transwell were stained with crystal violet and quantified.

VI. Discussion

Our data showed that PC-hASCs displayed a significantly higher migration capacity towards oxHOGd than control hASCs, both in standard conditions and after H_2O_2 stimulation, suggesting that PC-hASCs are able to respond more efficiently to rescue signals present in the secretome of oxHOGd . On the other hand, hASCs and PC-hASCs migrate more than hASCs and PC-hASCs previously subjected to oxidative stress, indicating that the oxidative stress insult reduced the migration ability of these cells, which was already demonstrated by other authors²⁵⁰.

In summary, this study shows that preconditioning with low doses of H_2O_2 enhances survival and adaptation of hASCs under oxidative stress conditions through two mechanisms, namely, antioxidant activity and metabolic plasticity. Therefore, as we explain in figure 55, PC-hASCs reduce intracellular ROS levels and attenuate the inflammatory response derived from an oxidative stress situation by overexpressing NRF2 and the subsequent antioxidant molecules. In addition, the reduction of ROS by the antioxidants seemed to allow the increase of mitochondrial activity and hence the production of ATP by this pathway. Moreover, the overexpression of HIF-1 α appears to be responsible for the increase in glycolysis and thus in ATP production, enabling PC-hASCs to meet the bioenergetic demand required to survive under stress conditions. Besides, these mechanisms seem to be also responsible for the enhanced therapeutic capacity of these cells demonstrated by the alleviation of oxidative stress effects on oxHOGd . Taken together, H_2O_2 preconditioning promotes the therapeutic effect of hASCs, on the one hand, increasing their tolerance to the harmful oxidative stress and, on the other, promoting the paracrine activity necessary to counteract ROS, which might lead to developing successful cell-based therapies.

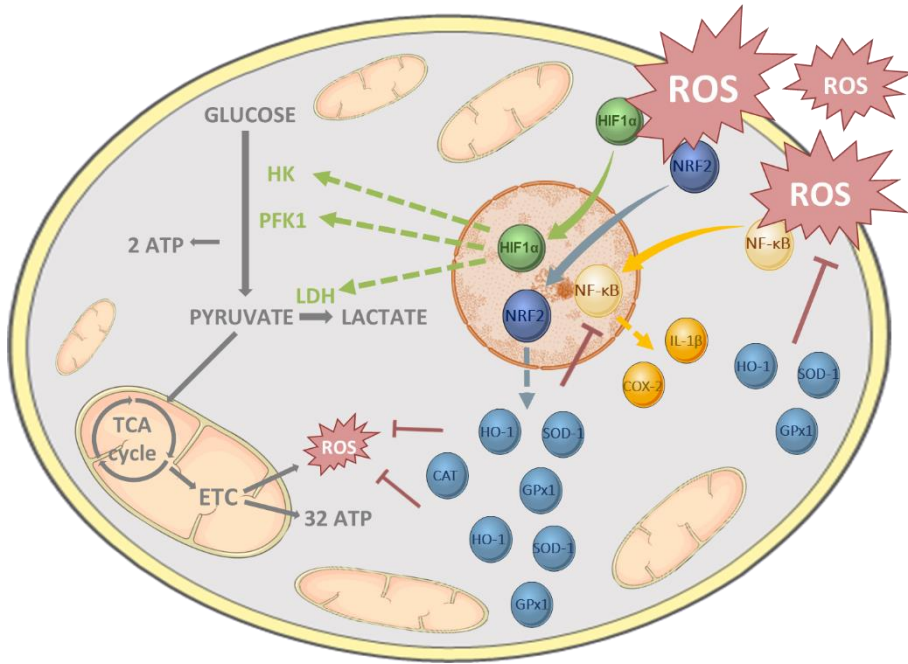


Figure 55. Schematic overview of PC-hASCs mechanisms to adapt to an oxidative stress environment.

VII. Conclusions

1. PC-hASCs show a higher resistance to oxidative stress than non-preconditioned cells.
2. PC-hASCs display an increased antioxidant response to overcome oxidative stress, as demonstrated by the overexpression of NRF2 and the antioxidant enzymes HO-1, SOD-1, GPx-1, and CAT.
3. Under oxidative stress conditions, PC-hASCs reduce the secretion of pro-inflammatory molecules COX-2 and IL-1 β by attenuating the expression of NF- κ B.
4. To facilitate the adaptation to an oxidative stress environment, PC-hASCs increase the total ATP production rate through the modulation of the energetic metabolism.
5. PC-hASCs produce more mitochondrial ATP than hASCs, which is associated with a higher respiration rate and $\Delta\psi_m$.
6. PC-hASCs produce more glycolytic ATP compared to hASCs, which correlates with an increase in glycolysis and the overexpression of HIF-1 α .
7. PC-hASCs show a heightened pro-recovery effect on an oxidized oligodendroglial cell model, promoting the antioxidant response of these damaged cells.

VIII. References

-
1. da Silva Meirelles, L., Fontes, A. M., Covas, D. T. & Caplan, A. I. Mechanisms involved in the therapeutic properties of mesenchymal stem cells. *Cytokine Growth Factor Rev.* **20**, 419–427 (2009).
 2. Caplan, A. I. Why are MSCs therapeutic? New data: new insight. *J. Pathol.* **217**, 318–324 (2009).
 3. Hu, C. & Li, L. Preconditioning influences mesenchymal stem cell properties in vitro and in vivo. *J. Cell. Mol. Med.* **22**, 1428–1442 (2018).
 4. Ni, J. *et al.* Therapeutic Potential of Human Adipose-Derived Stem Cell Exosomes in Stress Urinary Incontinence – An in Vitro and in Vivo Study. *Cell. Physiol. Biochem.* **48**, 1710–1722 (2018).
 5. Damia, E. *et al.* Adipose-Derived Mesenchymal Stem Cells: Are They a Good Therapeutic Strategy for Osteoarthritis? *Int. J. Mol. Sci.* **19**, 1926 (2018).
 6. Wang, N. *et al.* Mesenchymal stem cells-derived extracellular vesicles, via miR-210, improve infarcted cardiac function by promotion of angiogenesis. *Biochim. Biophys. Acta - Mol. Basis Dis.* **1863**, 2085–2092 (2017).
 7. Abbasi-Malati, Z., Roushandeh, A. M., Kuwahara, Y. & Roudkenar, M. H. Mesenchymal Stem Cells on Horizon: A New Arsenal of Therapeutic Agents. *Stem Cell Rev. Reports* **14**, 484–499 (2018).
 8. Birben, E., Sahiner, U. M., Sackesen, C., Erzurum, S. & Kalayci, O. Oxidative stress and antioxidant defense. *World Allergy Organ. J.* **5**, 9–19 (2012).
 9. Denu, R. A. & Hematti, P. Effects of Oxidative Stress on Mesenchymal

VIII. References

- Stem Cell Biology. *Oxid. Med. Cell. Longev.* **2016**, 2989076 (2016).
10. Chen, X. *et al.* Adipose-derived mesenchymal stem cells promote the survival of fat grafts via crosstalk between the Nrf2 and TLR4 pathways. *Cell Death Dis.* **7**, e2369–e2369 (2016).
 11. Cadenas, E. & Packer, L. Hydrogen peroxide and cell signaling. C LK - <https://ehu.on.worldcat.org/oclc/856866064>. *Methods in enzymology*; **528 TA - TT - 1** online resource. (2013).
 12. Loboda, A., Damulewicz, M., Pyza, E., Jozkowicz, A. & Dulak, J. Role of Nrf2/HO-1 system in development, oxidative stress response and diseases: an evolutionarily conserved mechanism. *Cell. Mol. Life Sci.* **73**, 3221–3247 (2016).
 13. Wei, R., Enaka, M. & Muragaki, Y. Activation of KEAP1/NRF2/P62 signaling alleviates high phosphate-induced calcification of vascular smooth muscle cells by suppressing reactive oxygen species production. *Sci. Rep.* **9**, 10366 (2019).
 14. Holmström, K. M., Kostov, R. V & Dinkova-Kostova, A. T. The multifaceted role of Nrf2 in mitochondrial function. *Curr. Opin. Toxicol.* **1**, 80–91 (2016).
 15. Nguyen, T., Nioi, P. & Pickett, C. B. The Nrf2-antioxidant response element signaling pathway and its activation by oxidative stress. *J. Biol. Chem.* **284**, 13291–13295 (2009).
 16. Mohammadzadeh, M. *et al.* Nrf-2 overexpression in mesenchymal stem cells reduces oxidative stress-induced apoptosis and cytotoxicity. *Cell Stress Chaperones* **17**, 553–565 (2012).

-
17. Ahmed, S. M. U., Luo, L., Namani, A., Wang, X. J. & Tang, X. Nrf2 signaling pathway: Pivotal roles in inflammation. *Biochim. Biophys. Acta - Mol. Basis Dis.* **1863**, 585–597 (2017).
 18. Karin, M., Yamamoto, Y. & Wang, Q. M. The IKK NF- κ B system: a treasure trove for drug development. *Nat. Rev. Drug Discov.* **3**, 17–26 (2004).
 19. Cachofeiro, V. *et al.* Oxidative stress and inflammation, a link between chronic kidney disease and cardiovascular disease: New strategies to prevent cardiovascular risk in chronic kidney disease. *Kidney Int.* **74**, S4–S9 (2008).
 20. Gloire, G., Legrand-Poels, S. & Piette, J. NF- κ B activation by reactive oxygen species: Fifteen years later. *Biochem. Pharmacol.* **72**, 1493–1505 (2006).
 21. Liu, T., Zhang, L., Joo, D. & Sun, S.-C. NF- κ B signaling in inflammation. *Signal Transduct. Target. Ther.* **2**, 17023 (2017).
 22. Nesci, S. *et al.* Characterization of metabolic profiles and lipopolysaccharide effects on porcine vascular wall mesenchymal stem cells. *J. Cell. Physiol.* **10**, 16685-16691 (2019).
 23. Liu, Y., Yuan, X., Muñoz, N., Logan, T. M. & Ma, T. Commitment to aerobic Glycolysis Sustains Immunosuppression of Human Mesenchymal Stem Cells. *Stem Cells Transl. Med.* **8(1)**, 93-106 (2019).
 24. Sokolova, I. M. Energy-limited tolerance to stress as a conceptual framework to integrate the effects of multiple stressors. *Integr. Comp. Biol.* **53**, 597–608 (2013).
 25. Yuan, X., Logan, T. M. & Ma, T. Metabolism in Human Mesenchymal

VIII. References

- Stromal Cells: A Missing Link Between hMSC Biomanufacturing and Therapy? . *Frontiers in Immunology* **10**, 977 (2019).
26. Amiri, F., Jahanian-Najafabadi, A. & Roudkenar, M. H. In vitro augmentation of mesenchymal stem cells viability in stressful microenvironments : In vitro augmentation of mesenchymal stem cells viability. *Cell Stress Chaperones* **20**, 237–251 (2015).
27. Silva, L. H. A. *et al.* Strategies to improve the therapeutic effects of mesenchymal stromal cells in respiratory diseases. *Stem Cell Res. Ther.* **9**, 45 (2018).
28. Lee, J. H., Yoon, Y. M. & Lee, S. H. Hypoxic Preconditioning Promotes the Bioactivities of Mesenchymal Stem Cells via the HIF-1 α -GRP78-Akt Axis. *Int. J. Mol. Sci.* **18**, 1320 (2017).
29. Oses, C. *et al.* Preconditioning of adipose tissue-derived mesenchymal stem cells with deferoxamine increases the production of pro-angiogenic, neuroprotective and anti-inflammatory factors: Potential application in the treatment of diabetic neuropathy. *PLoS One* **12**, e0178011 (2017).
30. Saparov, A., Ogay, V., Nurgozhin, T., Jumabay, M. & Chen, W. C. W. Preconditioning of Human Mesenchymal Stem Cells to Enhance Their Regulation of the Immune Response. *Stem Cells Int.* **2016**, 3924858 (2016).
31. Luna-López, A., González-Puertos, V. Y., López-Diazguerrero, N. E. & Königsberg, M. New considerations on hormetic response against oxidative stress. *J. Cell Commun. Signal.* **8**, 323–331 (2014).
32. Castro, B. *et al.* Cryopreserved H₂O₂-preconditioned human adipose-

-
- derived stem cells exhibit fast post-thaw recovery and enhanced bioactivity against oxidative stress. *J. Tissue Eng. Regen. Med.* **13**, 328–341 (2019).
33. Roy, S., Khanna, S., Nallu, K., Hunt, T. K. & Sen, C. K. Dermal wound healing is subject to redox control. *Mol. Ther.* **13(1)**, 211-220 (2006).
34. Zhuang, Y. *et al.* Resveratrol Attenuates Oxidative Stress-Induced Intestinal Barrier Injury through PI3K/Akt-Mediated Nrf2 Signaling Pathway. *Oxid. Med. Cell. Longev.* **2019**, 7591840 (2019).
35. Koundouros, N. & Poulogiannis, G. Phosphoinositide 3-Kinase/Akt Signaling and Redox Metabolism in Cancer . *Frontiers in Oncology* **8**, 160 (2018).
36. Garg, T. K. & Chang, J. Y. Oxidative stress causes ERK phosphorylation and cell death in cultured retinal pigment epithelium: prevention of cell death by AG126 and 15-deoxy-delta 12, 14-PGJ2. *BMC Ophthalmol.* **3**, 5 (2003).
37. Nouri, F., Nematollahi-Mahani, S. N. & Sharifi, A. M. Preconditioning of Mesenchymal Stem Cells with Non-Toxic Concentration of Hydrogen Peroxide Against Oxidative Stress Induced Cell Death: The Role of Hypoxia-Inducible Factor-1. *Adv. Pharm. Bull.* **9**, 76–83 (2019).
38. Cao, L., Liu, J., Zhang, L., Xiao, X. & Li, W. Curcumin inhibits H₂O₂-induced invasion and migration of human pancreatic cancer via suppression of the ERK/NF- κ B pathway. *Oncol. Rep.* **36(4)**, 2245-2251 (2016).
39. Nuschke, A., Rodrigues, M., Wells, A. W., Sylakowski, K. & Wells, A. Mesenchymal stem cells/multipotent stromal cells (MSCs) are glycolytic and thus glucose is a limiting factor of in vitro models of MSC starvation.

VIII. References

- Stem Cell Res. Ther.* **7**, 179 (2016).
40. Shum, L. C., White, N. S., Mills, B. N., Bentley, K. L. de M. & Eliseev, R. A. Energy Metabolism in Mesenchymal Stem Cells During Osteogenic Differentiation. *Stem Cells Dev.* **25**, 114–122 (2016).
41. dos Santos, F. *et al.* Ex vivo expansion of human mesenchymal stem cells: A more effective cell proliferation kinetics and metabolism under hypoxia. *J. Cell. Physiol.* **223**, 27–35 (2010).
42. Sifuentes-Franco, S., Pacheco-Moisés, F. P., Rodríguez-Carrizalez, A. D. & Miranda-Díaz, A. G. The Role of Oxidative Stress, Mitochondrial Function, and Autophagy in Diabetic Polyneuropathy. *J. Diabetes Res.* **2017**, 1673081 (2017).
43. Buntinx, M. *et al.* Characterization of three human oligodendroglial cell lines as a model to study oligodendrocyte injury: Morphology and oligodendrocyte-specific gene expression. *J. Neurocytol.* **32(1)**, 25-38. (2003).
44. De Arriba Zerpa, G. A. *et al.* Alternative splicing prevents transferrin secretion during differentiation of a human oligodendrocyte cell line. *J. Neurosci. Res.* **61(4)**, 388-395 (2000).
45. De Vries, G. H. & Boullerne, A. I. Glial cell lines: An overview. *Neurochem. Res.* **35(12)**, 1978-2000 (2010).
46. Schoenfeld, R. *et al.* Oligodendroglial differentiation induces mitochondrial genes and inhibition of mitochondrial function represses oligodendroglial differentiation. *Mitochondrion* **10**, 143–150 (2010).
47. Thurairajah, K., Broadhead, M. L. & Balogh, Z. J. Trauma and Stem Cells:

-
- Biology and Potential Therapeutic Implications. *Int. J. Mol. Sci.* **18**, 577 (2017).
48. Miller, L. W. Chapter 38 - New Strategies to Enhance Stem Cell Homing for Tissue Repair. in (eds. Perin, E. C., Miller, L. W., Taylor, D. A. & Willerson, J. T. B. T.-S. C. and G. T. for C. D.) 485–496 (Academic Press, 2016). <https://doi.org/10.1016/B978-0-12-801888-0.00038-2>
49. Contreras D, T. N. Viral Disease, Tissue Injury, Repair and Regeneration. *J. Mol. Genet. Med.* **8**, 148 (2014).
50. Sugimoto, M. A., Sousa, L. P., Pinho, V., Perretti, M. & Teixeira, M. M. Resolution of Inflammation: What Controls Its Onset? *Front. Immunol.* **7**, 160 (2016).
51. Mohan, S. & Gupta, D. Crosstalk of toll-like receptors signaling and Nrf2 pathway for regulation of inflammation. *Biomed. Pharmacother.* **108**, 1866–1878 (2018).
52. De la Fuente, M. Oxidation and Inflammation in the Immune and Nervous Systems, a Link Between Aging and Anxiety BT - Handbook of Immunosenescence: Basic Understanding and Clinical Implications. in (eds. Fulop, T., Franceschi, C., Hirokawa, K. & Pawelec, G.) 1–31 (Springer International Publishing, 2018). doi:10.1007/978-3-319-64597-1_115-1
53. Mao, A. S. & Mooney, D. J. Regenerative medicine: Current therapies and future directions. *Proc. Natl. Acad. Sci. U. S. A.* **112**, 14452–14459 (2015).
54. Rosenthal, N. & Badylak, S. Regenerative medicine: today's discoveries informing the future of medical practice. *NPJ Regen. Med.* **1**, 16007 (2016).

VIII. References

55. Liu, S. Q. *Bioregenerative Engineering: Principles and Applications*. (John Wiley & Sons Inc, 2006). doi:10.1002/0470116862
56. Daar, A. S. & Greenwood, H. L. A proposed definition of regenerative medicine. *J. Tissue Eng. Regen. Med.* **1**, 179–184 (2007).
57. Riazi, A. M., Kwon, S. Y. & Stanford, W. L. Stem Cell Sources for Regenerative Medicine. *Methods Mol Biol.* **482**, 55-90 (2009).
58. Dimmeler, S., Ding, S., Rando, T. A. & Trounson, A. Translational strategies and challenges in regenerative medicine. *Nat. Med.* **20**, 814 (2014).
59. Mahla, R. S. Stem Cells Applications in Regenerative Medicine and Disease Therapeutics. *Int. J. Cell Biol.* **2016**, 6940283 (2016).
60. Neidhart, M. Chapter 21 - DNA Methylation in Stem Cell Diseases. in (ed. Neidhart, M. B. T.-D. N. A. M. and C. H. D.) 357–370 (Academic Press, 2016). <https://doi.org/10.1016/B978-0-12-420194-1.00021-X>
61. Evans, M. J. & Kaufman, M. H. Establishment in culture of pluripotential cells from mouse embryos. *Nature* **292**, 154–156 (1981).
62. Martin, G. R. Isolation of a pluripotent cell line from early mouse embryos cultured in medium conditioned by teratocarcinoma stem cells. *Proc. Natl. Acad. Sci.* **78**, 7634 – 7638 (1981).
63. Doetschman, T. C., Eistetter, H. & Katz, M. The in vitro development of blastocyst-derived embryonic stem cell lines: Formation of visceral yolk sac, blood islands and myocardium. *J. Embryol. Exp. Morphol.* **87**, 27–45 (1985).

-
64. Takahashi, K. & Yamanaka, S. Induction of Pluripotent Stem Cells from Mouse Embryonic and Adult Fibroblast Cultures by Defined Factors. *Cell* **126(4)**, 663-676 (2006).
65. Young, R. A. Control of the Embryonic Stem Cell State. *Cell* **144**, 940–954 (2011).
66. Klimanskaya, I. Chapter 7 - Embryonic Stem Cells: Derivation, Properties, and Challenges. in (eds. Atala, A., Lanza, R., Mikos, A. G. & Nerem, R. B. T.-P. of R. M. (Third E.) 113–123 (Academic Press, 2019). <https://doi.org/10.1016/B978-0-12-809880-6.00007-2>
67. Volarevic, V. *et al.* Ethical and safety issues of stem cell-based therapy. *International Journal of Medical Sciences* **15(1)**, 36-45 (2018).
68. Takahashi, K. *et al.* Induction of Pluripotent Stem Cells from Adult Human Fibroblasts by Defined Factors. *Cell* **131**, 861–872 (2007).
69. Yoshihara, M., Hayashizaki, Y. & Murakawa, Y. Genomic Instability of iPSCs: Challenges Towards Their Clinical Applications. *Stem cell Rev. reports* **13**, 7–16 (2017).
70. Martin, U. Genome stability of programmed stem cell products. *Adv. Drug Deliv. Rev.* **120**, 108–117 (2017).
71. von Joest, M., Búa Aguín, S. & Li, H. Genomic stability during cellular reprogramming: Mission impossible? *Mutat. Res. Mol. Mech. Mutagen.* **788**, 12–16 (2016).
72. Carpenedo, R. L. & McDevitt, T. C. Chapter II.1.7 - Stem Cells: Key Concepts. in (eds. Ratner, B. D., Hoffman, A. S., Schoen, F. J. & Lemons, J. E. B. T.-B. S. (Third E.) 487–495 (Academic Press, 2013).

VIII. References

<https://doi.org/10.1016/B978-0-08-087780-8.00042-5>

73. Zhang, Y., Xu, L., Wang, S., Cai, C. & Yan, L. Concise Review: Differentiation of Human Adult Stem Cells Into Hepatocyte-like Cells In vitro. *Int. J. stem cells* **7**, 49–54 (2014).
74. Ullah, I., Subbarao, R. B. & Rho, G. J. Human mesenchymal stem cells - current trends and future prospective. *Biosci. Rep.* **35**, e00191 (2015).
75. Wakao, S., Kuroda, Y., Ogura, F., Shigemoto, T. & Dezawa, M. Regenerative Effects of Mesenchymal Stem Cells: Contribution of Muse Cells, a Novel Pluripotent Stem Cell Type that Resides in Mesenchymal Cells. *Cells* **1**, 1045–1060 (2012).
76. Volarevic, V., Nurkovic, J., Arsenijevic, N. & Stojkovic, M. Concise Review: Therapeutic Potential of Mesenchymal Stem Cells for the Treatment of Acute Liver Failure and Cirrhosis. *Stem Cells* **32**, 2818–2823 (2014).
77. Tewary, M., Shakiba, N. & Zandstra, P. W. Stem cell bioengineering: building from stem cell biology. *Nat. Rev. Genet.* **19**, 595–614 (2018).
78. Thomas, E. D., Lochte Jr, H. L., Cannon, J. H., Sahler, O. D. & Ferrebee, J. W. Supralethal whole body irradiation and isologous marrow transplantation in man. *J. Clin. Invest.* **38**, 1709–1716 (1959).
79. Till, J. E. & McCulloch, E. A. A Direct Measurement of the Radiation Sensitivity of Normal Mouse Bone Marrow Cells. *Radiat. Res.* **175(2)**, 145-149 (1961).
80. Thomson, J. A. Embryonic stem cell lines derived from human blastocysts. *Science.* **282(5391)**, 1145-1147 (1998).

-
81. Takahashi, K. & Yamanaka, S. Induction of Pluripotent Stem Cells from Mouse Embryonic and Adult Fibroblast Cultures by Defined Factors. *Cell* **126**, 663–676 (2006).
 82. Steinhoff, G. *et al.* Stem cells and heart disease - Brake or accelerator? *Adv. Drug Deliv. Rev.* **120**, 2–24 (2017).
 83. Henig, I. & Zuckerman, T. Hematopoietic stem cell transplantation-50 years of evolution and future perspectives. *Rambam Maimonides Med. J.* **5**, e0028–e0028 (2014).
 84. Friedenstein, A. J. Precursor Cells of Mechanocytes. *Int. Rev. Cytol.* **47**, 327-359. (1976).
 85. Locke, M., Windsor, J. & Dunbar, P. R. Human adipose-derived stem cells: Isolation, characterization and applications in surgery. *ANZ Journal of Surgery* **79(11)**, 856 (2009).
 86. Murphy, M. B., Moncivais, K. & Caplan, A. I. Mesenchymal stem cells: Environmentally responsive therapeutics for regenerative medicine. *Experimental and Molecular Medicine* **45**, e54 (2013).
 87. Mizukami, A. & Swiech, K. Mesenchymal stromal cells: From discovery to manufacturing and commercialization. *Stem Cells Int.* **2018**, 4083921 (2018).
 88. Dominici, M. *et al.* Minimal criteria for defining multipotent mesenchymal stromal cells. The International Society for Cellular Therapy position statement. *Cytotherapy* **8**, 315–317 (2006).
 89. Kang, S. K., Shin, I. S., Ko, M. S., Jo, J. Y. & Ra, J. C. Journey of mesenchymal stem cells for homing: strategies to enhance efficacy and safety of stem

VIII. References

- cell therapy. *Stem Cells Int.* **2012**, 342968 (2012).
90. Nitzsche, F. *et al.* Concise Review: MSC Adhesion Cascade—Insights into Homing and Transendothelial Migration. *Stem Cells* **35**, 1446–1460 (2017).
91. Ullah, M., Liu, D. D. & Thakor, A. S. Mesenchymal Stromal Cell Homing: Mechanisms and Strategies for Improvement. *iScience* **15**, 421–438 (2019).
92. Cho, K.-S. *et al.* IFATS Collection: Immunomodulatory Effects of Adipose Tissue-Derived Stem Cells in an Allergic Rhinitis Mouse Model. *Stem Cells* **27**, 259–265 (2009).
93. Saito, T., Kuang, J.-Q., Bittira, B., Al-Khaldi, A. & Chiu, R. C.-J. Xenotransplant cardiac chimera: immune tolerance of adult stem cells. *Ann. Thorac. Surg.* **74**, 19–24 (2002).
94. Zhao, R. C. *Essentials of mesenchymal stem cell biology and its clinical translation*. Dordrecht: Springer. (2013). doi:10.1007/978-94-007-6716-4
95. Gebler, A., Zabel, O. & Seliger, B. The immunomodulatory capacity of mesenchymal stem cells. *Trends Mol. Med.* **18**, 128–134 (2012).
96. Wang, Y., Chen, X., Cao, W. & Shi, Y. Plasticity of mesenchymal stem cells in immunomodulation: pathological and therapeutic implications. *Nat. Immunol.* **15**, 1009 (2014).
97. Yañez, R. *et al.* Adipose Tissue-Derived Mesenchymal Stem Cells Have In Vivo Immunosuppressive Properties Applicable for the Control of the Graft-Versus-Host Disease. *Stem Cells* **24**, 2582–2591 (2006).

-
98. Corcione, A. *et al.* Human mesenchymal stem cells modulate B-cell functions. *Blood* **107**, 367 – 372 (2006).
 99. Ramasamy, R. *et al.* Mesenchymal Stem Cells Inhibit Dendritic Cell Differentiation and Function by Preventing Entry Into the Cell Cycle. *Transplantation* **83 (1)**, 71-76 (2007).
 100. Lim, J.-H. *et al.* Immunomodulation of Delayed-Type Hypersensitivity Responses by Mesenchymal Stem Cells Is Associated with Bystander T Cell Apoptosis in the Draining Lymph Node. *J. Immunol.* **185**, 4022 – 4029 (2010).
 101. Le Blanc, K. *et al.* Treatment of severe acute graft-versus-host disease with third party haploidentical mesenchymal stem cells. *Lancet* **363**, 1439–1441 (2004).
 102. Sun, L. *et al.* Umbilical cord mesenchymal stem cell transplantation in severe and refractory systemic lupus erythematosus. *Arthritis Rheum.* **62**, 2467–2475 (2010).
 103. Dalal, J., Gandy, K. & Domen, J. Role of mesenchymal stem cell therapy in Crohn’s disease. *Pediatr. Res.* **71**, 445 (2012).
 104. da Costa Gonçalves, F. *et al.* Antioxidant properties of mesenchymal stem cells against oxidative stress in a murine model of colitis. *Biotechnol. Lett.* **39**, 613–622 (2017).
 105. Li, M. *et al.* Stem Cell Transplantation Increases Antioxidant Effects in Diabetic Mice. *Int. J. Biol. Sci.* **8**, 1335–1344 (2012).
 106. Yan, Y. *et al.* hucMSC Exosome-Derived GPX1 Is Required for the Recovery of Hepatic Oxidant Injury. *Mol. Ther.* **25**, 465–479 (2017).

VIII. References

107. Abdel-Mageed, A. S. *et al.* Intravenous administration of mesenchymal stem cells genetically modified with extracellular superoxide dismutase improves survival in irradiated mice. *Blood* **113**, 1201–1203 (2009).
108. Alekseenko, L. L. *et al.* Quiescent Human Mesenchymal Stem Cells Are More Resistant to Heat Stress than Cycling Cells. *Stem Cells Int.* **2018**, 3753547 (2018).
109. Liu, Y. & Ma, T. Metabolic regulation of mesenchymal stem cell in expansion and therapeutic application. *Biotechnol. Prog.* **31**, 468–481 (2015).
110. Buravkova, L. B. *et al.* Low ATP level is sufficient to maintain the uncommitted state of multipotent mesenchymal stem cells. *Biochim. Biophys. Acta - Gen. Subj.* **1830**, 4418–4425 (2013).
111. Ozge, K. M. *et al.* Mitochondrial Oxidative Stress Reduces the Immunopotency of Mesenchymal Stromal Cells in Adults With Coronary Artery Disease. *Circ. Res.* **122**, 255–266 (2018).
112. Caplan, A. I. & Dennis, J. E. Mesenchymal stem cells as trophic mediators. *J. Cell. Biochem.* **98**, 1076–1084 (2006).
113. Haynesworth, S. E., Baber, M. A. & Caplan, A. I. Cytokine expression by human marrow-derived mesenchymal progenitor cells in vitro: Effects of dexamethasone and IL-1 α . *J. Cell. Physiol.* **166**, 585–592 (1996).
114. Park, W. S., Ahn, S. Y., Sung, S. I., Ahn, J.-Y. & Chang, Y. S. Strategies to enhance paracrine potency of transplanted mesenchymal stem cells in intractable neonatal disorders. *Pediatr. Res.* **83**, 214 (2017).
115. Rani, S., Ryan, A. E., Griffin, M. D. & Ritter, T. Mesenchymal Stem Cell-

-
- derived Extracellular Vesicles: Toward Cell-free Therapeutic Applications. *Mol. Ther.* **23**, 812–823 (2015).
116. Driscoll, J. & Patel, T. The mesenchymal stem cell secretome as an acellular regenerative therapy for liver disease. *J. Gastroenterol.* **54**, 763–773 (2019).
117. Keshtkar, S., Azarpira, N. & Ghahremani, M. H. Mesenchymal stem cell-derived extracellular vesicles: novel frontiers in regenerative medicine. *Stem Cell Res. Ther.* **9**, 63 (2018).
118. Djouad, F., Bouffi, C., Ghannam, S., Noël, D. & Jorgensen, C. Mesenchymal stem cells: innovative therapeutic tools for rheumatic diseases. *Nat. Rev. Rheumatol.* **5**, 392 (2009).
119. Baez-Jurado, E. *et al.* Secretome of Mesenchymal Stem Cells and Its Potential Protective Effects on Brain Pathologies. *Mol. Neurobiol.* **56**, 6902–6927 (2019).
120. Morigi, M. *et al.* Life-Sparing Effect of Human Cord Blood-Mesenchymal Stem Cells in Experimental Acute Kidney Injury. *Stem Cells* **28**, 513–522 (2010).
121. Yang, J. *et al.* Extracellular Vesicles Derived from Bone Marrow Mesenchymal Stem Cells Protect against Experimental Colitis via Attenuating Colon Inflammation, Oxidative Stress and Apoptosis. *PLoS One* **10**, e0140551 (2015).
122. Teng, X. *et al.* Mesenchymal Stem Cell-Derived Exosomes Improve the Microenvironment of Infarcted Myocardium Contributing to Angiogenesis and Anti-Inflammation. *Cell. Physiol. Biochem.* **37**, 2415–2424 (2015).

VIII. References

123. Zhao, F., Qu, Y., Liu, H., Du, B. & Mu, D. Umbilical cord blood mesenchymal stem cells co-modified by TERT and BDNF: A novel neuroprotective therapy for neonatal hypoxic-ischemic brain damage. *Int. J. Dev. Neurosci.* **38**, 147–154 (2014).
124. Zuk, P. A. *et al.* Human Adipose Tissue Is a Source of Multipotent Stem Cells. *Mol. Biol. Cell* **13**, 4279–4295 (2002).
125. Safford, K. M. *et al.* Neurogenic differentiation of murine and human adipose-derived stromal cells. *Biochem. Biophys. Res. Commun.* **294**, 371–379 (2002).
126. Wang, Y. *et al.* Human adipose-derived mesenchymal stem cells are resistant to HBV infection during differentiation into hepatocytes in vitro. *Int. J. Mol. Sci.* **15**, 6096–6110 (2014).
127. Choi, Y. S. *et al.* Differentiation of human adipose-derived stem cells into beating cardiomyocytes. *J. Cell. Mol. Med.* **14**, 878–889 (2010).
128. Galipeau, J. & Sensébé, L. Mesenchymal Stromal Cells: Clinical Challenges and Therapeutic Opportunities. *Cell Stem Cell* **22**, 824–833 (2018).
129. Busser, H. *et al.* Isolation and Characterization of Human Mesenchymal Stromal Cell Subpopulations: Comparison of Bone Marrow and Adipose Tissue. *Stem Cells Dev.* **24(18)**, 2142-2157 (2015).
130. Drela, K., Stanaszek, L., Nowakowski, A., Kuczynska, Z. & Lukomska, B. Experimental Strategies of Mesenchymal Stem Cell Propagation: Adverse Events and Potential Risk of Functional Changes. *Stem Cells Int.* **2019**, 7012692 (2019).
131. Hayflick, L. The limited in vitro lifetime of human diploid cell strains. *Exp.*

-
- Cell Res.* **37**, 614-636 (1965).
132. Ma, L. *et al.* Maintained Properties of Aged Dental Pulp Stem Cells for Superior Periodontal Tissue Regeneration. *Aging Dis.* **10**, 793–806 (2019).
133. Jin, H. J. *et al.* Comparative analysis of human mesenchymal stem cells from bone marrow, adipose tissue, and umbilical cord blood as sources of cell therapy. *Int. J. Mol. Sci.* **14**, 17986–18001 (2013).
134. Vidal, M. A., Walker, N. J., Napoli, E. & Borjesson, D. L. Evaluation of senescence in mesenchymal stem cells isolated from equine bone marrow, adipose tissue, and umbilical cord tissue. *Stem Cells Dev.* **21(2)**, 273-283 (2012).
135. Mazini, L., Rochette, L., Amine, M. & Malka, G. Regenerative Capacity of Adipose Derived Stem Cells (ADSCs), Comparison with Mesenchymal Stem Cells (MSCs). *Int. J. Mol. Sci.* **20**, 2523 (2019).
136. Li, Y. *et al.* Senescence of mesenchymal stem cells (Review). *Int. J. Mol. Med.* **39(4)**, 775-782 (2017).
137. Soto-Gamez, A. & Demaria, M. Therapeutic interventions for aging: the case of cellular senescence. *Drug Discov. Today* **22**, 786–795 (2017).
138. Passos, J. F. *et al.* Mitochondrial Dysfunction Accounts for the Stochastic Heterogeneity in Telomere-Dependent Senescence. *PLOS Biol.* **5**, e110 (2007).
139. Turinetto, V., Vitale, E. & Giachino, C. Senescence in Human Mesenchymal Stem Cells: Functional Changes and Implications in Stem Cell-Based Therapy. *Int. J. Mol. Sci.* **17**, 1164 (2016).

VIII. References

140. Chen, C. *et al.* Metabolic reprogramming by HIF-1 activation enhances survivability of human adipose-derived stem cells in ischaemic microenvironments. *Cell Prolif.* **50**, e12363 (2017).
141. Ezquer, F. E., Ezquer, M. E., Vicencio, J. M. & Calligaris, S. D. Two complementary strategies to improve cell engraftment in mesenchymal stem cell-based therapy: Increasing transplanted cell resistance and increasing tissue receptivity. *Cell Adh. Migr.* **11**, 110–119 (2017).
142. Chan, E. C., Jiang, F., Peshavariya, H. M. & Dusting, G. J. Regulation of cell proliferation by NADPH oxidase-mediated signaling: Potential roles in tissue repair, regenerative medicine and tissue engineering. *Pharmacol. Ther.* **122**, 97–108 (2009).
143. J., F. S., S., K. D., S., H. M., Qian, X. & K., G. K. Reactive Oxygen Species in Metabolic and Inflammatory Signaling. *Circ. Res.* **122**, 877–902 (2018).
144. Chang, W. *et al.* Anti-death strategies against oxidative stress in grafted mesenchymal stem cells. *Histology and Histopathology* **28(12)**, 1529-1536 (2013).
145. Gilmore, A. P. Anoikis. *Cell Death Differ.* **12**, 1473–1477 (2005).
146. Reddig, P. J. & Juliano, R. L. Clinging to life: cell to matrix adhesion and cell survival. *Cancer Metastasis Rev.* **24**, 425–439 (2005).
147. Song, H. *et al.* Reactive Oxygen Species Inhibit Adhesion of Mesenchymal Stem Cells Implanted into Ischemic Myocardium via Interference of Focal Adhesion Complex. *Stem Cells* **28**, 555–563 (2010).
148. Lee, S., Choi, E., Cha, M.-J. & Hwang, K.-C. Cell adhesion and long-term survival of transplanted mesenchymal stem cells: a prerequisite for cell

-
- therapy. *Oxid. Med. Cell. Longev.* **2015**, 632902 (2015).
149. Becherucci, V. *et al.* Human platelet lysate in mesenchymal stromal cell expansion according to a GMP grade protocol: a cell factory experience. *Stem Cell Res. Ther.* **9**, 124 (2018).
150. Shanbhag, S., Stavropoulos, A., Suliman, S., Hervig, T. & Mustafa, K. Efficacy of Humanized Mesenchymal Stem Cell Cultures for Bone Tissue Engineering: A Systematic Review with a Focus on Platelet Derivatives. *Tissue Eng. Part B Rev.* **23**, 552–569 (2017).
151. Ng, F. *et al.* PDGF, TGF- β , and FGF signaling is important for differentiation and growth of mesenchymal stem cells (MSCs): transcriptional profiling can identify markers and signaling pathways important in differentiation of MSCs into adipogenic, chondrogenic, and oste. *Blood* **112**, 295 – 307 (2008).
152. Horn, P. *et al.* Impact of individual platelet lysates on isolation and growth of human mesenchymal stromal cells. *Cytotherapy* **12**, 888–898 (2010).
153. Burnouf, T., Strunk, D., Koh, M. B. C. & Schallmoser, K. Human platelet lysate: Replacing fetal bovine serum as a gold standard for human cell propagation? *Biomaterials* **76**, 371–387 (2016).
154. Elseberg, C., Leber, J., Weidner, T. & Czermak, P. The Challenge of Human Mesenchymal Stromal Cell Expansion: Current and Prospective Answers. in *New Insights into Cell Culture Technology* (2017). doi:10.5772/66901
155. Atashi, F., Jaconi, M. E. E., Pittet-Cuénod, B. & Modarressi, A. Autologous Platelet-Rich Plasma: A Biological Supplement to Enhance Adipose-Derived Mesenchymal Stem Cell Expansion. *Tissue Eng. Part C Methods*

- 21**, 253–262 (2014).
156. Vogel, J. P. *et al.* Platelet-rich plasma improves expansion of human mesenchymal stem cells and retains differentiation capacity and in vivo bone formation in calcium phosphate ceramics. *Platelets* **17**, 462–469 (2006).
157. Fekete, N. *et al.* Platelet lysate from whole blood-derived pooled platelet concentrates and apheresis-derived platelet concentrates for the isolation and expansion of human bone marrow mesenchymal stromal cells: production process, content and identification of active comp. *Cytotherapy* **14**, 540–554 (2012).
158. Van Pham, P. *et al.* Activated platelet-rich plasma improves adipose-derived stem cell transplantation efficiency in injured articular cartilage. *Stem Cell Res. Ther.* **4**, 91 (2013).
159. Mishra, A. *et al.* Buffered Platelet-Rich Plasma Enhances Mesenchymal Stem Cell Proliferation and Chondrogenic Differentiation. *Tissue Eng. Part C Methods* **15**, 431–435 (2009).
160. Chadid, T. *et al.* Reversible secretome and signaling defects in diabetic mesenchymal stem cells from peripheral arterial disease patients. *J. Vasc. Surg.* **68**, 137S-151S.e2 (2018).
161. Forte, D. *et al.* Human cord blood-derived platelet lysate enhances the therapeutic activity of adipose-derived mesenchymal stromal cells isolated from Crohn’s disease patients in a mouse model of colitis. *Stem Cell Res. Ther.* **6**, 170 (2015).
162. Moisle, K. M. *et al.* Optimising proliferation and migration of mesenchymal stem cells using platelet products: A rational approach to

-
- bone regeneration. *J. Orthop. Res.* **37**, 1329–1338 (2019).
163. Wu, X. *et al.* Serum and xeno-free, chemically defined, no-plate-coating-based culture system for mesenchymal stromal cells from the umbilical cord. *Cell Prolif.* **49**, 579–588 (2016).
164. Lee, M.-S. *et al.* Enhanced Cell Growth of Adipocyte-Derived Mesenchymal Stem Cells Using Chemically-Defined Serum-Free Media. *Int. J. Mol. Sci.* **18**, 1779 (2017).
165. van der Valk, J. *et al.* Fetal Bovine Serum (FBS): Past - Present - Future. *ALTEX.* **35(1)**, 99-118 (2018).
166. Park, J. S., Suryaprakash, S., Lao, Y.-H. & Leong, K. W. Engineering mesenchymal stem cells for regenerative medicine and drug delivery. *Methods* **84**, 3–16 (2015).
167. Devetzi, M. *et al.* Genetically-modified stem cells in treatment of human diseases: Tissue kallikrein (KLK1)-based targeted therapy (Review). *International Journal of Molecular Medicine.* **41(3)**, 1177-1186 (2018).
168. Bouard, D., Alazard-Dany, D. & Cosset, F.-L. Viral vectors: from virology to transgene expression. *Br. J. Pharmacol.* **157**, 153–165 (2009).
169. Xu, X. *et al.* Efficient homology-directed gene editing by CRISPR/Cas9 in human stem and primary cells using tube electroporation. *Sci. Rep.* **8**, 11649 (2018).
170. Mangi, A. A. *et al.* Mesenchymal stem cells modified with Akt prevent remodeling and restore performance of infarcted hearts. *Nat. Med.* **9**, 1195–1201 (2003).

VIII. References

171. Zeng, B., Lin, G., Ren, X., Zhang, Y. & Chen, H. Over-expression of HO-1 on mesenchymal stem cells promotes angiogenesis and improves myocardial function in infarcted myocardium. *J. Biomed. Sci.* **17**, 80 (2010).
172. Shu, T., Zeng, B., Ren, X. & Li, Y. HO-1 modified mesenchymal stem cells modulate MMPs/TIMPs system and adverse remodeling in infarcted myocardium. *Tissue Cell* **42**, 217–222 (2010).
173. Yuan, L. *et al.* VEGF-modified human embryonic mesenchymal stem cell implantation enhances protection against cisplatin-induced acute kidney injury. *Am. J. Physiol. Physiol.* **300**, F207–F218 (2010).
174. Chen, Y. *et al.* Hepatocyte Growth Factor Modification Promotes the Amelioration Effects of Human Umbilical Cord Mesenchymal Stem Cells on Rat Acute Kidney Injury. *Stem Cells Dev.* **20**, 103–113 (2010).
175. Mattson, M. P. Hormesis defined. *Ageing Res. Rev.* **7**, 1–7 (2008).
176. Hong, Y., Kim, Y.-S., Hong, S.-H. & Oh, Y.-M. Therapeutic effects of adipose-derived stem cells pretreated with pioglitazone in an emphysema mouse model. *Exp. & Mol. Med.* **48**, e266 (2016).
177. Beegle, J. *et al.* Hypoxic Preconditioning of Mesenchymal Stromal Cells Induces Metabolic Changes, Enhances Survival, and Promotes Cell Retention In Vivo. *Stem Cells* **33**, 1818–1828 (2015).
178. Perdoni, C., McGrath, J. A. & Tolar, J. Preconditioning of mesenchymal stem cells for improved transplantation efficacy in recessive dystrophic epidermolysis bullosa. *Stem Cell Res. Ther.* **5**, 121 (2014).
179. Yeo, E.-J. Special issue on hypoxia. *Exp. Mol. Med.* **51**, 69 (2019).

-
180. Sandvig, I. *et al.* Strategies to Enhance Implantation and Survival of Stem Cells After Their Injection in Ischemic Neural Tissue. *Stem Cells Dev.* **26**, 554–565 (2017).
181. Baldari, S. *et al.* Challenges and strategies for improving the regenerative effects of mesenchymal stromal cell-based therapies. *International Journal of Molecular Sciences.* **18(10)**, e2087 (2017).
182. Shojaei, F., Rahmati, S. & Banitalebi Dehkordi, M. A review on different methods to increase the efficiency of mesenchymal stem cell-based wound therapy. *Wound Repair Regen.* **27(6)**, 661-671, (2019).
183. Hung, S.-C. *et al.* Short-Term Exposure of Multipotent Stromal Cells to Low Oxygen Increases Their Expression of CX3CR1 and CXCR4 and Their Engraftment In Vivo. *PLoS One* **2**, e416 (2007).
184. He, A. *et al.* The antiapoptotic effect of mesenchymal stem cell transplantation on ischemic myocardium is enhanced by anoxic preconditioning. *Can. J. Cardiol.* **25**, 353–358 (2009).
185. Lee, E. Y. *et al.* Hypoxia-enhanced wound-healing function of adipose-derived stem cells: Increase in stem cell proliferation and up-regulation of VEGF and bFGF. *Wound Repair Regen.* **17**, 540–547 (2009).
186. Liu, L. *et al.* Hypoxia-Inducible Factor-1 α Is Essential for Hypoxia-Induced Mesenchymal Stem Cell Mobilization into the Peripheral Blood. *Stem Cells Dev.* **20**, 1961–1971 (2011).
187. Estrada, J. C. *et al.* Culture of human mesenchymal stem cells at low oxygen tension improves growth and genetic stability by activating glycolysis. *Cell Death Differ.* **19**, 743–755 (2012).

VIII. References

188. Liu, J. *et al.* Hypoxia Regulates the Therapeutic Potential of Mesenchymal Stem Cells Through Enhanced Autophagy. *Int. J. Low. Extrem. Wounds* **14**, 63–72 (2015).
189. Bader, A. M. *et al.* Hypoxic Preconditioning Increases Survival and Pro-Angiogenic Capacity of Human Cord Blood Mesenchymal Stromal Cells In Vitro. *PLoS One* **10**, e0138477–e0138477 (2015).
190. Lehninger, A. L., Nelson, D. L., Cox, M. M., Nelson, D. L. & Cox, M. M. *Lehninger principles of biochemistry. TA - TT* - (W.H. Freeman, 2013).
191. Tsujimoto, Y. Apoptosis and necrosis: Intracellular ATP level as a determinant for cell death modes. *Cell Death Differ.* **4**, 429 (1997).
192. Moya, A. *et al.* Quiescence Preconditioned Human Multipotent Stromal Cells Adopt a Metabolic Profile Favorable for Enhanced Survival under Ischemia. *Stem Cells.* **35(1)**, 181-196 (2017).
193. Cheung, T. H. & Rando, T. A. Molecular regulation of stem cell quiescence. *Nat. Rev. Mol. Cell Biol.* **14**, 329–340 (2013).
194. Li, D., Xu, Y., Gao, C. Y. & Zhai, Y. P. Adaptive protection against damage of preconditioning human umbilical cord-derived mesenchymal stem cells with hydrogen peroxide. *Genet. Mol. Res.* **13(3)**, 7304-7317 (2014).
195. Li, S., Deng, Y., Feng, J. & Ye, W. Oxidative preconditioning promotes bone marrow mesenchymal stem cells migration and prevents apoptosis. *Cell Biol. Int.* **33**, 411–418 (2009).
196. Khatlani, T. *et al.* Preconditioning by Hydrogen Peroxide Enhances Multiple Properties of Human Decidua Basalis Mesenchymal Stem/Multipotent Stromal Cells. *Stem Cells Int.* **2018**, 6480793 (2018).

-
197. Kennelly, H., Mahon, B. P. & English, K. Human mesenchymal stromal cells exert HGF dependent cytoprotective effects in a human relevant pre-clinical model of COPD. *Sci. Rep.* **6**, 38207 (2016).
198. Usha Shalini, P., Vidyasagar, J. V. S., Kona, L. K., Ponnana, M. & Chelluri, L. K. In vitro allogeneic immune cell response to mesenchymal stromal cells derived from human adipose in patients with rheumatoid arthritis. *Cell. Immunol.* **314**, 18–25 (2017).
199. Sun, J., Zhang, Y., Song, X., Zhu, J. & Zhu, Q. The Healing Effects of Conditioned Medium Derived from Mesenchymal Stem Cells on Radiation-Induced Skin Wounds in Rats. *Cell Transplant.* **28(1)**, 105-115 (2018).
200. Wiśniewski, J. R., Zougman, A., Nagaraj, N. & Mann, M. Universal sample preparation method for proteome analysis. *Nat. Methods* **6**, 359–362 (2009).
201. Cox, J. & Mann, M. MaxQuant enables high peptide identification rates, individualized p.p.b.-range mass accuracies and proteome-wide protein quantification. *Nat. Biotechnol.* **26**, 1367–1372 (2008).
202. Cox, J. *et al.* Andromeda: A peptide search engine integrated into the MaxQuant environment. *J. Proteome Res.* **10(4)**, 1794-1805 (2011).
203. Cox, J. *et al.* Accurate proteome-wide label-free quantification by delayed normalization and maximal peptide ratio extraction, termed MaxLFQ. *Mol. Cell. Proteomics* **13**, 2513–2526 (2014).
204. Tyanova, S. *et al.* The Perseus computational platform for comprehensive analysis of (prote)omics data. *Nature Methods* **13(9)**, 731-40 (2016).

VIII. References

205. Rosner, M., Schipany, K. & Hengstschläger, M. Merging high-quality biochemical fractionation with a refined flow cytometry approach to monitor nucleocytoplasmic protein expression throughout the unperturbed mammalian cell cycle. *Nat. Protoc.* **8**, 602 (2013).
206. Ajit, D. *et al.* Phytochemicals and botanical extracts regulate NF- κ B and Nrf2/ARE reporter activities in DI TNC1 astrocytes. *Neurochem. Int.* **97**, 49–56 (2016).
207. Barnham, K. J., Masters, C. L. & Bush, A. I. Neurodegenerative diseases and oxidative stress. *Nat. Rev. Drug Discov.* **3**, 205–214 (2004).
208. Gandhi, S. & Abramov, A. Y. Mechanism of oxidative stress in neurodegeneration. *Oxidative Medicine and Cellular Longevity.* **2012**, 428010 (2012).
209. Liessem-Schmitz, A. *et al.* Nrf2 Signaling in Sodium Azide-Treated Oligodendrocytes Restores Mitochondrial Functions. *J. Mol. Neurosci.* **66**, 229–237 (2018).
210. Brand, A., Schonfeld, E., Isharel, I. & Yavin, E. Docosahexaenoic acid-dependent iron accumulation in oligodendroglia cells protects from hydrogen peroxide-induced damage. *J. Neurochem.* **105**, 1325–1335 (2008).
211. Maltman, D. J., Hardy, S. A. & Przyborski, S. A. Role of mesenchymal stem cells in neurogenesis and nervous system repair. *Neurochem. Int.* **59**, 347–356 (2011).
212. Sachan, T. T. and V. Mesenchymal Stem Cells: Potential in Treatment of Neurodegenerative Diseases. *Current Stem Cell Research & Therapy* **9**, 513–521 (2014).

-
213. Zhang, H.-T., Liu, Z.-L., Yao, X.-Q., Yang, Z.-J. & Xu, R.-X. Neural differentiation ability of mesenchymal stromal cells from bone marrow and adipose tissue: a comparative study. *Cytotherapy* **14**, 1203–1214 (2012).
214. Parimisetty, A. *et al.* Secret talk between adipose tissue and central nervous system via secreted factors-an emerging frontier in the neurodegenerative research. *J. Neuroinflammation* **13**, 67 (2016).
215. Tazón-Diego, F. Influencia de las células madre mesenquimales en la recuperación de oligodendrocitos sometidos a estrés oxidativo. (University of the Basque Country (UPV/EHU), 2014).
216. Maqueda, A. & Rodriguez, F. J. Efficacy of human HC016 cell transplants on neuroprotection and functional recovery in a rat model of acute spinal cord injury. *J. Tissue Eng. Regen. Med.* (2019) doi: 10.1002/term.2995. [Epub ahead of print]
217. M., J. *et al.* CSF interleukin-1 beta, tumor necrosis factor-alpha and free radicals production in relation to clinical outcome in acute bacterial meningitis. *Indian pediatrics.* **37(6)**, 608-614 (2000).
218. Zeng, W. *et al.* Antioxidant treatment enhances human mesenchymal stem cell anti-stress ability and therapeutic efficacy in an acute liver failure model. *Sci. Rep.* **5**, 11100 (2015).
219. Wang, S. *et al.* A novel cytoprotective peptide protects mesenchymal stem cells against mitochondrial dysfunction and apoptosis induced by starvation via Nrf2/Sirt3/FoxO3a pathway. *J. Transl. Med.* **15**, 33 (2017).
220. Oh, J. Y. *et al.* 17 β -Estradiol protects mesenchymal stem cells against high glucose-induced mitochondrial oxidants production via

VIII. References

- Nrf2/Sirt3/MnSOD signaling. *Free Radic. Biol. Med.* **130**, 328–342 (2019).
221. Valle-Prieto, A. & Conget, P. A. Human Mesenchymal Stem Cells Efficiently Manage Oxidative Stress. *Stem Cells Dev.* **19**, 1885–1893 (2010).
222. Bonilla-Porras, A. R., Jimenez-Del-Rio, M. & Velez-Pardo, C. N-acetylcysteine blunts 6-hydroxydopamine- and l-buthionine-sulfoximine-induced apoptosis in human mesenchymal stromal cells. *Mol. Biol. Rep.* **46**, 4423–4435 (2019).
223. Lin, W. *et al.* Sulforaphane suppressed LPS-induced inflammation in mouse peritoneal macrophages through Nrf2 dependent pathway. *Biochem. Pharmacol.* **76**, 967–973 (2008).
224. Bellezza, I. *et al.* Inhibition of NF- κ B nuclear translocation via HO-1 activation underlies α -tocopheryl succinate toxicity. *J. Nutr. Biochem.* **23**, 1583–1591 (2012).
225. Cuadrado, A., Martín-Moldes, Z., Ye, J. & Lastres-Becker, I. Transcription Factors NRF2 and NF- κ B Are Coordinated Effectors of the Rho Family, GTP-binding Protein RAC1 during Inflammation. *J. Biol. Chem.* **289**, 15244–15258 (2014).
226. Chen, C.-T., Shih, Y.-R. V, Kuo, T. K., Lee, O. K. & Wei, Y.-H. Coordinated Changes of Mitochondrial Biogenesis and Antioxidant Enzymes During Osteogenic Differentiation of Human Mesenchymal Stem Cells. *Stem Cells* **26**, 960–968 (2008).
227. Bartrons, R. & Caro, J. Hypoxia, glucose metabolism and the Warburg's effect. *J. Bioenerg. Biomembr.* **39**, 223–229 (2007).

-
228. Woo, Y. M. *et al.* Inhibition of Aerobic Glycolysis Represses Akt/mTOR/HIF-1 α Axis and Restores Tamoxifen Sensitivity in Antiestrogen-Resistant Breast Cancer Cells. *PLoS One* **10**, e0132285 (2015).
229. Basse, A. L. *et al.* Regulation of glycolysis in brown adipocytes by HIF-1 α . *Sci. Rep.* **7**, 4052 (2017).
230. Del Rey, M. J. *et al.* Hif-1 α Knockdown Reduces Glycolytic Metabolism and Induces Cell Death of Human Synovial Fibroblasts Under Normoxic Conditions. *Sci. Rep.* **7**, 3644 (2017).
231. Cerychova, R. & Pavlinkova, G. HIF-1, Metabolism, and Diabetes in the Embryonic and Adult Heart. *Front. Endocrinol. (Lausanne)*. **9**, 460 (2018).
232. Brand, K. Aerobic Glycolysis by Proliferating Cells: Protection against Oxidative Stress at the Expense of Energy Yield. *J. Bioenerg. Biomembr.* **29**, 355–364 (1997).
233. Chandel, N. S. *et al.* Reactive oxygen species generated at mitochondrial Complex III stabilize hypoxia-inducible factor-1 α during hypoxia: A mechanism of O₂ sensing. *J. Biol. Chem.* **275(33)**, 25130-25138 (2000).
234. Guzy, R. D. *et al.* Mitochondrial complex III is required for hypoxia-induced ROS production and cellular oxygen sensing. *Cell Metab.* **1**, 401–408 (2005).
235. Lassmann, H. & van Horssen, J. Oxidative stress and its impact on neurons and glia in multiple sclerosis lesions. *Biochim. Biophys. Acta - Mol. Basis Dis.* **1862**, 506–510 (2016).
236. Barreto, G. E., Gonzalez, J., Capani, F. & Morales, L. Neuroprotective

VIII. References

- Agents in Brain Injury: A Partial Failure? *Int. J. Neurosci.* **122**, 223–226 (2012).
237. Constantin, G. *et al.* Adipose-Derived Mesenchymal Stem Cells Ameliorate Chronic Experimental Autoimmune Encephalomyelitis. *Stem Cells* **27**, 2624–2635 (2009).
238. Lopatina, T. *et al.* Adipose-derived stem cells stimulate regeneration of peripheral nerves: BDNF secreted by these cells promotes nerve healing and axon growth de novo. *PLoS One* **6**, e17899–e17899 (2011).
239. Marconi, S. *et al.* Systemic treatment with adipose-derived mesenchymal stem cells ameliorates clinical and pathological features in the amyotrophic lateral sclerosis murine model. *Neuroscience* **248**, 333–343 (2013).
240. Mendes-Pinheiro, B. *et al.* Bone Marrow Mesenchymal Stem Cells' Secretome Exerts Neuroprotective Effects in a Parkinson's Disease Rat Model. *Front. Bioeng. Biotechnol.* **7**, 294 (2019).
241. Bodart-Santos, V. *et al.* Extracellular vesicles derived from human Wharton's jelly mesenchymal stem cells protect hippocampal neurons from oxidative stress and synapse damage induced by amyloid- β oligomers. *Stem Cell Res. Ther.* **10**, 332 (2019).
242. Lee, H. J. *et al.* The therapeutic potential of human umbilical cord blood-derived mesenchymal stem cells in Alzheimer's disease. *Neurosci. Lett.* **481**, 30–35 (2010).
243. Fitzpatrick, E. *et al.* Coculture with Mesenchymal Stem Cells Results in Improved Viability and Function of Human Hepatocytes. *Cell Transplant.* **24**, 73–83 (2015).

-
244. Nitti, M. *et al.* Heme Oxygenase 1 in the Nervous System: Does It Favor Neuronal Cell Survival or Induce Neurodegeneration? *Int. J. Mol. Sci.* **19**, 2260 (2018).
245. Rosa, P. M., Martins, L. A. M., Souza, D. O. & Quincozes-Santos, A. Glioprotective Effect of Resveratrol: an Emerging Therapeutic Role for Oligodendroglial Cells. *Mol. Neurobiol.* **55**, 2967–2978 (2018).
246. Veiga, S., Ly, J., Chan, P. H., Bresnahan, J. C. & Beattie, M. S. SOD1 overexpression improves features of the oligodendrocyte precursor response in vitro. *Neurosci. Lett.* **503**, 10–14 (2011).
247. Baud, O. *et al.* Glutathione peroxidase-catalase cooperativity is required for resistance to hydrogen peroxide by mature rat oligodendrocytes. *J. Neurosci.* **24**, 1531–1540 (2004).
248. Li, L. *et al.* Overexpression of Heme Oxygenase-1 in Mesenchymal Stem Cells Augments Their Protection on Retinal Cells In Vitro and Attenuates Retinal Ischemia/Reperfusion Injury In Vivo against Oxidative Stress. *Stem Cells Int.* **2017**, 4985323 (2017).
249. Thimraj, T. A., George, L., Asrafuzzaman, S., Upadhyay, S. & Ganguly, K. Chapter 7 - Oxidative Signaling in Chronic Obstructive Airway Diseases. in (eds. Chatterjee, S., Jungraithmayr, W. & Bagchi, D. B. T.-I. and I. in H. and D.) 79–98 (Academic Press, 2018). <https://doi.org/10.1016/B978-0-12-805417-8.00007-X>
250. Hu, C., Zhao, L., Peng, C. & Li, L. Regulation of the mitochondrial reactive oxygen species: Strategies to control mesenchymal stem cell fates ex vivo and in vivo. *J. Cell. Mol. Med.* **22**, 5196–5207 (2018).

